

AD-A085 132

BELL HELICOPTER TEXTRON FORT WORTH TX
CONCEPTUAL DESIGN OF A HELICOPTER COMPOSITE TRUSS TAIL BOOM. (U)
APR 80 D A GALLIAN

F/G 1/3

DAAK51-78-C-0016

UNCLASSIFIED

USAAVRADCOM-TR-80-D-R

NL

1/2

2/2

3/2

4/2

5/2

6/2

7/2

8/2

9/2

10/2

11/2

12/2

13/2

14/2

15/2

16/2

17/2

18/2

19/2

20/2

21/2

22/2

23/2

24/2

25/2

26/2

27/2

28/2

29/2

30/2

31/2

32/2

33/2

34/2

35/2

36/2

37/2

38/2

39/2

40/2

41/2

42/2

43/2

44/2

45/2

46/2

47/2

48/2

49/2

50/2

51/2

52/2

53/2

54/2

55/2

56/2

57/2

58/2

59/2

60/2

61/2

62/2

63/2

64/2

65/2

66/2

67/2

68/2

69/2

70/2

71/2

72/2

73/2

74/2

75/2

76/2

77/2

78/2

79/2

80/2

81/2

82/2

83/2

84/2

85/2

86/2

87/2

88/2

89/2

90/2

91/2

92/2

93/2

94/2

95/2

96/2

97/2

98/2

99/2

100/2

101/2

102/2

103/2

104/2

105/2

106/2

107/2

108/2

109/2

110/2

111/2

112/2

113/2

114/2

115/2

116/2

117/2

118/2

119/2

120/2

121/2

122/2

123/2

124/2

125/2

126/2

127/2

128/2

129/2

130/2

131/2

132/2

133/2

134/2

135/2

136/2

137/2

138/2

139/2

140/2

141/2

142/2

143/2

144/2

145/2

146/2

147/2

148/2

149/2

150/2

151/2

152/2

153/2

154/2

155/2

156/2

157/2

158/2

159/2

160/2

161/2

162/2

163/2

164/2

165/2

166/2

167/2

168/2

169/2

170/2

171/2

172/2

173/2

174/2

175/2

176/2

177/2

178/2

179/2

180/2

181/2

182/2

183/2

184/2

185/2

186/2

187/2

188/2

189/2

190/2

191/2

192/2

193/2

194/2

195/2

196/2

197/2

198/2

199/2

200/2

201/2

202/2

203/2

204/2

205/2

206/2

207/2

208/2

209/2

210/2

211/2

212/2

213/2

214/2

215/2

216/2

217/2

218/2

219/2

220/2

221/2

222/2

223/2

224/2

225/2

226/2

227/2

228/2

229/2

230/2

231/2

232/2

233/2

234/2

235/2

236/2

237/2

238/2

239/2

240/2

241/2

242/2

243/2

244/2

245/2

246/2

247/2

248/2

249/2

250/2

251/2

252/2

253/2

254/2

255/2

256/2

257/2

258/2

259/2

260/2

261/2

262/2

263/2

264/2

265/2

266/2

267/2

268/2

269/2

270/2

271/2

272/2

273/2

274/2

275/2

276/2

277/2

278/2

279/2

280/2

281/2

282/2

283/2

284/2

285/2

286/2

287/2

288/2

289/2

290/2

291/2

292/2

293/2

294/2

295/2

296/2

297/2

298/2

299/2

300/2

301/2

302/2

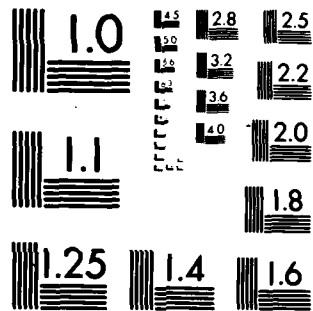
303/2

304/2

305/2

306/2

307/2



MICROCOPY RESOLUTION TEST CHART
NATIONAL BUREAU OF STANDARDS-1963 A

USAAVRADCOM-TR-80-D-8

12

J.L



LEVEL

CONCEPTUAL DESIGN OF A HELICOPTER COMPOSITE TRUSS TAIL BOOM

David A. Gallian
BELL HELICOPTER TEXTRON
P. O. Box 482
Fort Worth, Texas 76101

ADA 085132

April 1980

Final Report

DTIC
ELECTE
JUN 5 1980

Approved for public release;
distribution unlimited.

Prepared for

APPLIED TECHNOLOGY LABORATORY

U. S. ARMY RESEARCH AND TECHNOLOGY LABORATORIES (AVRADCOM)

Fort Eustis, Va. 23604

NC FILE COPY

80 6 5 04 6

APPLIED TECHNOLOGY LABORATORY POSITION STATEMENT

This report was prepared by Bell Helicopter Textron under the terms of Contract DAAK51-78-C-0016. Objectives of this effort were to establish design criteria, design, investigate manufacturing techniques, fabricate, and ballistically test a composite truss tail boom section comparable to an OH-58 tail boom.

Results of this effort show that a satisfactory design was achieved and a filament winding manufacturing technique was developed and used to fabricate the specimens. The specimen met the structural requirements of the comparable tail boom and proved to be ballistically tolerant to the small High-Explosive threat.

The conclusions contained herein are concurred in by the Applied Technology Laboratory. This concurrence is limited to technical accomplishment and does not imply the practicality of the proposed approach for application to current Army aircraft.

The technical monitor for this contract was Mr. George T. McAllister, Aeronautical Systems Division.

DISCLAIMERS

The findings in this report are not to be construed as an official Department of the Army position unless so designated by other authorized documents.

When Government drawings, specifications, or other data are used for any purpose other than in connection with a definitely related Government procurement operation, the United States Government thereby incurs no responsibility nor any obligation whatsoever; and the fact that the Government may have formulated, furnished, or in any way supplied the said drawings, specifications, or other data is not to be regarded by implication or otherwise as in any manner licensing the holder or any other person or corporation, or conveying any rights or permission, to manufacture, use, or sell any patented invention that may in any way be related thereto.

Trade names cited in this report do not constitute an official endorsement or approval of the use of such commercial hardware or software.

DISPOSITION INSTRUCTIONS

Destroy this report when no longer needed. Do not return it to the originator.

Unclassified

SECURITY CLASSIFICATION OF THIS PAGE (When Data Entered)

REPORT DOCUMENTATION PAGE		READ INSTRUCTIONS BEFORE COMPLETING FORM
1. REPORT NUMBER 18 USAAVRADCOM TR-80-D-8	2. GOVT ACCESSION NO. 19 ADA085132	3. RECIPIENT'S CATALOG NUMBER
4. TITLE (and Subtitle) 6 CONCEPTUAL DESIGN OF A HELICOPTER COMPOSITE TRUSS TAIL BOOM	5. TYPE OF REPORT & PERIOD COVERED 9 Final Report	6. PERFORMING ORG. REPORT NUMBER
7. AUTHOR(s) 10 David A. Gallian	8. CONTRACT OR GRANT NUMBER(s) 15 DAAK51-78-C-0016	9. PROGRAM ELEMENT, PROJECT, TASK AREA & WORK UNIT NUMBERS 16 1209A 1L162209AH76 00 249 EK
9. PERFORMING ORGANIZATION NAME AND ADDRESS Bell Helicopter Textron P. O. Box 482 Fort Worth, Texas 76101	10. CONTROLLING OFFICE NAME AND ADDRESS 11 Applied Technology Laboratory, U. S. Army Research and Technology Laboratories (AVRADCOM) Fort Eustis, Virginia 23604	11. REPORT DATE Apr 80
14. MONITORING AGENCY NAME & ADDRESS (if different from Controlling Office)	12. NUMBER OF PAGES 115	13. SECURITY CLASS. (of this report) Unclassified
16. DISTRIBUTION STATEMENT (of this Report) Approved for public release; distribution unlimited.		15a. DECLASSIFICATION/DOWNGRADING SCHEDULE
17. DISTRIBUTION STATEMENT (of the abstract entered in Block 20, if different from Report)		
18. SUPPLEMENTARY NOTES		
19. KEY WORDS (Continue on reverse side if necessary and identify by block number) Composite Helicopter Tail Boom Truss Ballistic Tolerant		
20. ABSTRACT (Continue on reverse side if necessary and identify by block number) This report presents the results of a conceptual study of a helicopter composite truss tail boom. The study included the following tasks: design criteria, material properties, truss design and analysis, manufacturing techniques, and fabrication and ballistic testing. The results of the study indicate that a composite truss is a viable concept for a ballistically tolerant tail boom.		

DD FORM 1 JAN 73 1473 EDITION OF 1 NOV 65 IS OBSOLETE

Unclassified

SECURITY CLASSIFICATION OF THIS PAGE (When Data Entered)

054200 [Signature]

TABLE OF CONTENTS

	<u>Page</u>
LIST OF ILLUSTRATIONS.	4
LIST OF TABLES	6
INTRODUCTION	7
DESIGN CRITERIA.	9
DETERMINATION OF MATERIAL PROPERTIES	10
DESIGN AND ANALYSIS.	14
FABRICATION.	49
BALLISTIC TESTING.	52
STATIC LOAD CORRELATION.	68
DYNAMIC LOAD IMPULSES.	79
CONCLUSIONS AND RECOMMENDATIONS.	82
REFERENCES	84
APPENDIX A - COMPOSITE TAIL BOOM TESTS	85

LIST OF ILLUSTRATIONS

<u>Figure</u>		<u>Page</u>
1	Coupon Fabrication Mandrel.	12
2	Truss Configurations 4T and 4T/C.	16
3	Truss Configurations 5T and 5T/C.	17
4	Truss Configurations 6T and 6T/C.	18
5	Truss Configurations 7T and 7T/C.	19
6	Truss Configurations 8T and 8T/C.	20
7	NASTRAN Model Stiffness Correlation	21
8	Typical Damage State 2.	23
9	Deflection - Configuration 4T	24
10	Deflection Damage - Configuration 4T/C.	25
11	Deflection - Configuration 5T	26
12	Deflection - Configuration 5T/C	27
13	Deflection - Configuration 6T	28
14	Deflection - Configuration 6T/C	29
15	Deflection - Configuration 7T	30
16	Deflection - Configuration 7T/C	31
17	Deflection - Configuration 8T	32
18	Deflection - Configuration 8T/C	33
19	Configuration Characteristics	35
20	Member Joint Testing.	39
21	Member Joint Specimen After Failure	40
22	Member Joint Geometry	40
23	Machined Attachment Fitting	41
24	Welded Attachment Fitting	43

<u>Figure</u>		<u>Page</u>
25	Truss Boom Weight Comparison.	44
26	Final Truss Design.	45
27	Pinned End Rigid Bars	48
28	Wooden Tooling Pattern.	50
29	Sand Casting Mold	50
30	Sand Casting.	51
31	Wet Lay-Up	51
32	Truss Loading Diagram	53
33	Load Application Frame.	54
34	Targeted Impact Area, Specimen 1.	55
35	Exit Side Damage, Specimen 1.	56
36	Individual Member Damage, Specimen 1.	57
37	Boom Deflection After Impact, Specimen 1.	58
38	Targeted Impact Area, Specimen 2.	58
39	Projectile Entry Hole, Specimen 2	59
40	Exit Side Fragment Damage, Specimen 2	60
41	Exit Side of Entry Hole, Specimen 2	61
42	Individual Member Damage, Specimen 2.	62
43	Boom Deflection After Impact, Specimen 2.	63
44	Targeted Impact Area, Specimen 3.	64
45	Fragment Damage, Specimen 3	65
46	Upper Tension Longeron, Specimen 3.	66
47	Typical Fragment Damage	67
48	Strain Gage Locations, Specimen 1	69
49	NASTRAN Loads, Member 1, Specimen 1	71

<u>Figure</u>		<u>Page</u>
50	NASTRAN LOADS, Member 4, Specimen 1.	73
51	Strain Gage Locations, Specimen 2.	76
52	Strain Gage Locations, Specimen 3.	77

LIST OF TABLES

<u>Table</u>		<u>Page</u>
1	Resin System Properties, LRF-092	10
2	Summary of Material Properties	13
3	Truss Configuration Descriptions	15
4	Preliminary Sizing Study Results	34
5	Member Column Buckling Test Results.	37
6	Member Joint Test Loads.	39
7	Attachment Fitting Test Results.	42
8	Finite Element Section Properties.	47
9	NASTRAN Predicted Member Buckling Allowables .	48
10	Specimen Applied Loads	52
11	Correlation of Member Loads Before Ballistic Impact - Test 1.	68
12	NASTRAN Member Forces and Moments.	70
13	Correlation of Member Loads Before Ballistic Impact - Test 2.	75
14	Correlation of Member Loads Before Ballistic Impact - Test 3.	78
15	Dynamic Impulse Strain, Test 1	80
16	Dynamic Impulse Strain, Test 2	81

INTRODUCTION

Military activities in the past ten years have subjected the helicopter to increased exposure of air defense measures. The vulnerability of helicopters has increased due to the larger caliber weapons that may be encountered when performing air mobility missions in mid-intensity warfare. Reducing helicopter vulnerability is a major factor in improving helicopter combat effectiveness. Attrition analysis performed by the Army shows that tail boom damage could be a significant contributor to helicopter combat loss.

The primary threat to the helicopter tail boom is an HEI delayed-fuse round. Basically, the fuse is activated upon contact with the structure and detonates after some finite time delay. The combined effect of the fragmentation and the high blast pressure associated with the detonation can cause catastrophic structural failure when occurring within a confined volume such as that found in a conventional tailboom.

An attempt to reduce the vulnerability of very small diameter tail booms would mean an excessive weight increase and/or a large modification cost.

To determine a methodology for the solution to the tail boom vulnerability problem, the design options available to the aircraft designer are monocoque, semimonocoque, or truss. Both the monocoque and semimonocoque are standard methods of aircraft construction. Since each completely encloses a volume, they are more vulnerable to the HEI threat than an open truss design. When the HEI comes into contact with the surface of a conventional tail boom, its fuse is activated and detonation occurs within the confined volume. The resulting fragments and pressure on the structure generally cause extensive damage.

The truss has many vulnerability reduction advantages.

Because of the openness of the truss, the projectile could simply pass through the tail boom without being activated. If a hit does occur, there is an equal probability of the round striking a member on the exit as on the entrance side of the tail boom envelope. If the hit occurs on the exit side, the round, because of the time-delay fuse, would detonate outside the envelope and cause little damage. If the hit occurs on the entrance side, the blast pressure is vented through the truss and damage is greatly reduced.

Another advantage of a truss is that it can be designed with alternate load paths (or redundancy) by providing additional secondary members.

Potentially, the most important characteristic of an open truss design is that it is insensitive to threat velocity and size of the threat. Thus, when new and larger threats are encountered in the future, the open truss design will not become obsolete.

Additional advantages can be realized from an open truss design if the truss is constructed from composite materials. Composites have relatively high ballistic tolerance, have high specific strength and stiffness (which will allow a high level of redundancy for minimum weight), and are relatively corrosion free. All these directly contribute to reduced weight and maintainability.

A truss constructed from composite materials also lends itself to automatic fabrication through the use of filament winding techniques.

In September of 1978, the Applied Technology Laboratory, Fort Eustis, Virginia, awarded a contract to Bell Helicopter Textron to design and build three composite truss tailboom specimens.

The effort was divided into five separate tasks: design criteria, material properties, truss design and analysis, manufacturing techniques, and fabrication and ballistic testing.

This report presents the results of this study and the conclusions reached after analysis of the results.

DESIGN CRITERIA

The design criteria established for the truss tail boom test section are as follows:

1. Truss specimens shall be of sufficient size, that is an envelope not greater than 15 inches in diameter by a length of 60 inches, to evaluate the effects of damage due to a 23mm HEI projectile.
2. Test section will be able to carry design limit loads before sustaining any damage. The stiffness of the test section will be comparable to the stiffness of a Model OH-58 tail boom before sustaining any damage.
3. After sustaining damage, the test section will be capable of carrying loads that would be developed during a lg high-speed level flight condition. Deflections resulting from the application of these loads to the damaged section will not be of such magnitude as to exceed the allowable driveshaft cocking angle.

Damage criteria will be as follows:

1. A compression side longeron joint and one opposite diagonal member will be considered ineffective.

Should the damage criterion above prove to be too severe, then the alternate damage criteria will be,

2. A compression longeron and one opposite diagonal will be considered ineffective.

Accession For	
NTIS GRA&I	<input checked="" type="checkbox"/>
DDC TAB	<input type="checkbox"/>
Unannounced Justification	<input type="checkbox"/>
By _____	
Distribution/	
Availability Codes	
Dist	Avail and/or special
A	

DETERMINATION OF MATERIAL PROPERTIES

T/300 graphite with a 280-degree cure adhesive was used for construction of the truss specimens. Although the properties of Union Carbide Corporation's Thornel 300 carbon fiber are well documented, its properties, when combined with an adhesive matrix suitable for use with filament winding techniques, are not. Prior to final analysis of the truss specimens, tension, compression, and shearing strength tests were performed to determine the mechanical properties of the graphite and adhesive mixture.

The resin system selected for use in the fabrication of the truss specimens, LRF-092,* is comprised of Epon 828 resin, MNA hardener, and BDMA accelerator. This resin system is particularly well suited for filament winding fabrication techniques.

The physical properties of this resin system, as measured in the Brunswick Corporation's material laboratory, are shown in Table 1.

TABLE 1. RESIN SYSTEM PROPERTIES, LRF-092

Tensile Strength, psi	8,477
Tensile Modulus, psi x 10 ⁶	.424
Percent Elongation	3.1
Compressive Strength, psi	16,458
Compressive Modulus, psi x 10 ⁶	.560
Flexural Strength, psi	17,799
Flexural Modulus, psi x 10 ⁶	.395
Shear Strength, ppsi	7,863
Thermal Expansion Coefficient, in./in.°F	2.98 x10 ⁻⁵
Density, lb/in. ³	.044
Cure Shrinkage, in./10 in.	.067

* LRF-Lincoln Resin Formula, a product of Brunswick Corporation, Lincoln, Nebraska.

In order to obtain test coupons that would be representative of the completed truss specimens, a rectangular steel mandrel was fabricated for filament winding of the coupons. Slots were machined into one end of the mandrel to aid in the fabrication of constant cross-section coupons. The mandrel is depicted in Figure 1. The test coupons were filament wound using a graphite/adhesive mix identical to the mixture that would be used to fabricate the truss specimens. The longitudinal, compression, tension, and shear coupons were prepared from the material wound into the mandrel slots. Transverse coupons were made from the panels wound on the straight section of the mandrel.

Tension specimens were prepared as 1 inch wide x 9 inches long straight-sided coupons with metal tabs bonded on each end. The coupons were loaded axially in a Satec Testing Machine, and strains were monitored using a strain transducer.

Longitudinal and transverse compression tests were performed per ASTM 695-69.

Horizontal shear strength was evaluated using procedures outlined in ASTM D 2344-72.

The results of these tests are summarized in Table 2. Values obtained by averaging the results of six coupons for each test type are tabulated and compared with published results from the Air Force Material Laboratory Design Guide.¹

¹ADVANCED COMPOSITE DESIGN GUIDE, Rockwell International Corporation, Contract F33615-74-C-5075, Air Force Flight Dynamics Laboratory, Air Force Systems Command, Wright-Patterson Air Force Base, Ohio, April 1976.

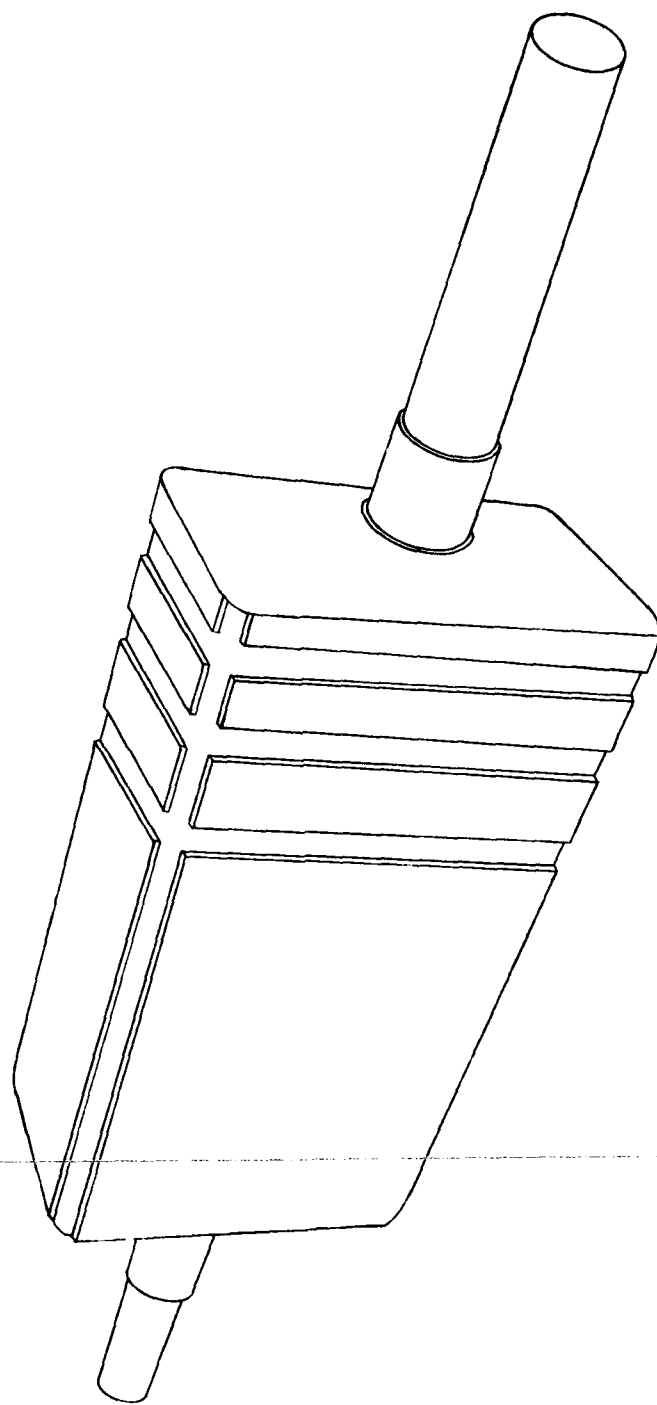


Figure 1. Coupon Fabrication Mandrel

TABLE 2. SUMMARY OF MATERIAL PROPERTIES
(THORNEL 300/LRF-092)

	Brunswick	AFML*
Longitudinal Tension		
Strength, psi x 10 ³	185.4	180.0
Modulus, psi x 10 ⁶	18.88	19.0
Longitudinal Compression		
Strength, psi x 10 ³	116.70**	180.0
Modulus, psi x 10 ⁶	18.37	19.0
Traverse Tension		
Strength, psi x 10 ³	4.62	5.0
Modulus, psi x 10 ⁶	2.62	1.5
Traverse Compression		
Strength, psi x 10 ³	22.88	25.0
Modulus, psi x 10 ⁶	1.53	--
Short Beam Shear, psi	10.77	11.5

* Published results from Air Force Material Laboratory Design Guide for High Strength Graphite in an Epoxy Resin.¹

** All specimens had premature edge failure.

DESIGN AND ANALYSIS

Phase one of the design and analysis task was to determine the best truss configuration. Truss configurations were judged on the basis of weight, deflection after impact, increase in longeron and diagonal load after impact, the amount of open area, and various manufacturing considerations. Of the configurations studied, all designs which required internal bracing to support the frame members were rejected due to manufacturing considerations. The use of filament-winding techniques requires that a solid winding mandrel be used. The use of such a tool eliminates the possibility of including any internal members in the truss design. With the elimination of all internal bracing, only those configurations incorporating frame members with bending continuity could be considered further.

Those truss configurations chosen for further investigation are shown in Table 3 and Figures 2 through 6.

These ten truss configurations were sized to match the stiffness of the existing Model OH-58 tail boom. The configurations were sized such that the stiffness (as measured by the deflection of a point in the center of the truss frames) of each configuration closely matched that of the first 60 inches of the existing Model OH-58 boom. This stiffness correlation is shown in Figure 7.

To aid in this preliminary sizing and to determine each configuration's deflection characteristics after ballistic impact, a NASTRAN (Reference 2) finite element model of each truss configuration was constructed.

A finite element generator program was written to aid in this task. Basic input consisted of geometry definition at the forward and aft end of the truss section; longeron, diagonal, and frame properties for each bay; and the number of bays. A complete, ready-to-run NASTRAN model was output. Computer time expended per truss configuration generated was less than 1 second.

Results of the preliminary sizing efforts and the deflection characteristics of the various configurations after ballistic impact are shown in Figures 8 through 18. Shown with each undamaged stiffness plot is the deflection exhibited after

² McCormick, Caleb W., NASA SP-222(03) NASTRAN USER'S MANUAL, National Aeronautics and Space Administration, Washington, D.C., July 1978

TABLE 3. TRUSS CONFIGURATION DESCRIPTIONS

	Configuration I.D.
4 Longeron Truss	
- Diagonals capable of taking tension only	4T
- Diagonals capable of taking tension and compression	4T/C
5 Longeron Truss	
- Diagonals capable of taking tension only	5T
- Diagonals capable of taking tension and compression	5T/C
6 Longeron Truss	
- Diagonals capable of taking tension only	6T
- Diagonals capable of taking tension and compression	6T/C
7 Longeron Truss	
- Diagonals capable of taking tension only	7T
- Diagonals capable of taking tension and compression	7T/C
8 Longeron Truss	
- Diagonals capable of taking tension only	8T
- Diagonals capable of taking tension and compression	8T/C

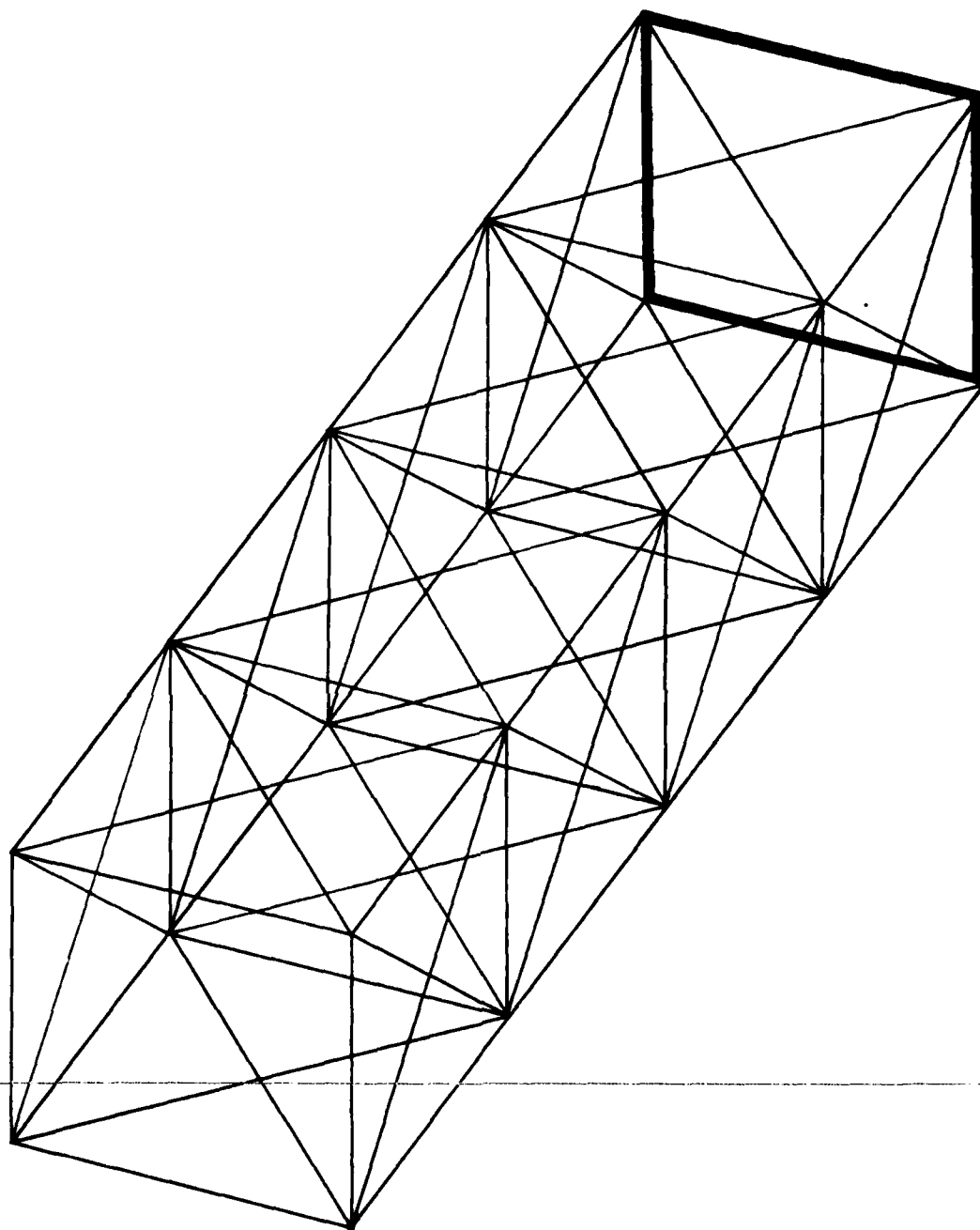


Figure 2. Truss Configurations 4T and 4T/C

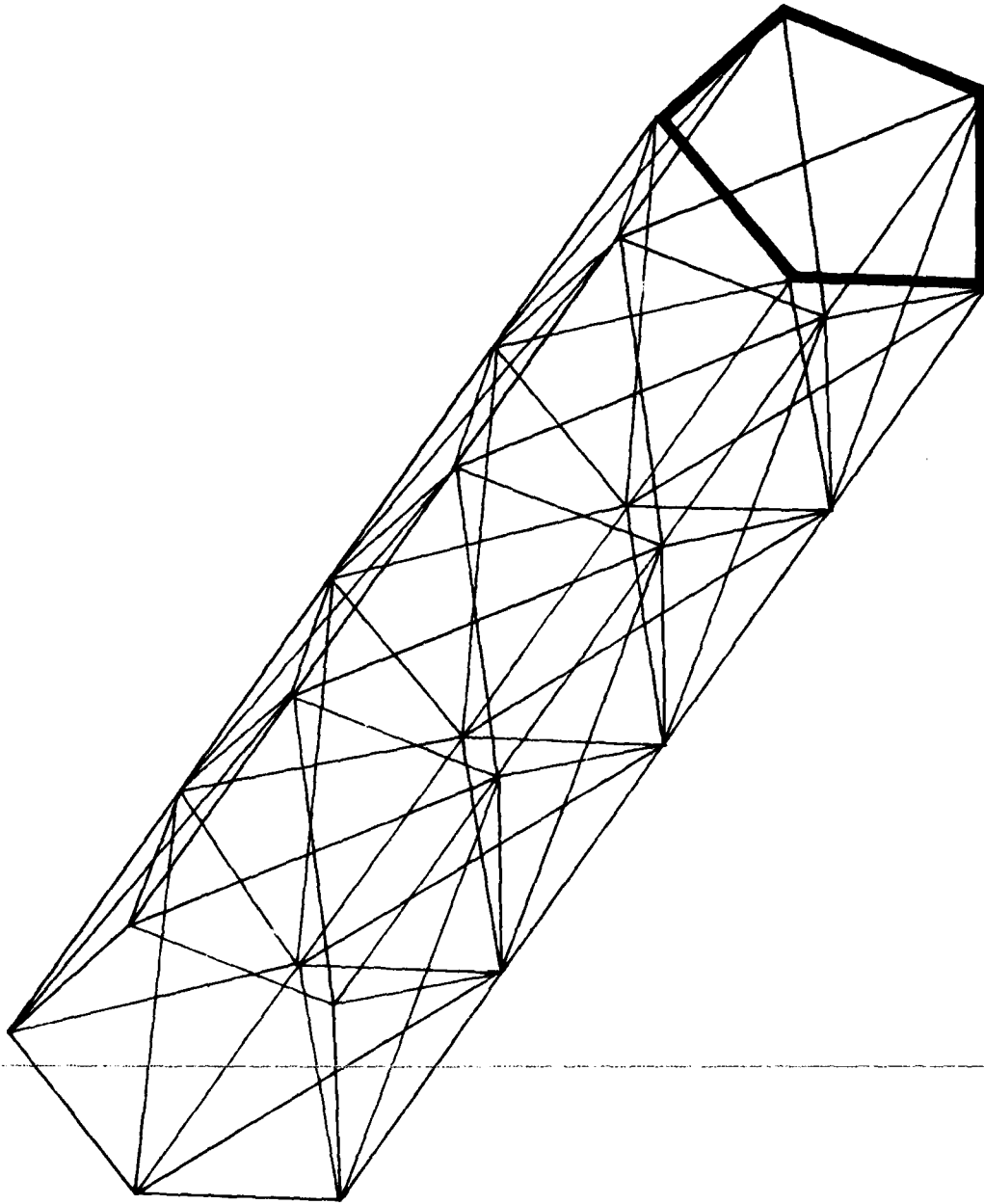


Figure 3. Truss Configurations 5T and 5T/C

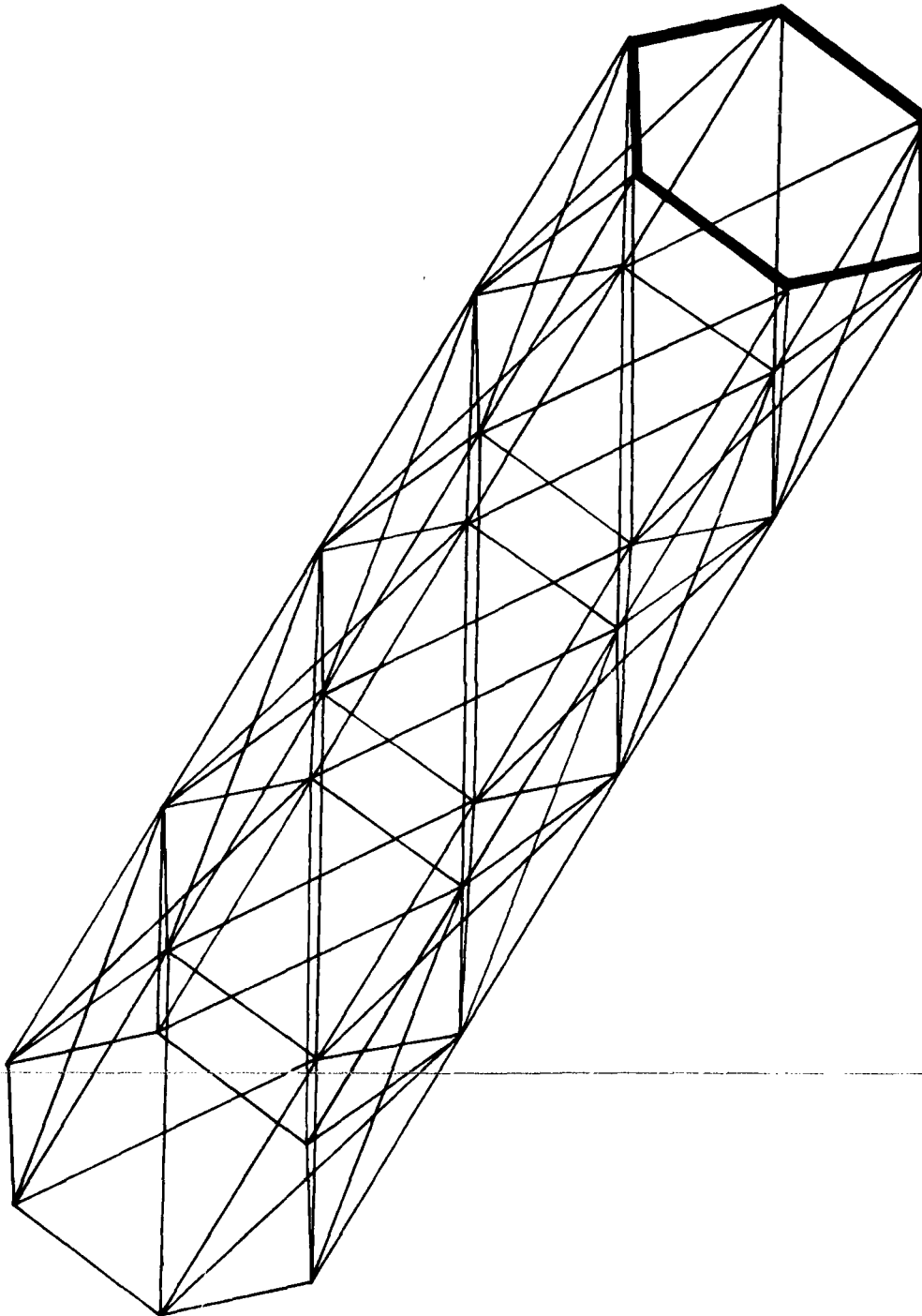


Figure 4. Truss Configurations 6T and 6T/C

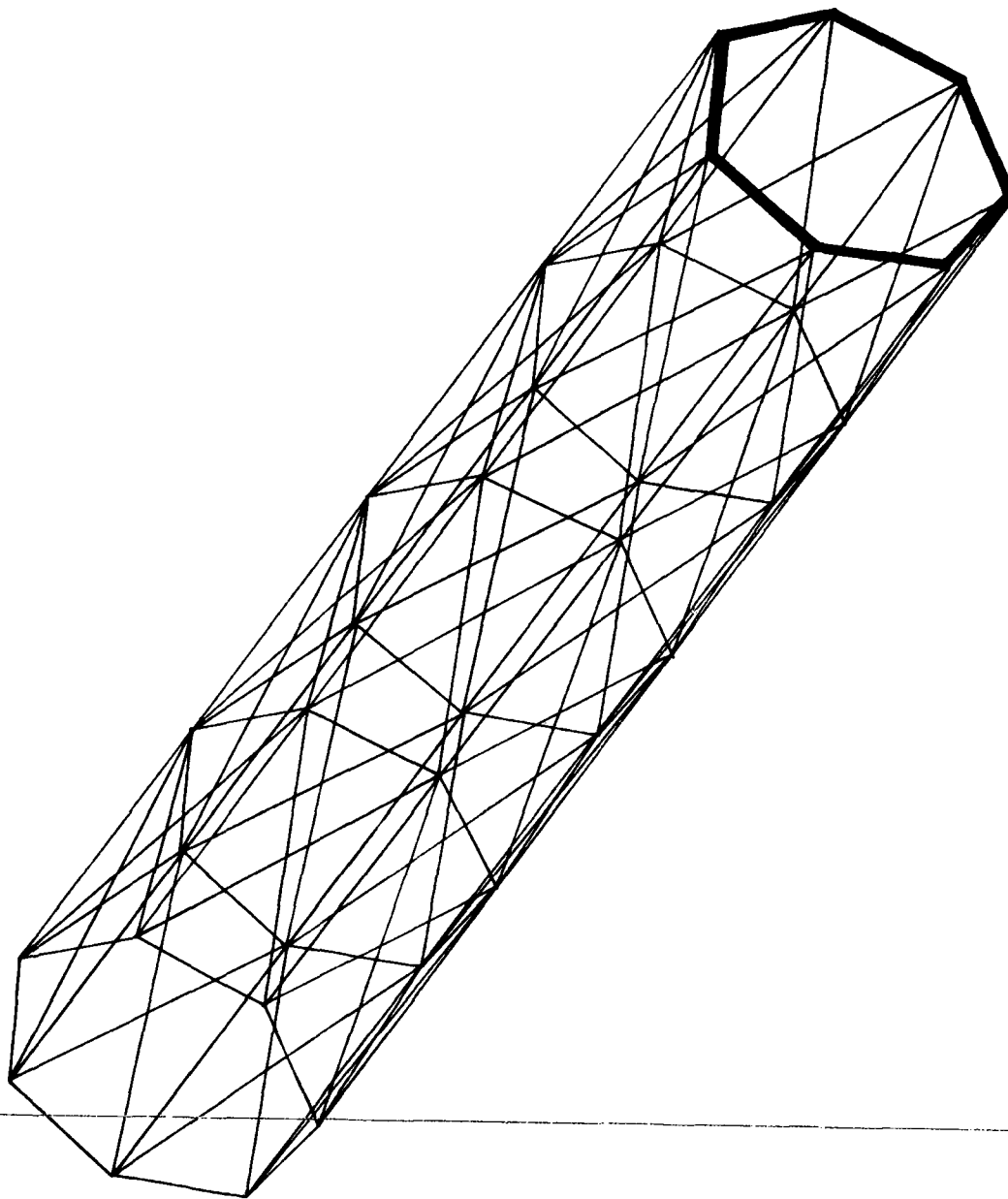


Figure 5. Truss Configurations 7T and 7T/C

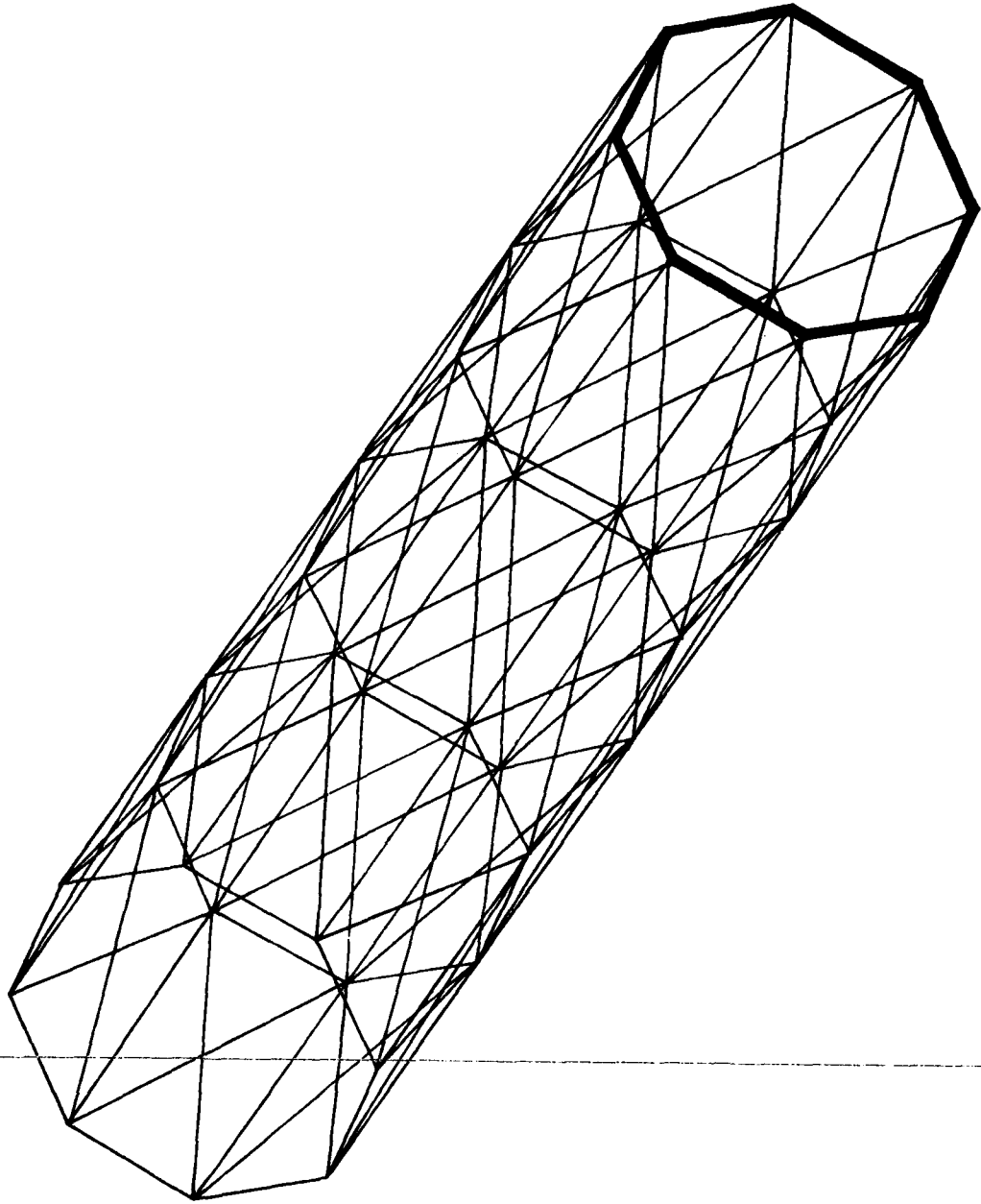


Figure 6. Truss Configurations 8T and 8T/C

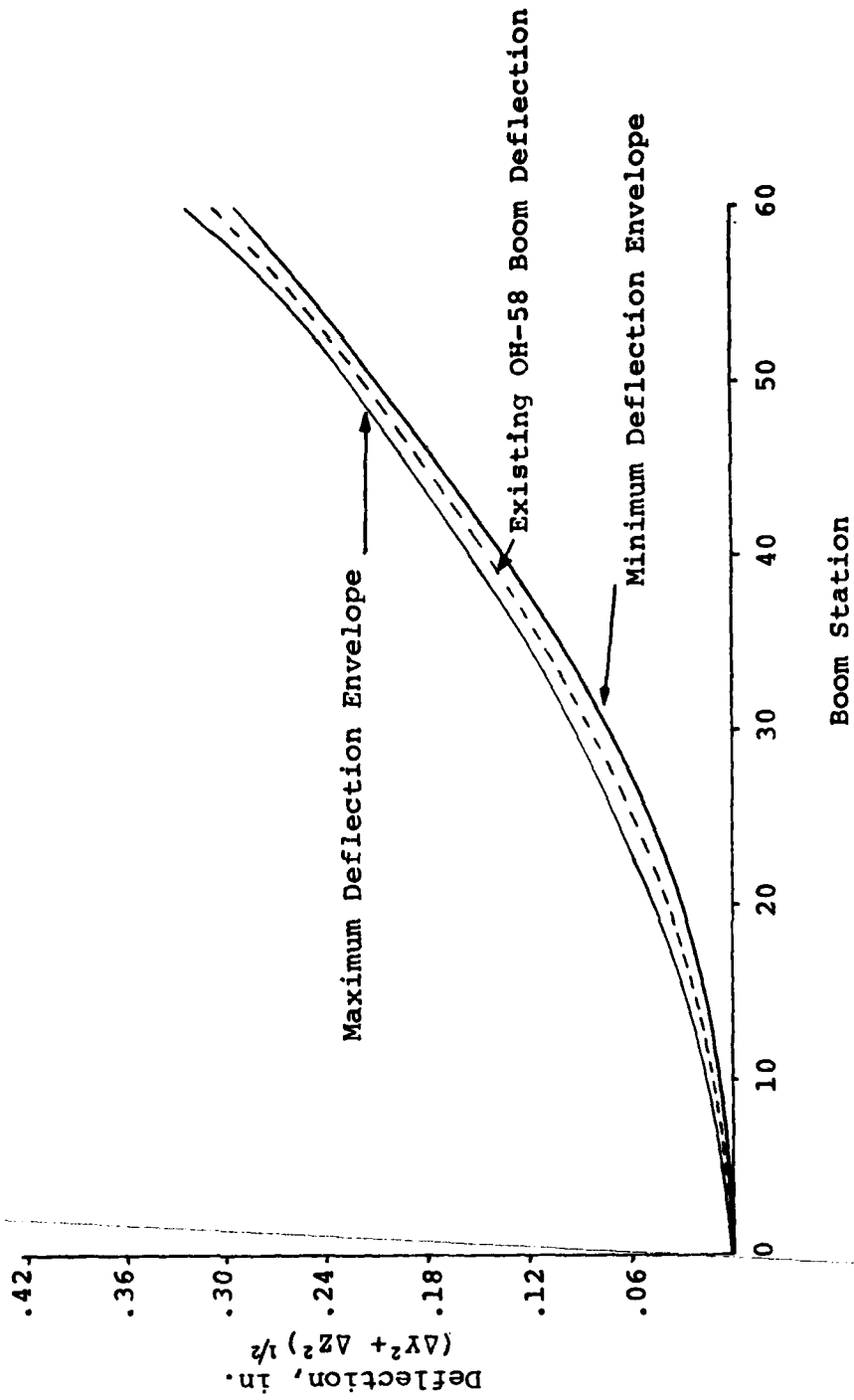


Figure 7. NASTRAN Model Stiffness Correlation

application of the two damage criteria. Damage state one refers to the loss of a single longeron and one opposite side diagonal member. Damage state two refers to the loss of a longeron joint and one opposite side diagonal member. Both the longeron and joint were removed from the compression side of the loaded truss model. A 1.5-degree slope line is also included on each graph. This line represents the maximum allowable tail rotor driveshaft coupling misalignment angle.

After each configuration was sized for stiffness, the mass generator in NASTRAN was used to calculate the weight of each truss configuration. A mass density of .056 lb/in.³ was used in this calculation. The weight used for comparison purposes was for the truss only and did not include any provisions for end fittings.

The amount of open area was based on the following assumed member geometry:

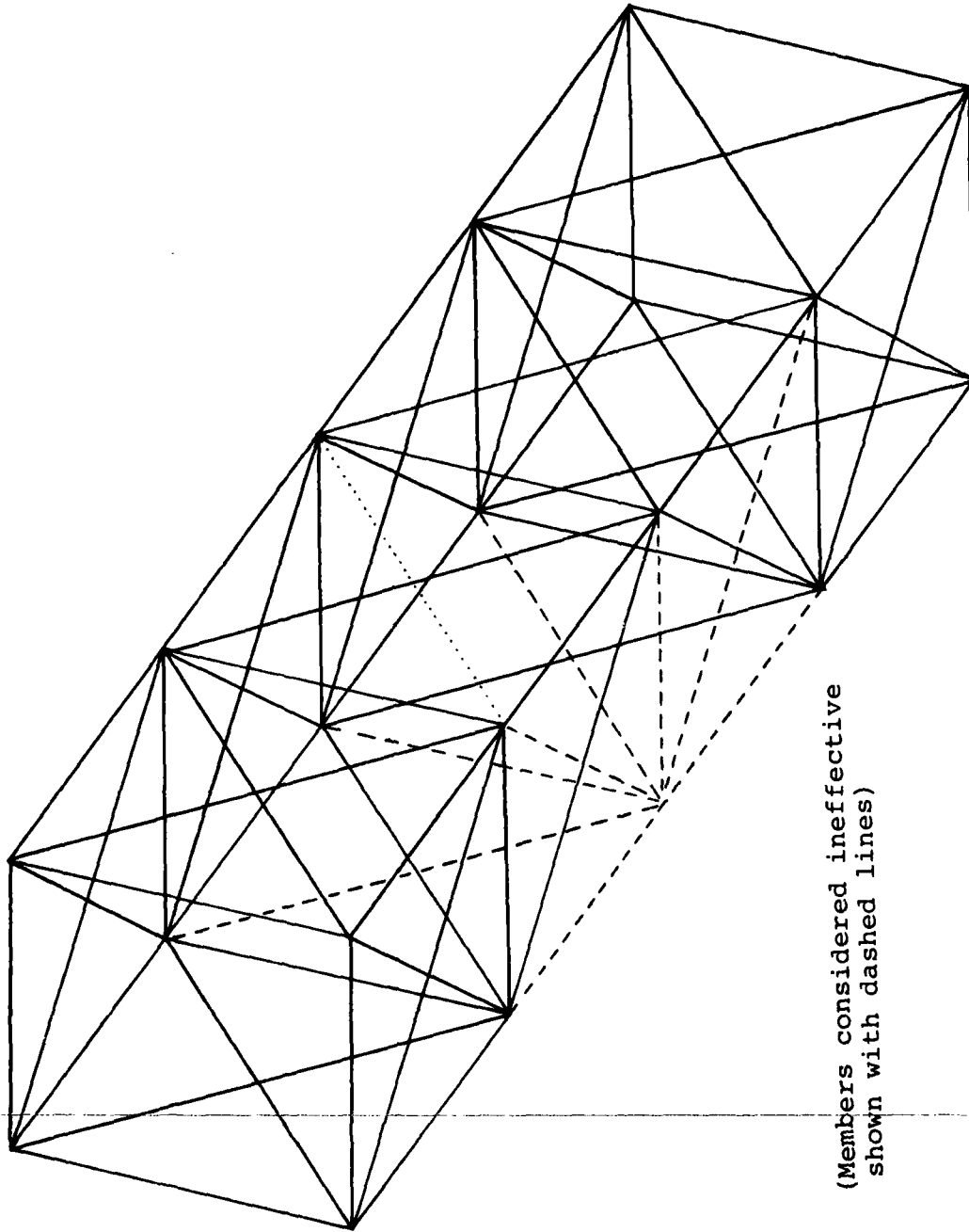
- All longerons had 1-inch flanges
- All diagonals had .5-inch flanges
- All frames had 1-inch flanges

The amount of open area presented by a particular truss configuration was calculated as

(circumferential area - member area).

Ballistically induced dynamic impulse loads were felt to be a significant yet unknown design input. It was assumed that the truss configuration that exhibited the smallest change in static longeron and diagonal load after impact would be the configuration that would be less susceptible to large dynamic impulses. Using the NASTRAN models, individual member loads were tabulated for the various truss configurations both before and after the removal of a longeron joint.

As shown in Figure 9, truss configuration 4T exceeded the deflection criterion after damage. Configuration 7T was eliminated from further consideration because of an inability to converge on a tension-only solution. In order to match the stiffness of the existing Model OH-58 boom, both 8 longeron configurations required such a small diameter boom that they approached becoming a solid tube. Both of these configurations were eliminated from further consideration because of this condition. The results from the preliminary sizing study for the remaining six truss configurations are shown in Table 4.



(Members considered ineffective
shown with dashed lines)

Figure 8. Typical Damage State 2

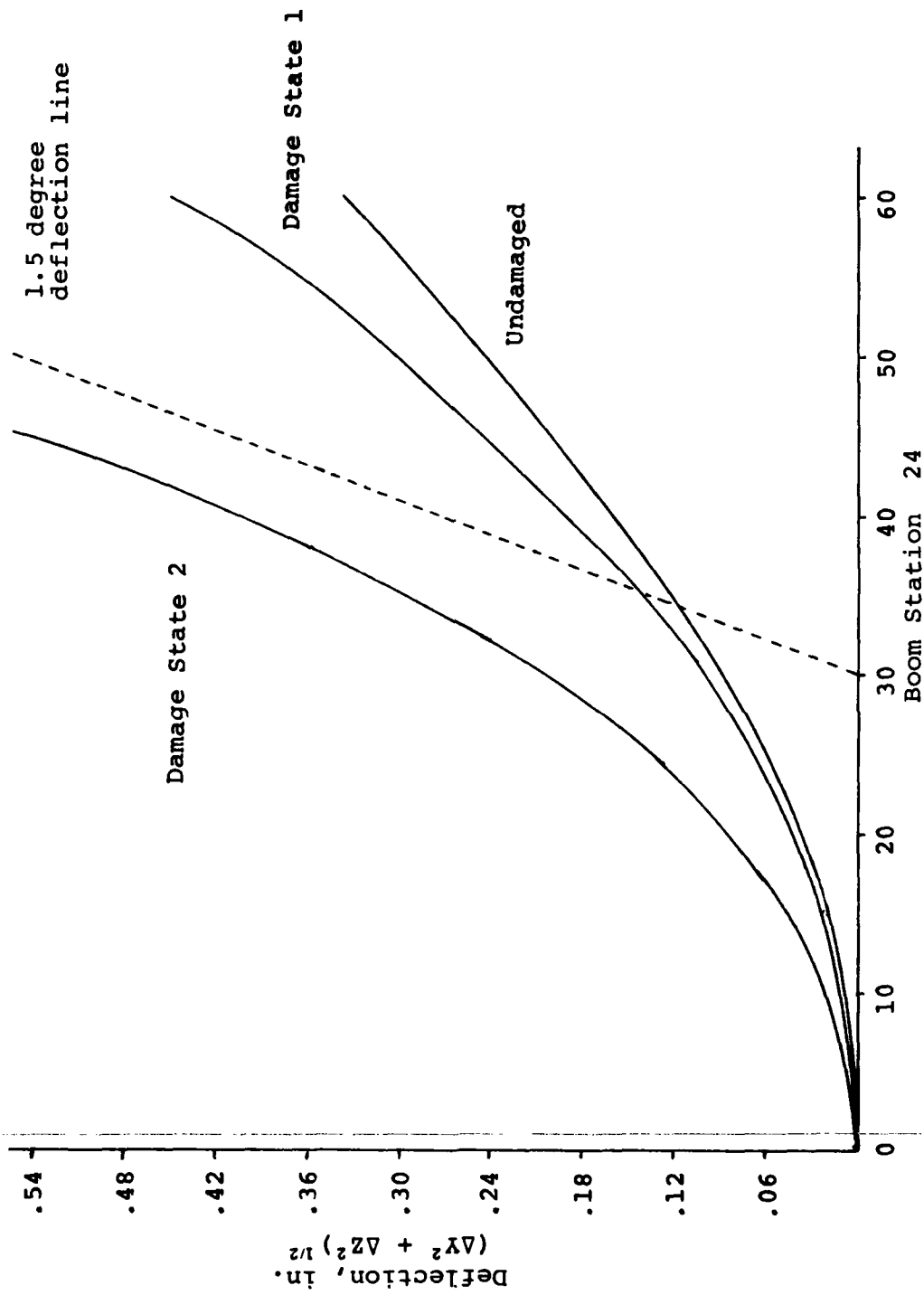


Figure 9. Deflection - Configuration 4T

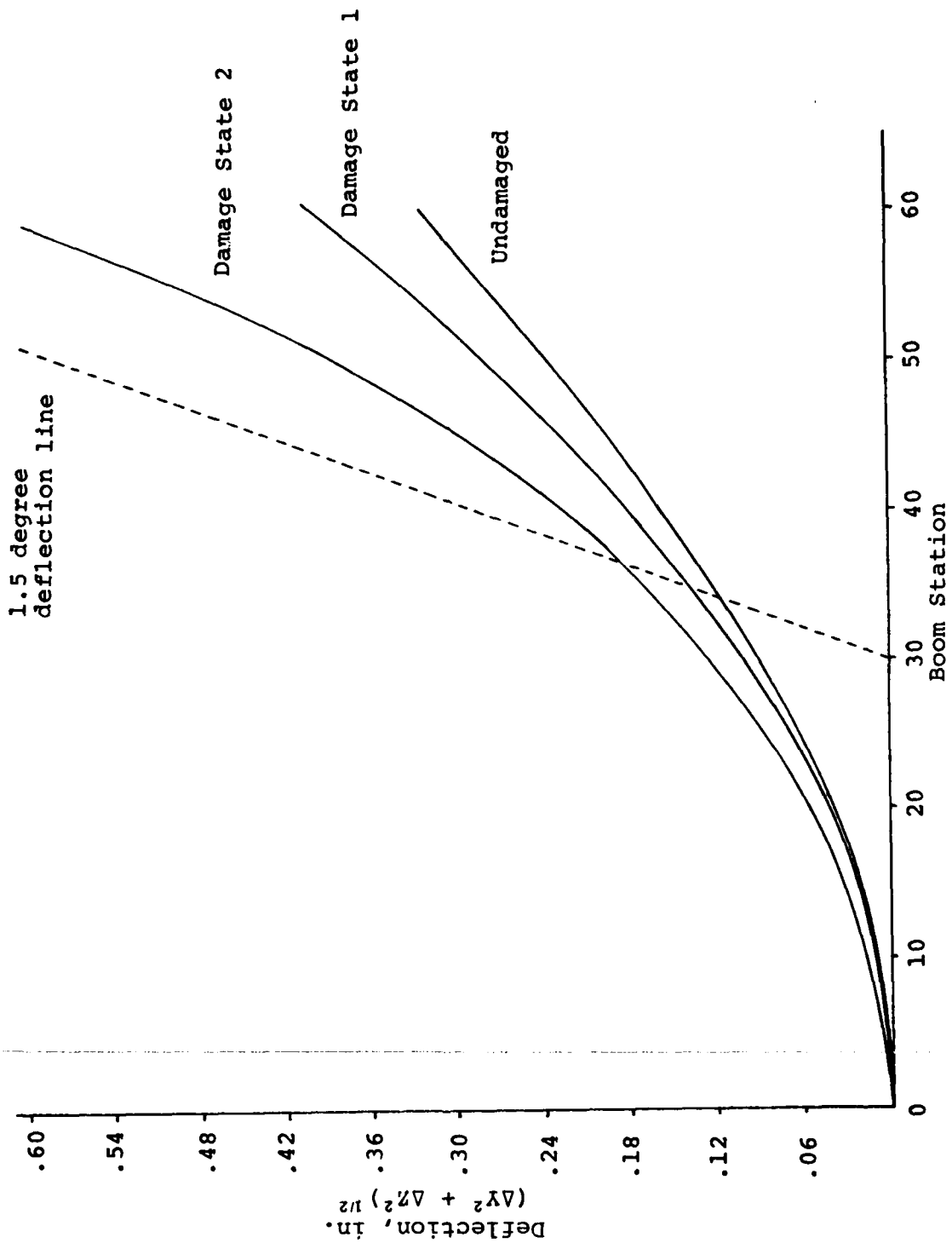


Figure 10. Deflection Damage - Configuration 4T/C

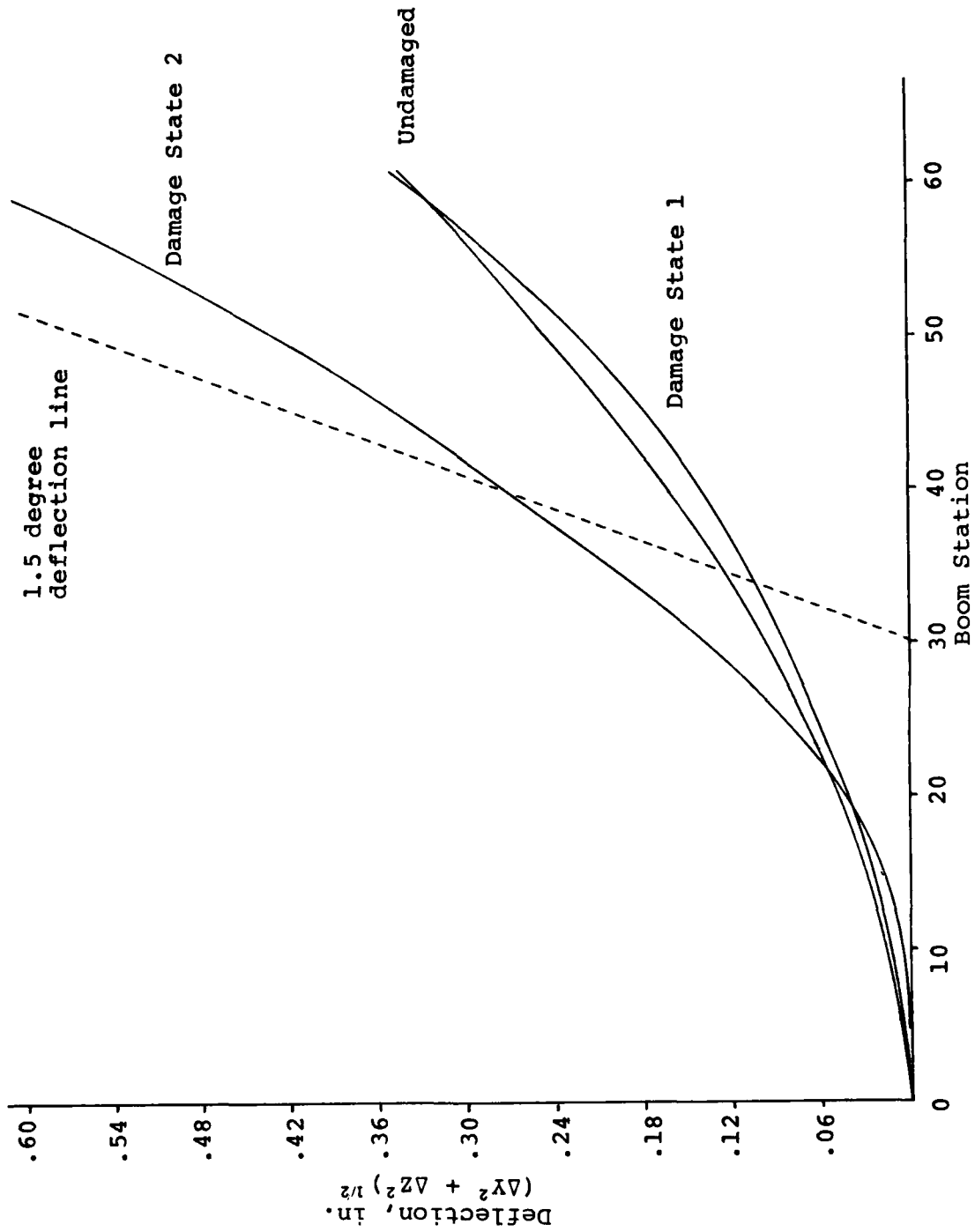


Figure 11. Deflection - Configuration 5T

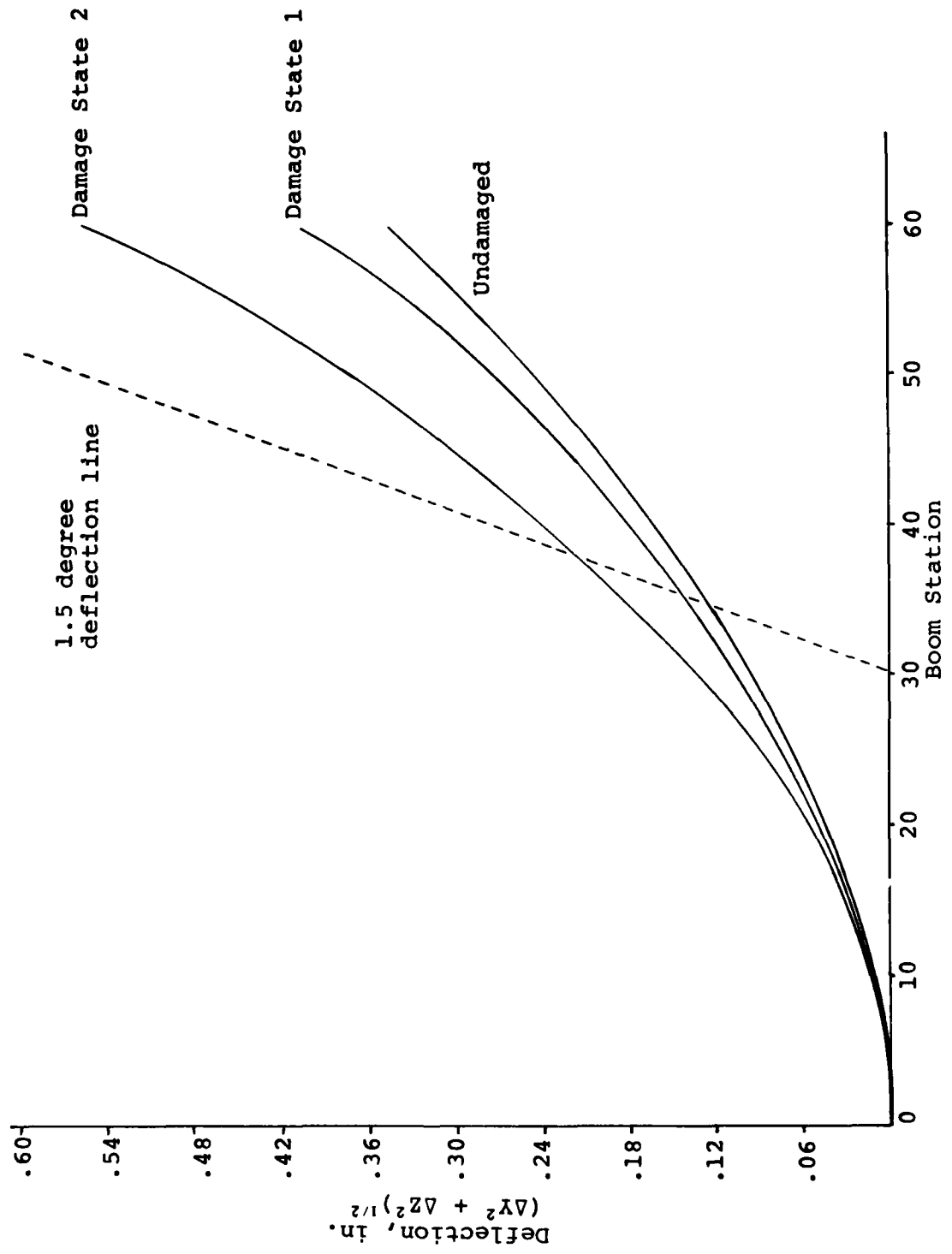


Figure 12. Deflection - Configuration 5T/C

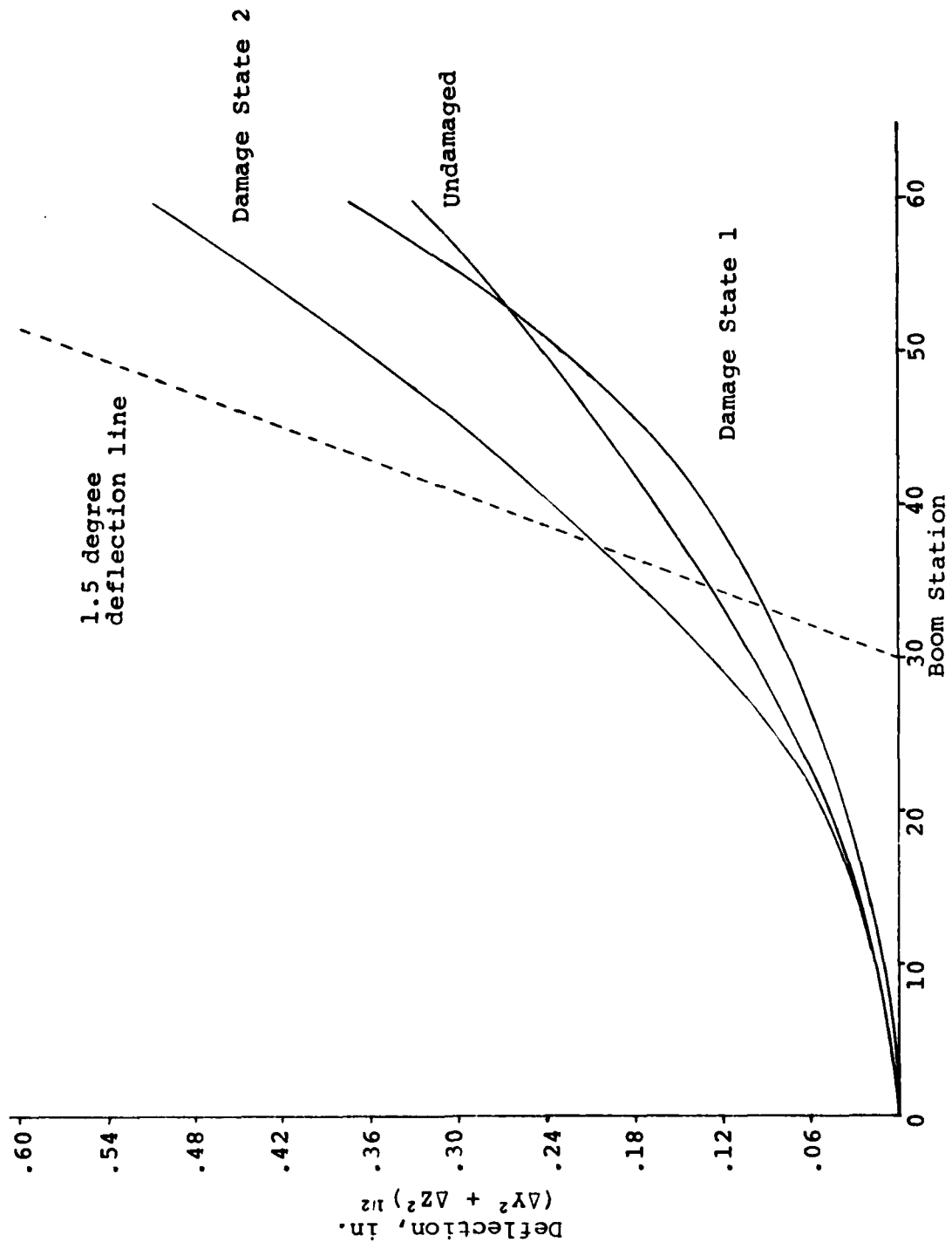


Figure 13. Deflection - Configuration 6T

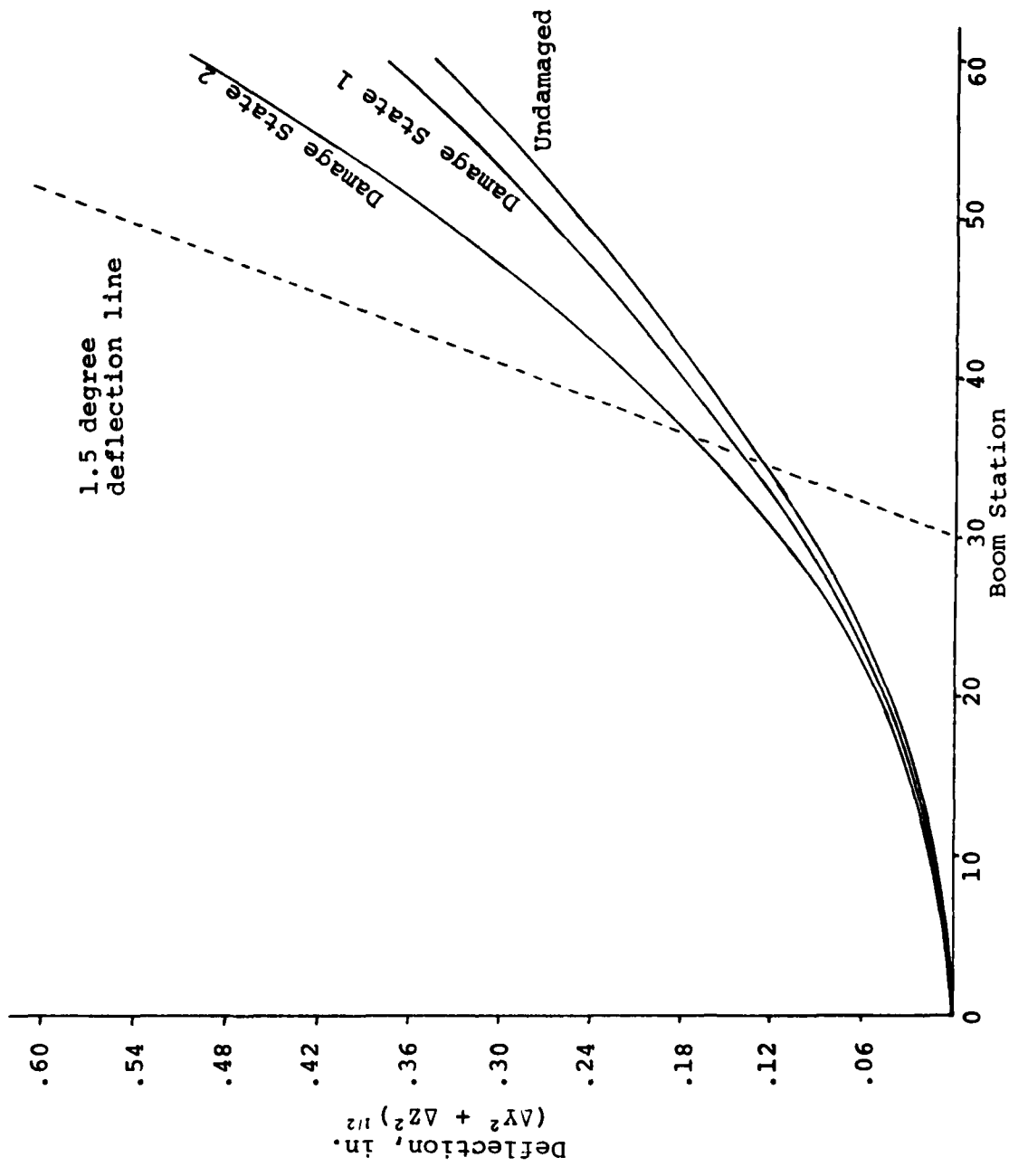


Figure 14. Deflection - Configuration 6T/C

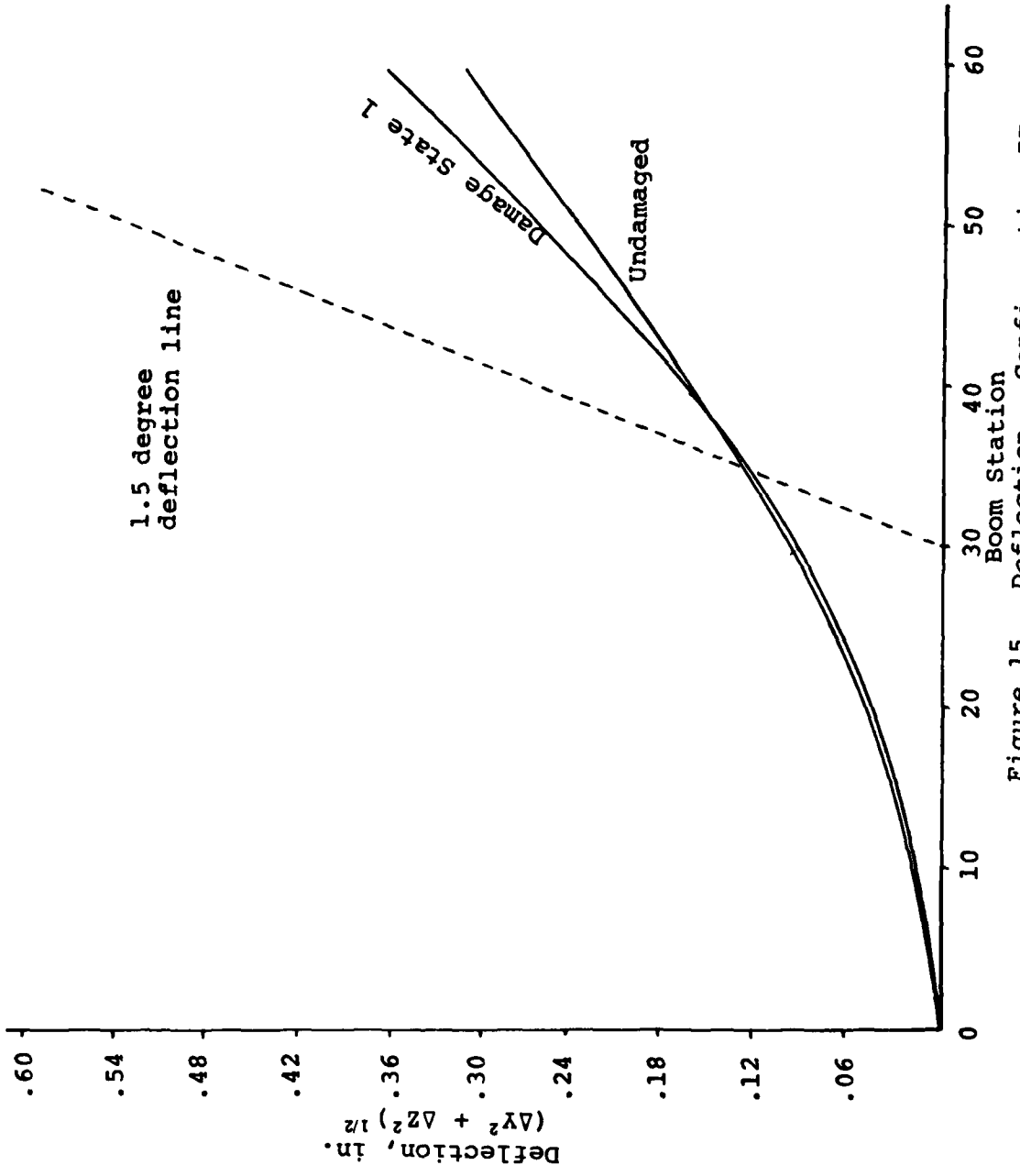


Figure 15. Deflection - Configuration 7T

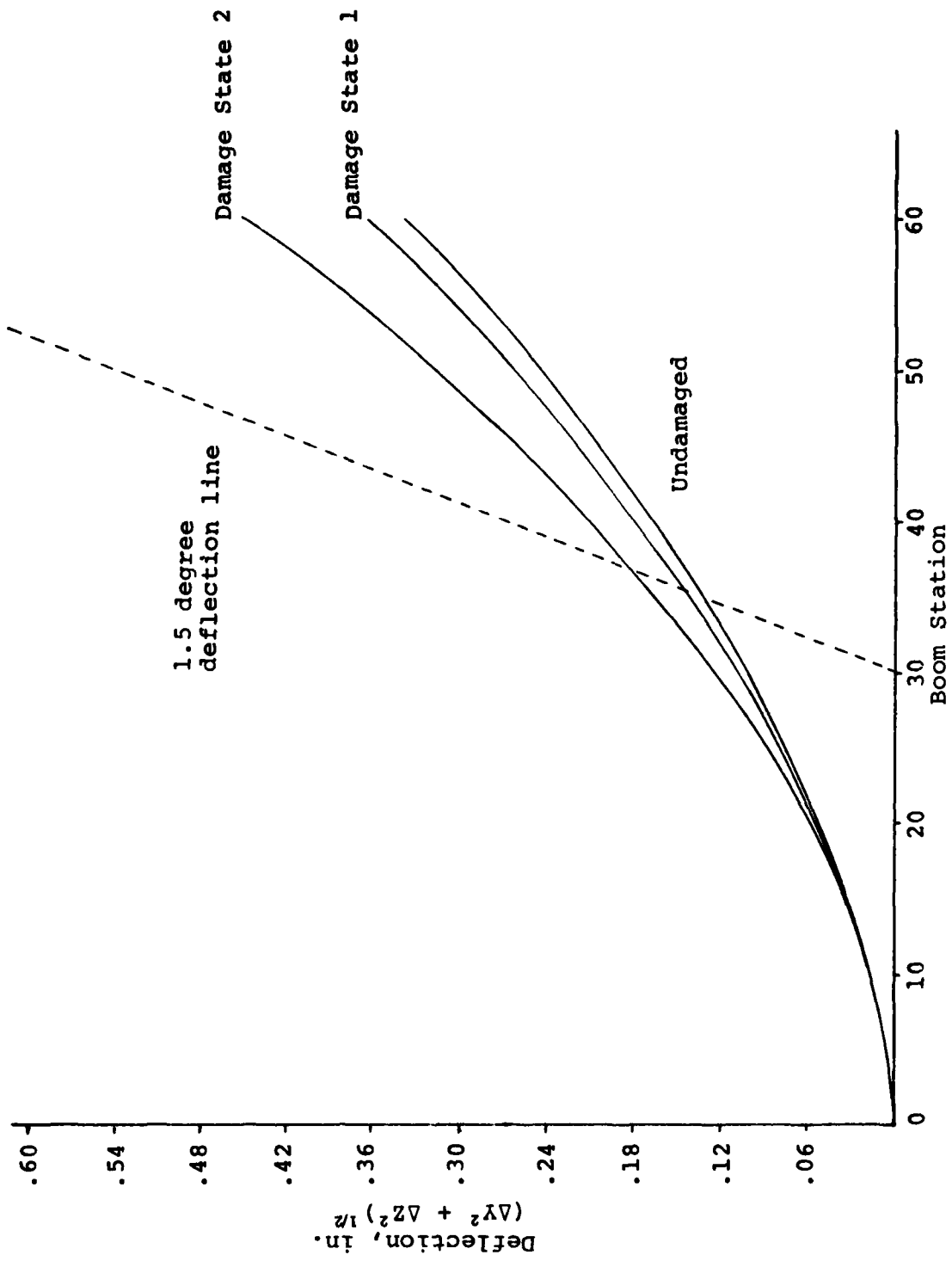


Figure 16. Deflection - Configuration 7T/C

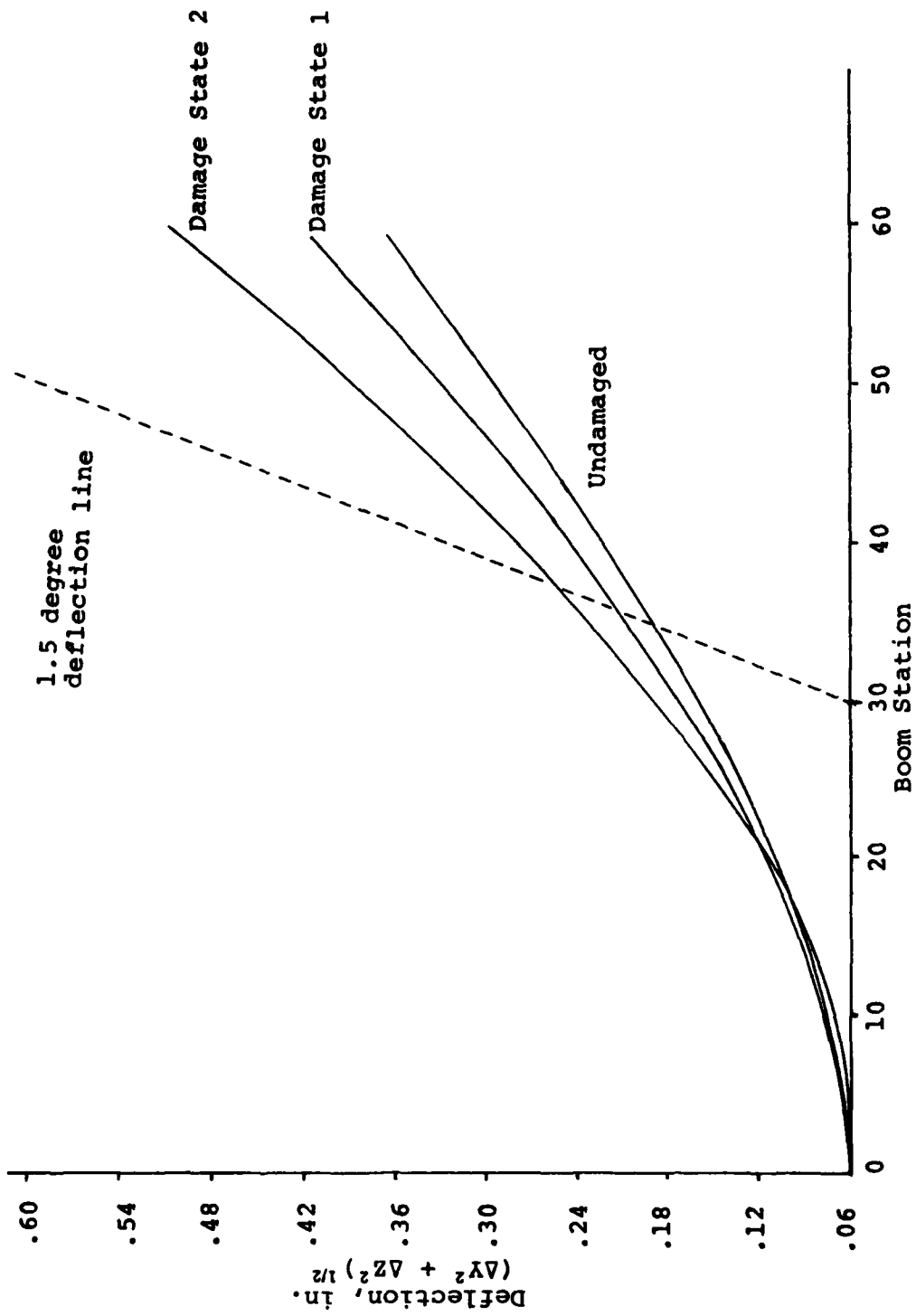


Figure 17. Deflection - Configuration 8T

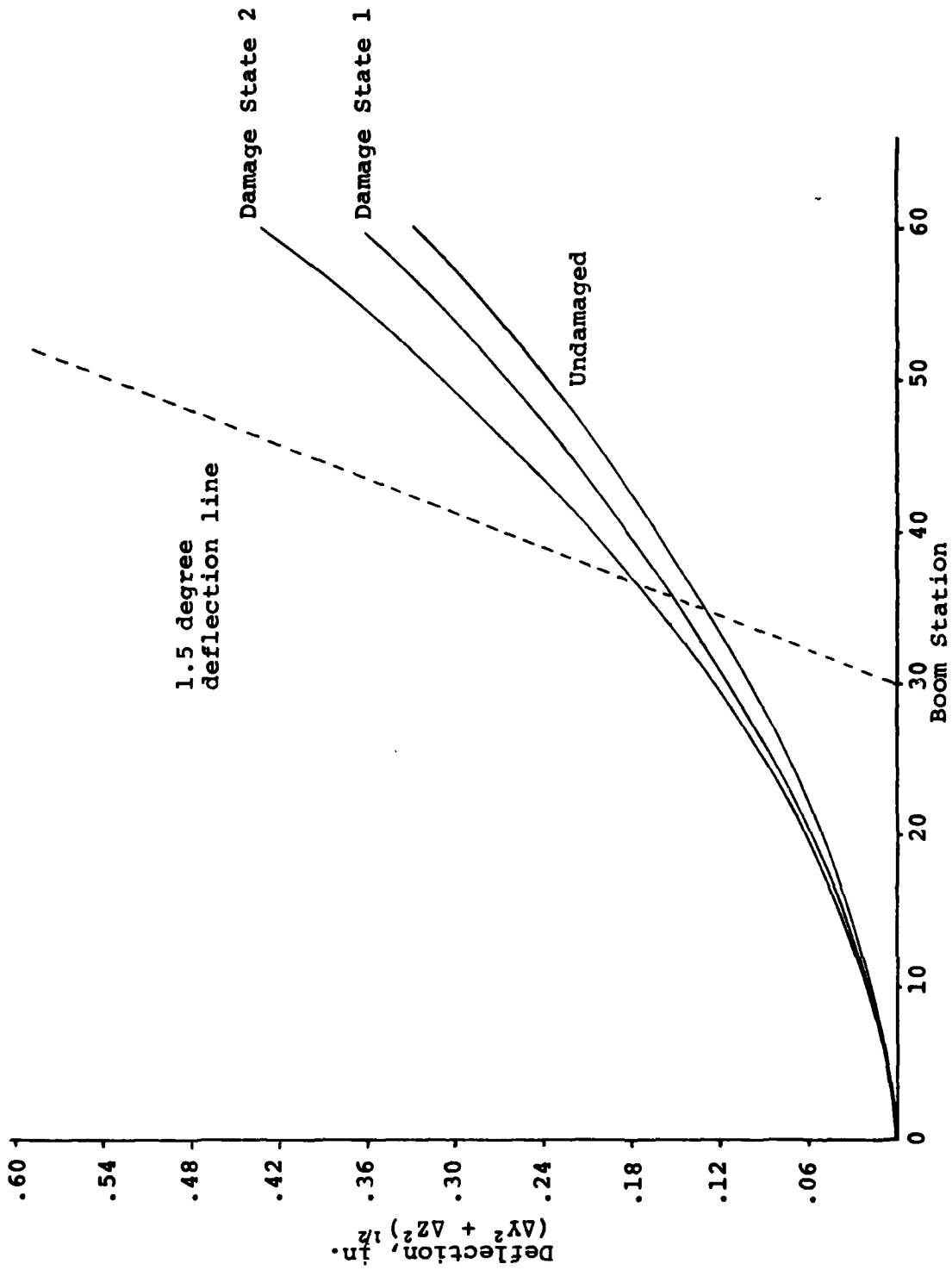


Figure 18. Deflection - Configuration 8T/C

TABLE 4. PRELIMINARY SIZING STUDY RESULTS

	CONFIGURATION					
	4T/C	5T/C	5T	6T/C	6T	7T/C
WEIGHT, LB/50 in.	3.76	7.66	9.81	7.96	10.29	8.94
% OPEN AREA	67	56	56	48	48	32
DEFLECTION AFTER IMPACT (DAMAGE STATE 2), IN. $(\Delta Y^2 + \Delta Z^2)^{1/2}$.457	.339	.595	.309	.316	.281
% CHANGE IN LONG- ERON LOAD AFTER IMPACT	109	83	60	46	33	26
% CHANGE IN DIA- GONAL LOAD AFTER IMPACT, LB	109	86	254	20	236	38

The key parameters of weight, amount of solid area, deflection after ballistic damage, and increase in longeron and diagonal load after damage are graphically compared in Figure 19. In this chart, the maximum values in each category are plotted as 100 percent. Lesser values are then shown as a percentage of the maximum values. As would be expected, the amount of solid (or presented) area is greater for those configurations having a larger number of longerons.

Likewise, the weight is generally less for those configurations having the fewer longerons.

The configurations that used diagonal members capable of taking only a tensile load were judged to be the worst overall designs. They were heavier than their tension/compression diagonal counterparts and exhibited a large increase in diagonal load after damage. During the initial sizing of these configurations, it became readily apparent that the stiffness of these two configurations was a function of the applied load. Since the stiffness of the existing Model OH-58 boom is constant throughout the range of design loads, any design that does not exhibit such a constant stiffness could possibly pass through a critical frequency as various flight loads were applied. For these reasons, truss configurations 5T and 6T were eliminated from the design selection.

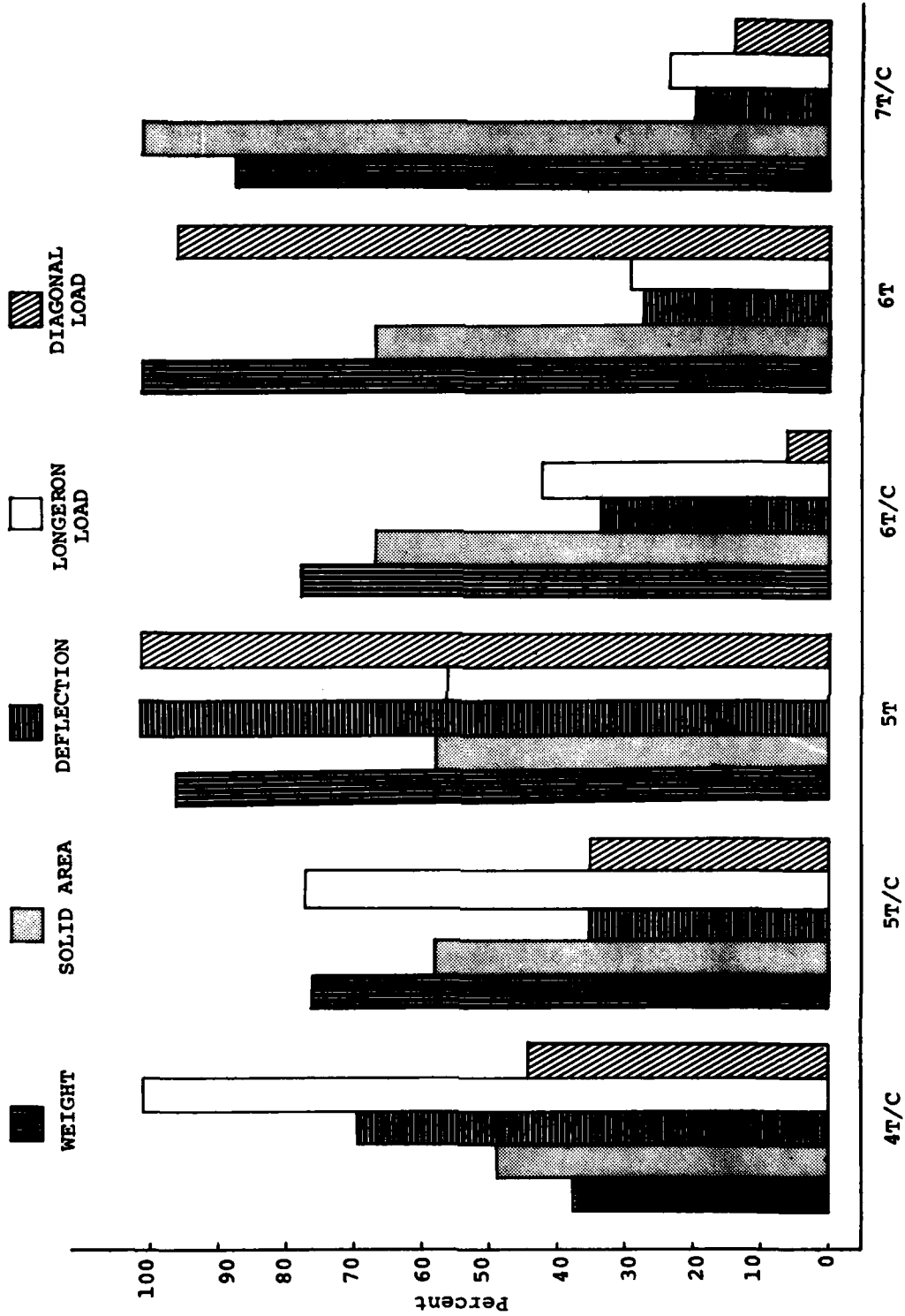


Figure 19. Configuration Characteristics

Configuration 4T/C exhibited a deflection pattern after the removal of a longeron joint that came very close to exceeding the 1.5-degree deflection limit. The remaining longerons also had the largest change in static load after damage. Even though configuration 4T/C was the lightest of the proposed designs and had the largest amount of open area, the potential for exceeding the tail rotor driveshaft bearing misalignment angle and the possible large dynamic impulse loads in the remaining longeron members eliminated configuration 4T/C from consideration.

Of the remaining three designs, configuration 6 T/C exhibits the best overall characteristics. The amount of solid area is only slightly higher than 5T/C and is 33 percent less than 7T/C. Configuration 6T/C exhibits a relatively small amount of increased deflection after the loss of a longeron joint. It offers only one-half of the longeron load redistribution of configuration 5T/C and only one-third of the diagonal load redistribution. Manufacturing studies indicate that it would be significantly easier (and thus less expensive) to build a configuration having an even number of longerons. For these reasons, configuration 6T/C was chosen as the best overall truss design. It should be noted that none of the original truss designs were optimized for weight or any other design parameter. The characteristics used for the configuration selection are believed to be representative of their respective designs but should not be considered the best obtainable. The selected truss configuration was optimized during the final truss analysis and design phase.

After selecting configuration 6T/C as the best overall design, the final design phase was begun.

Using the preliminary design loads obtained from the NASTRAN model developed during the configuration selection phase, prototype longeron, diagonal, truss joints, and attachment joints were designed and fabricated. The specimens were designed by Bell Helicopter and fabricated by Brunswick. All specimens were filament wound on a break-apart steel mandrel and autoclave cured in order to achieve production representative properties. All specimens were fabricated using unidirectional Thornel 300 graphite in an LRF-092 epoxy matrix. In all, four different shapes were tested to determine column buckling design allowables. Test results are shown in Table 5.

Manufacturing considerations pointed to the Tee as being the most desirable cross-section for the frame and diagonal members. Member tests showed that they were indeed stable under compressive loads but that the dimensions should be changed in order to prevent local flange separation that occurred

TABLE 5. MEMBER COLUMN BUCKLING TEST RESULTS

TEST	MEMBER SHAPE	ρ (IN.)	LENGTH (IN.)	P YIELD (LB)	P FAIL (LB)	AVG YIELD (LB)	FAILURE MODE
1	Square	.0817	16.5	1480	1530	1440	Column Buckling
2	Square	.0817	16.5	1400	1460		Column Buckling
3	Channel	.0655	16.5	540	570	580	Flange Separation
4	Channel	.0655	16.5	620	660		Longitudinal Split in Web
5	120° angle	.338	15.0	2100	2520	2250	Longitudinal Split
6	120° angle	.338	15.0	2400	2770		Longitudinal Split
7	Tee	.0926	8.0	4790	4900	4915	Flange Separation
8	Tee	.0926	8.0	5040	5150		Flange Separation

NOTE: All specimens were tested as fixed end columns

$$\rho = \sqrt{\frac{I}{A}}$$

in all of the specimens. The only shape practicable for use in the construction of the longeron members was the 120 degree angle. All of these specimens failed due to a split down the center of the angle member. This indicated that the unidirectional fiber stacking sequence was providing an insufficient amount of transverse shear strength.

After reviewing the results of the 120-degree angle column buckling tests, it was decided to include several layers of 90-degree filament-wound T300 graphite cloth in the stacking sequence. While this design change meant that the truss could no longer be completely wound by machine, it was felt that the inclusion of the 90-degree fibers would yield a significantly stronger section. Schedule and budget constraints prevented the fabrication and testing of the new longeron sections. Instead, a NASTRAN model of the longeron was constructed. Using the test data obtained with the 100 percent unidirectional fibers as a baseline, the model was fine tuned to achieve compatible results. A mesh size of 6 x 56 was chosen to represent the longeron. This mesh size represents a set of 336 NASTRAN CQUAD1 elements each .25-inch square. Element material properties were determined using Bell Helicopter composite material analysis program SC1701 (Reference 3). Program input consisted of the lamina stacking sequence and lamina mechanical properties as obtained from the material testing described earlier. As shown in Table 5, the average buckling load for the 120-degree angle test sections was 2250 pounds. The NASTRAN prediction for the failure was 2252 pounds.

Once the NASTRAN model was shown to be representative of the longeron structure, a new stacking sequence was input to program SC1701 to determine the laminate stiffness and bending matrix. These values were input to the NASTRAN model and a new buckling load was calculated for the longeron member. Several interactions were tried until a stacking sequence having the best strength-to-weight ratio was determined. The selected stacking sequence was optimized with 16 plies as (0, 0, 90, 0, 0, 0, 90, 0, 0, 0, 90, 0, 0, 0, 90, 0).

Besides the individual member tests, member joint tests were performed to verify that sufficient capability exists to transfer loads among the members. The specimens were loaded in tension as shown in Figure 20.

³ Wilson, H.E., COMPOSITE ANALYSIS PROGRAM SC1701, Bell Helicopter Textron Report 599-162-927, April 1, 1977.



Figure 20. Member Joint Testing

Machined aluminum end fittings were attached to the constraint and load application members. These fittings were attached to the joint specimen members in double shear with a high strength epoxy bond. A single bolt hole was drilled in each fitting to provide for a pinned attachment. Before failure, the member joint was able to successfully transfer 150 percent of the maximum longeron load predicted by the design configuration study NASTRAN model (see Table 6). Failure of all specimens was a result of a compression failure in diagonal member 3 (see Figure 21). No spreading or ply delamination took place at the member joint of either specimen (Reference Figure 22).

TABLE 6. MEMBER JOINT TEST LOADS

Specimen	Longeron Load At Failure	Required Transfer Load*
1	6898	3950
2	5999	

* Maximum longeron load obtained from joint out condition, design configuration study NASTRAN model.

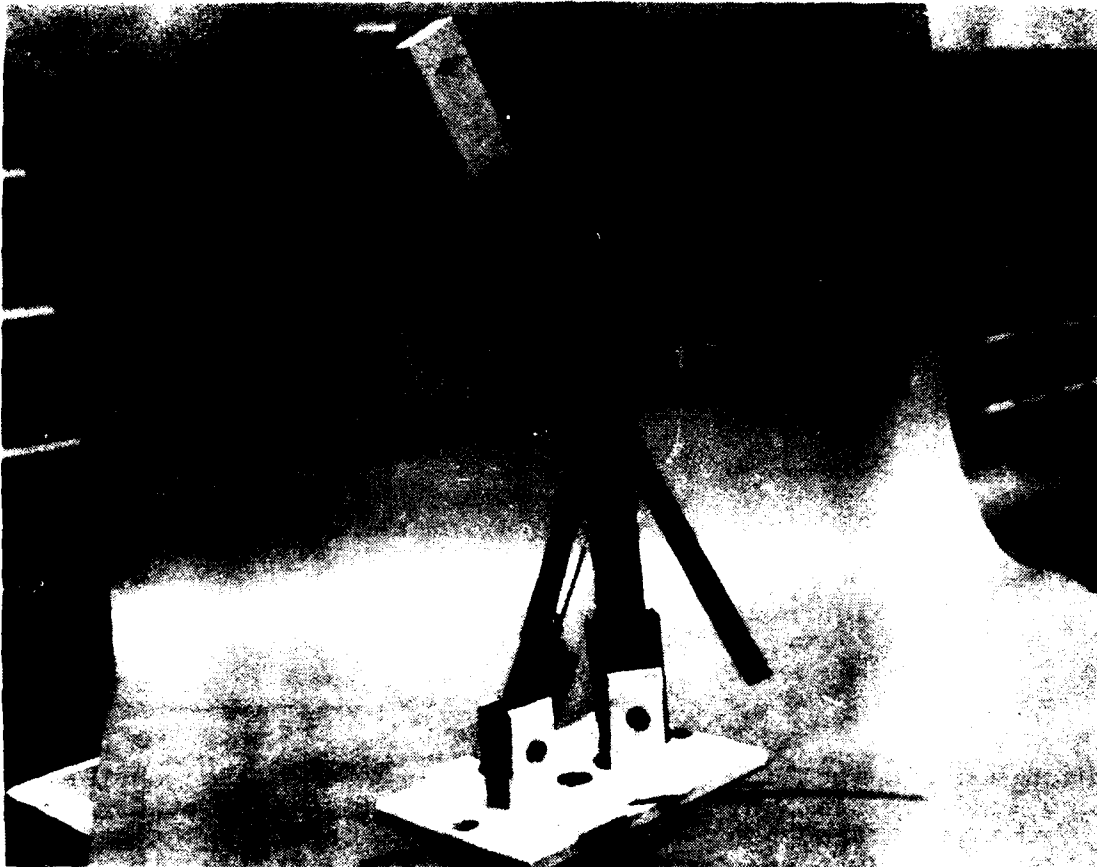


Figure 21. Member Joint After Testing

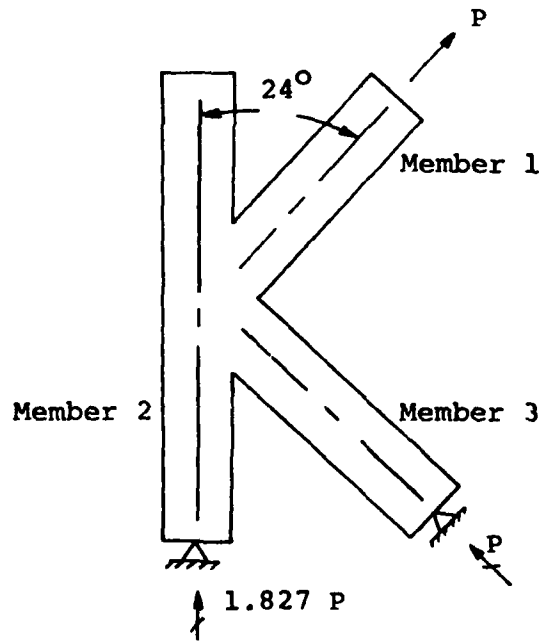


Figure 22. Member Joint Geometry

Fuselage-to-tail boom attachment joints were tested to verify fitting design and the fitting-to-longeron attachment method. The fittings detailed in Figure 23 were machined from hexagonal bar stock. They were attached to a sample longeron section with six protruding head rivets and a single layer of adhesive.

A 5/16-inch-diameter bolt was used to apply loading to the fitting. A fiberglass grip pad was built up on the other end of the longeron section. A tensile load was applied to the fitting. Test results are shown in Table 7.

Both specimens failed due to shear tearout at the bolt hole. This failure was directly related to the marginal e/D ratio provided by this design.

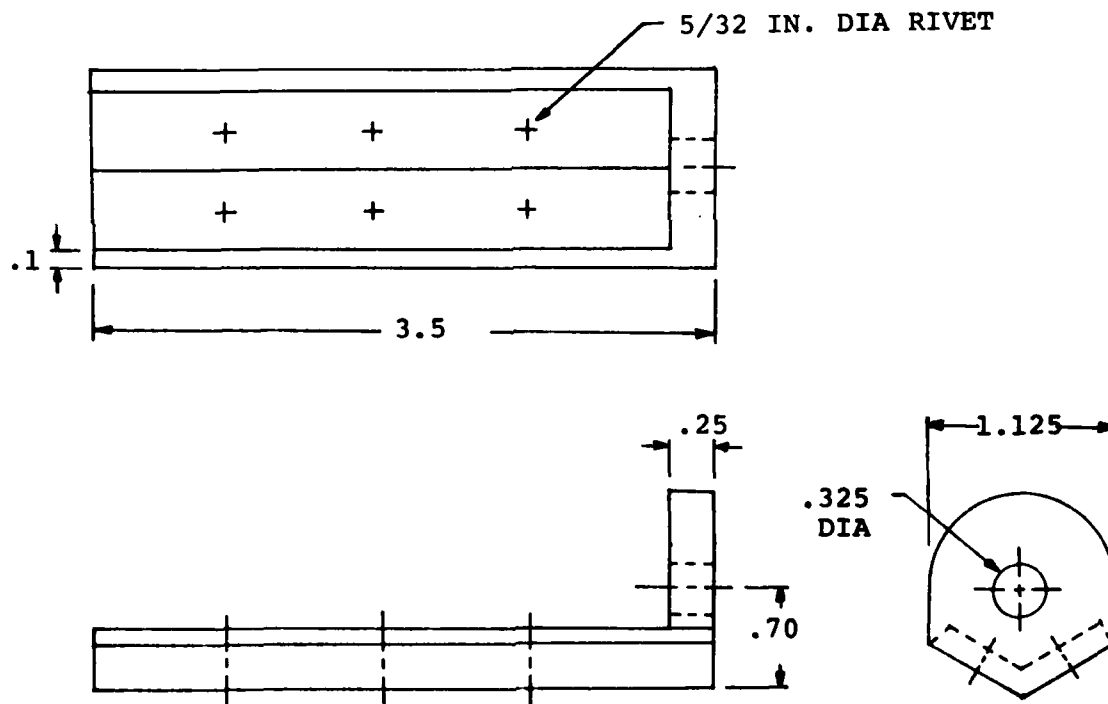


Figure 23. Machined Attachment Fitting

TABLE 7. ATTACHMENT FITTING TEST RESULTS

Test Number	Failure Load	Required Load *
1	5300	4680
2	5500	

* Maximum bolt load predicted by design configuration study NASTRAN model for a joint-out condition.

Although this fitting design and attachment procedure provided a 13-percent margin of safety, it proved to be costly both in terms of manufacturing cost and in the calendar time required for fabrication. While the use of rivets and adhesive to secure the fitting to the longeron was a working solution, it was not altogether satisfactory. The single shear bond failed at 2120 pounds for specimen 1, and 2640 pounds for specimen 2. Careful examination of the specimens after failure revealed that a slight (<.01 inch) amount of movement in the fitting relative to the longeron was noticeable. This movement was due to a bearing failure around the rivet holes in the longeron member.

Based on the results of these tests, the attachment joint fitting was redesigned and the method of attachment to the longeron was revised. Manufacturing cost and scheduling, and problems associated with obtaining hexagonal bar stock in a diameter required to produce a lug having a sufficient e/D ratio forced a complete redesign of the attachment fitting. The new design, as detailed in Figure 24, was constructed of 4130 alloy steel plate.

The angle was cold formed to fit the outside longeron contour. The face plate was cut from the same steel plate and welded to the angle. A 5/16-inch-diameter hole was drilled and tapped into the face plate. This allowed the attachment bolt to be positioned nearer the angle centroid since a nut bearing diameter and weld radius clearance did not have to be incorporated into the design.

Two additional attachment joint specimens were built and tested in order to verify the structural integrity of the welded endplate. Both specimens were loaded in excess of 200 percent of design load. No failure or material yielding was observed at this load level.

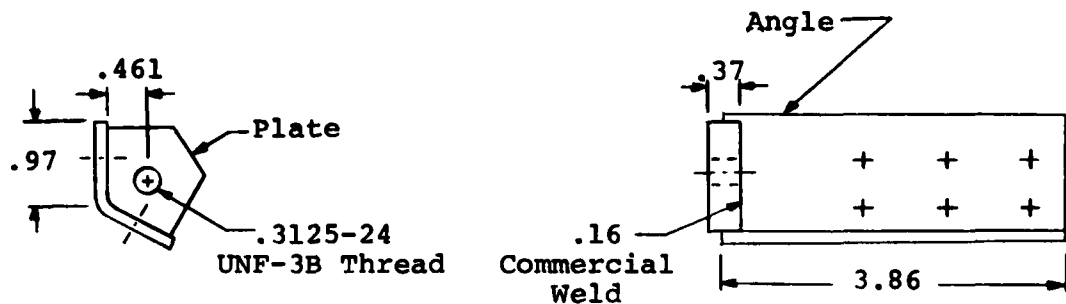


Figure 24. Welded Attachment Fitting

Two design changes were incorporated to alleviate the rivet bearing. First, the rivet diameter was increased from 5/32 inch to 3/16 inch. Second, two layers of fiberglass cloth were included in the longeron stacking sequence in the area of the attachment fittings. It was felt that the glass would provide a superior bearing surface than would the graphite by itself.

After analysis of the individual member, member joint, and attachment joint tests, design changes were incorporated into a second-generation design and an optimization analysis of the truss was begun. The design configuration study NASTRAN model was used as the starting point for the design optimization study. Being careful to stay within the design envelope of a 15-inch maximum diameter, the truss diameter, area and bending properties of the longeron, frame, and diagonal members were changed to develop the lightest structure possible while still maintaining compatibility with the existing Model OH-58 tail-boom stiffness. This optimization was done solely with a "try-and-see" approach. While this approach does not assure an optimum design, a weight savings of 2 pounds was realized when the weight of the truss boom is compared with the first 60 inches of an existing Model OH-58 boom. Additional weight savings could be realized if a tapered boom section were constructed. This approach was not considered for this program because of manufacturing considerations. Slightly more complicated tooling and winding computer programs would be required, but such a design could be readily produced in a production environment.

A weight comparison between the first 60 inches of the existing Model OH-58 boom and the three truss specimens is shown in Figure 25.

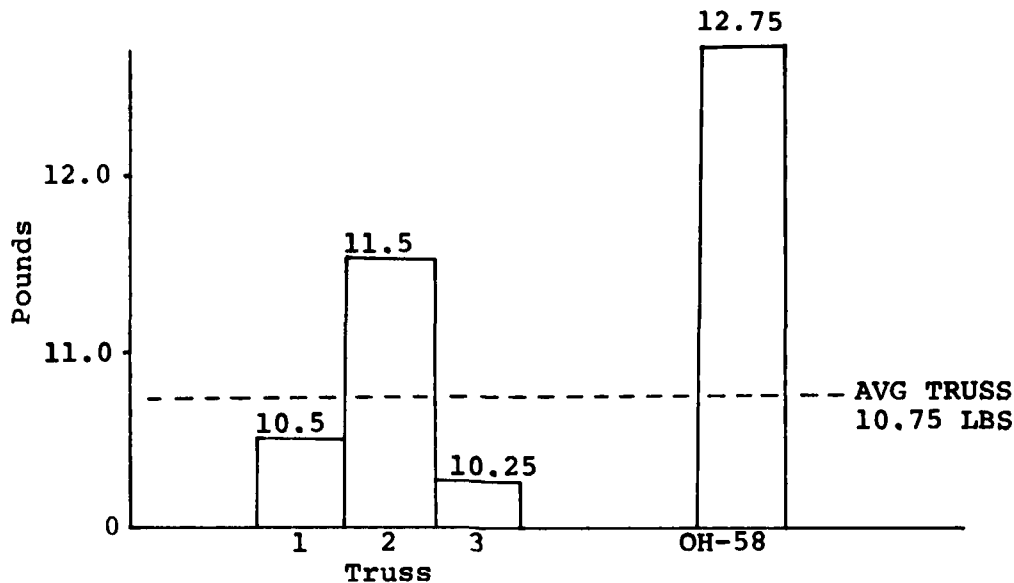


Figure 25. Truss Boom Weight Comparison (60 in. specimen)

The variation in weight between the three truss specimens was due to excess resin. The amount of fibers was constant in each specimen.

The final truss design (Figure 26) had an outside diameter of 14.50 inches and was 60.0 inches long, excluding the end fittings. Inclusion of the end fittings increased the overall length to 60.96 inches. The effective diameter as measured to the attachment bolt centroid was 13.4 inches.

The final NASTRAN model of the truss was constructed entirely of BAR elements. Complete moment continuity was assumed at each joint. Area and bending property values used in the model are shown in Table 8.

The model was fixed against translation at the forward end. Rigid ($A = 2.0$, $I = 2.0$) bars were connected to a mid-point grid established in the plane of the aft-most bulkhead. These bars were considered to be pinned at the truss frame. All loads were applied to mid-point grid and transferred to the truss structure by means of a shear distribution (Figure 27).

Output from the NASTRAN model consisted of the grid point displacement, forces and moments in each member, and $MC/I + P/A$ stresses at 4 points on each member. NASTRAN was used to compare these calculated stresses with input allowables and to compute the margin of safety for each member.

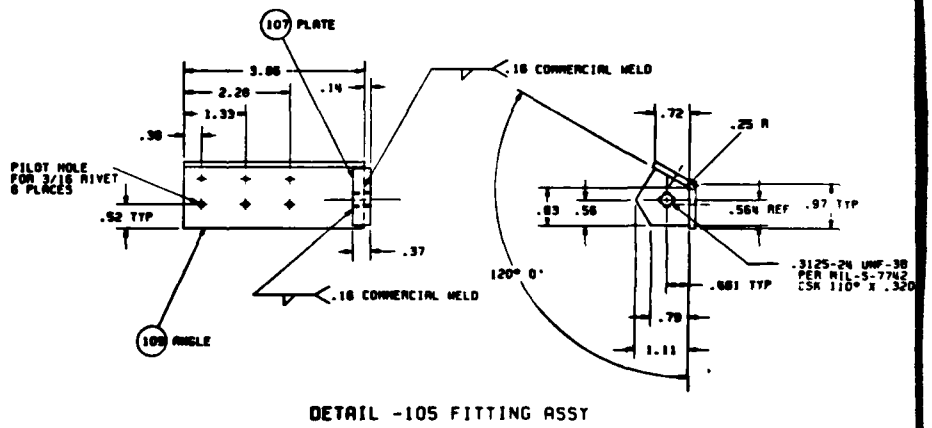
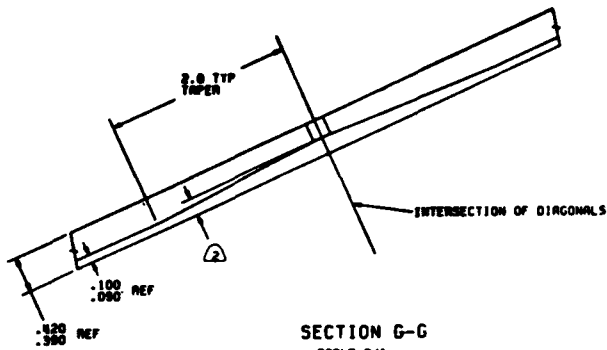
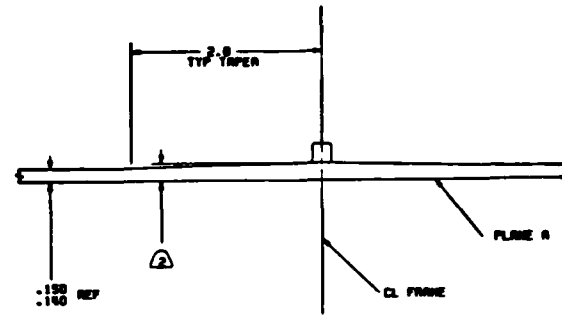


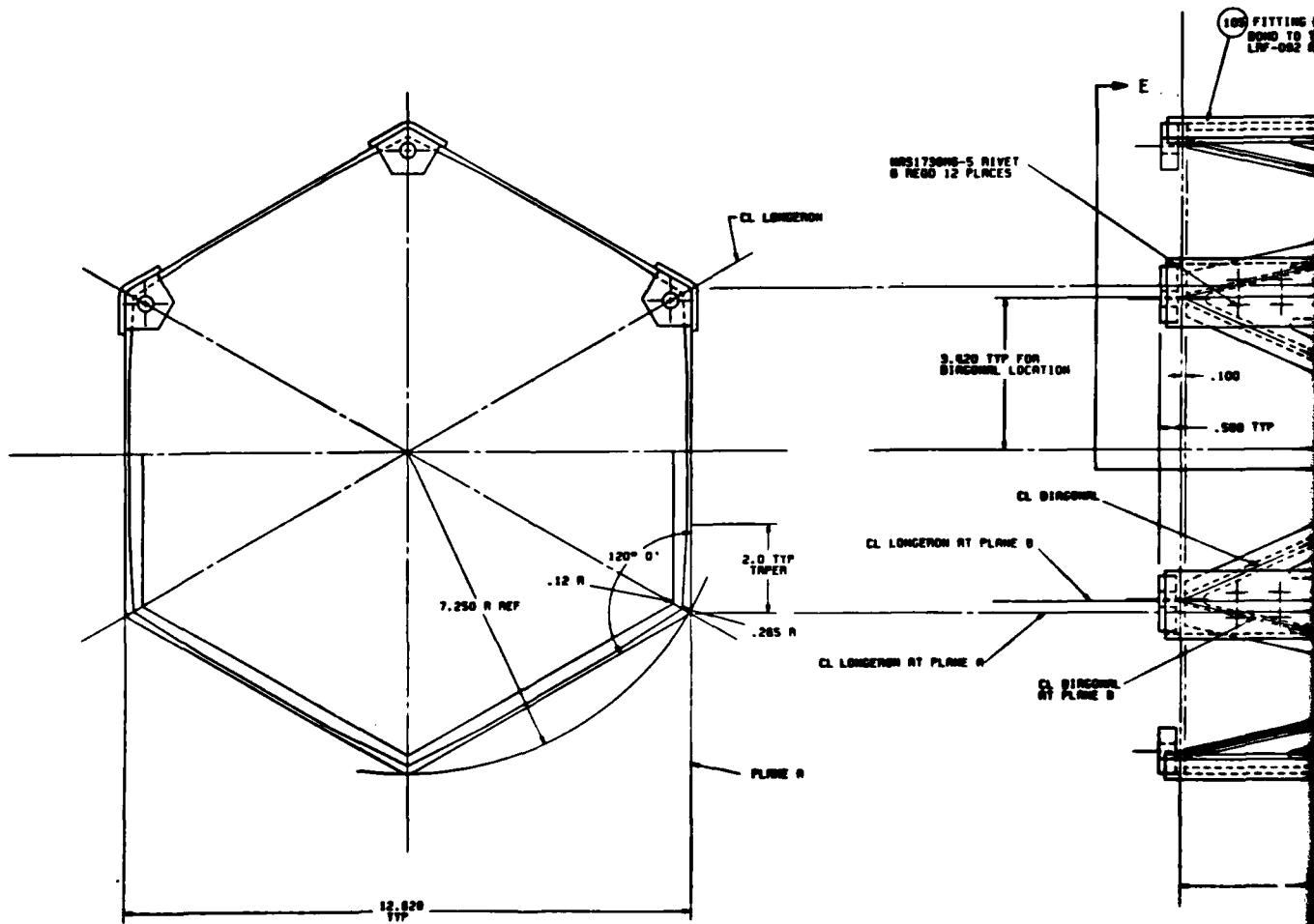
Figure 26. Final Truss Design



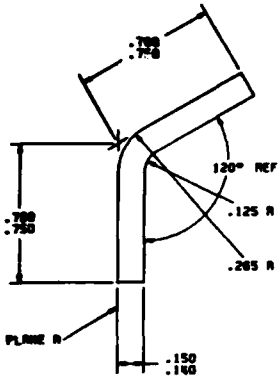
SECTION G-G
SCALE 2/1
TYP DIAGONAL TAPER



SECTION F-F
SCALE 2/1
TYP LONGERON TAPER



SECTION E-E



SECTION A-A
TYP LONGERON SECTION
SCALE 4/1

NOTES:

- ⚠ MATERIAL TO BE T300 GRAPHITE FIBERS WITH LW 082 EPOXY RESINE
- STICKING SEQUENCE:
FRAMES AND DIAGONALS (ALL 0°)
LONGERONS (0,0,90,0,0,0,90,0,0,0,90,0,0,90,0)
- ⚠ THICKNESS BUILD UP AT JOINTS AS REQUIRED
- 3 FRAMES, LONGERONS, AND DIAGONAL MEMBERS ARE TO BE WOUND ALTERNATELY TO ACHIEVE AN INTERSPERSING OF FIBERS AT JOINTS

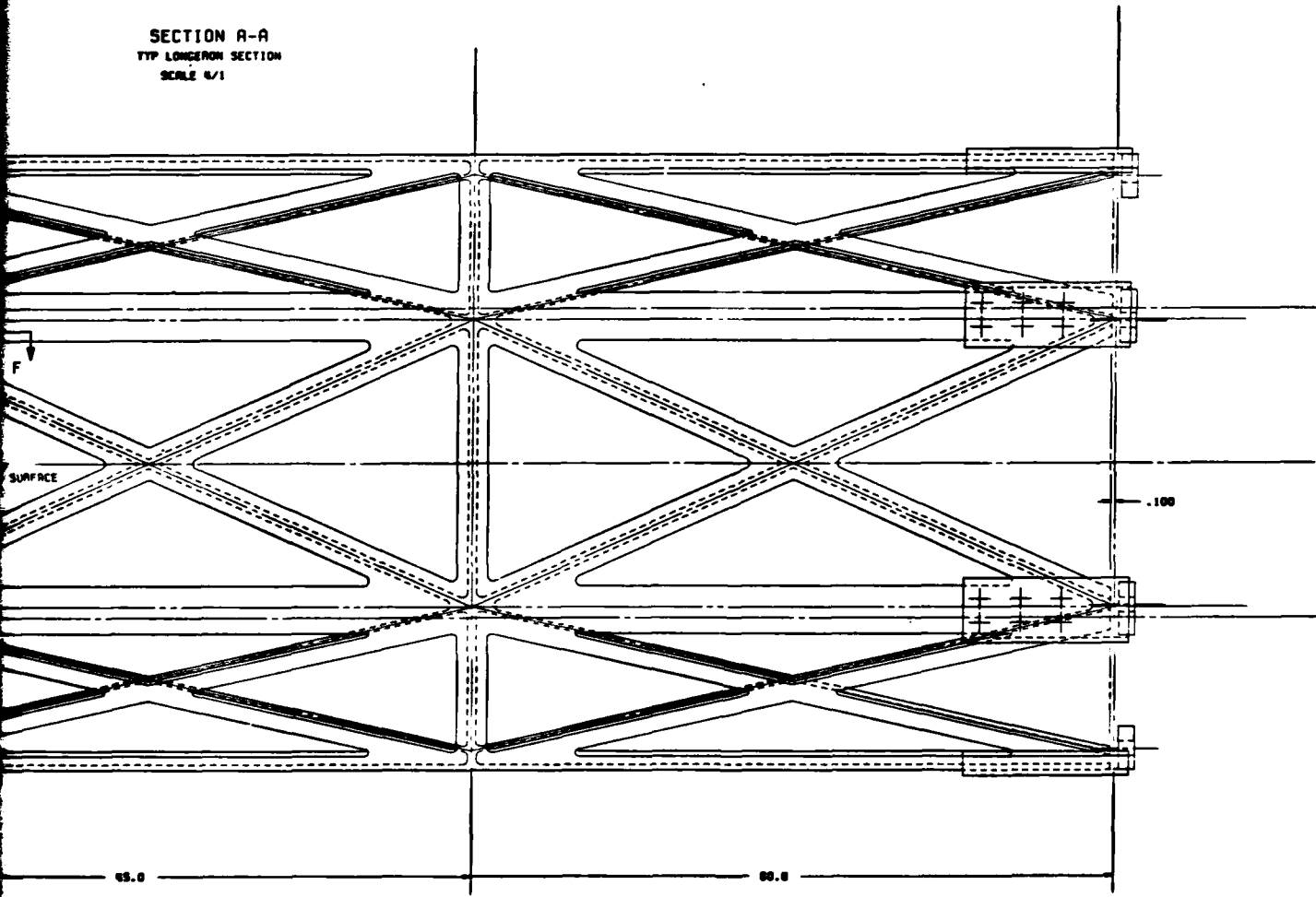
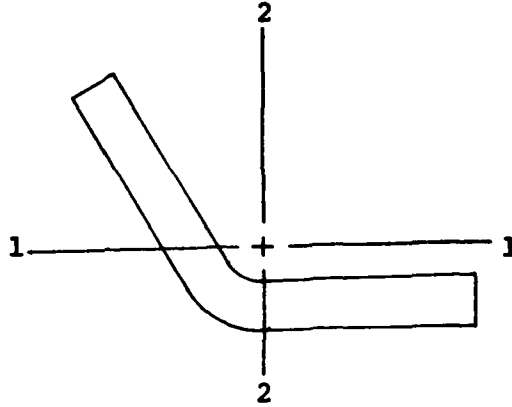
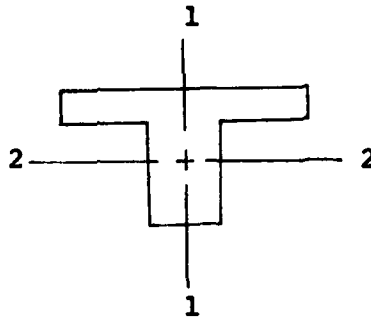


TABLE 8. FINITE ELEMENT SECTION PROPERTIES

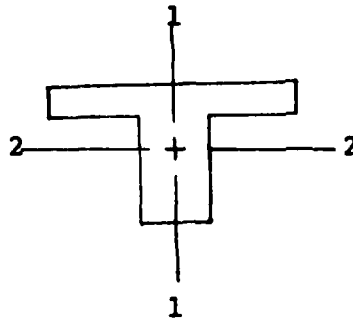
Member	Shape	Area (in. ²)	I_1 (in. ⁴)	I_2 (in. ⁴)	J_p (in. ⁴)
Longeron	Angle	.1957	.007946	.019372	.00001 (assumed)



Diagonal Tee		.1347	.001896	.00322	.00001
--------------	--	-------	---------	--------	--------



Frame Tee		.1203	.00113	.00316	.00001
-----------	--	-------	--------	--------	--------



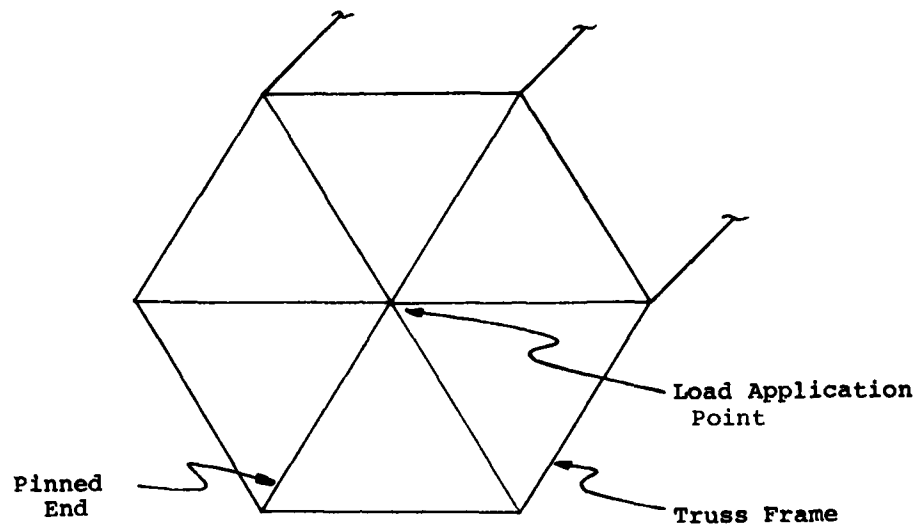


Figure 27. Pinned End Rigid Bars

The design allowables were determined from NASTRAN models of the individual frame, diagonal, and longeron members. To ensure that the models used were representative of the actual structure, the individual member test specimens were first modeled. The finite element mesh size was then adjusted until the NASTRAN-predicted buckling load was compatible with the test results. Using the same mesh philosophy, models representative of the final member designs were constructed and run to determine design allowables. The NASTRAN predicted allowables for the various members are shown in Table 9.

TABLE 9. NASTRAN-PREDICTED MEMBER BUCKLING ALLOWABLES

Member	Shape	Length (in.)	Buckling Stress (psi)
Longeron	120° Angle	15	29539
Diagonal	Tee	16.5	24591
Frame	Tee	6.75	88637

Predicted member loading and the correlation to actual static stresses are presented in the Static Load Correlation Section.

FABRICATION

Once the final truss design was developed, work was begun on the tooling required for fabrication. First, a female truss pattern was machined on six wooden segments. The hexagonal shape was attained by assembling the six segments and securing them in place with two bulkheads (Reference Figure 28). The outer shell for the sand casting was fabricated using six flat wooden pieces held in place by metal angles. The edges of these pieces were cut at an angle to form a tight hexagonal shape. A silicone rubber male pattern of the truss was cast between the wooden female pattern and the outer shell. This rubber pattern was removed from the wooden inner mandrel and attached to the outer shell (Figure 29). A metal wind axis was installed inside the mold, the interior was filled with a water soluble sand, and the assembly was oven cured. The wooden outer shell was removed after curing and the sand mandrel was exposed by peeling back the rubber pattern (Figure 30).

The sand mandrel was prepared for filament winding by taping all grooves with Teflon tape. A winding program developed by Brunswick Corporation was used to achieve an automatic winding sequence. First, the deep web grooves for the frame and diagonal members were wound. These members were wound alternately to achieve an interweaving of fibers. Once the deep web grooves were filled level to the lower surface of the sand mandrel, the longeron, frame, and diagonal flange winding was begun. As with the deep webs, the winding of the longeron, frame, and diagonal flanges was done on an alternate basis in order to achieve interwoven fibers at the member joints. All winding was accomplished with numerically controlled winding machines with the exception of the 90-degree ply fibers included in the longeron stacking sequence. These plies were laid up by hand.

Once the mandrel grooves were filled with the required number of pre-preg graphite fibers (Figure 31), the entire mandrel was wrapped in a highly absorbent cloth. The purpose of this cloth is to absorb the excess resin squeezed out of the windings during the cure cycle. Caul plates were then laid on top of the cloth, parallel to each member. These plates were secured with heat shrink tape. The entire assembly was then placed in a vacuum bag and autoclave cured.

After curing, the caul plates and cloth were removed and the sand mandrel was washed away from the truss structure. The truss was then cut to length. This step was necessary because of the fiber buildup at each end. This buildup was a result of the continuous fibers forming a closed-end loop as they reversed winding direction.

End fittings were attached with six NAS1738M6 "blind" rivets and an .01-inch layer of FM-123 adhesive oven cured at 250° F.

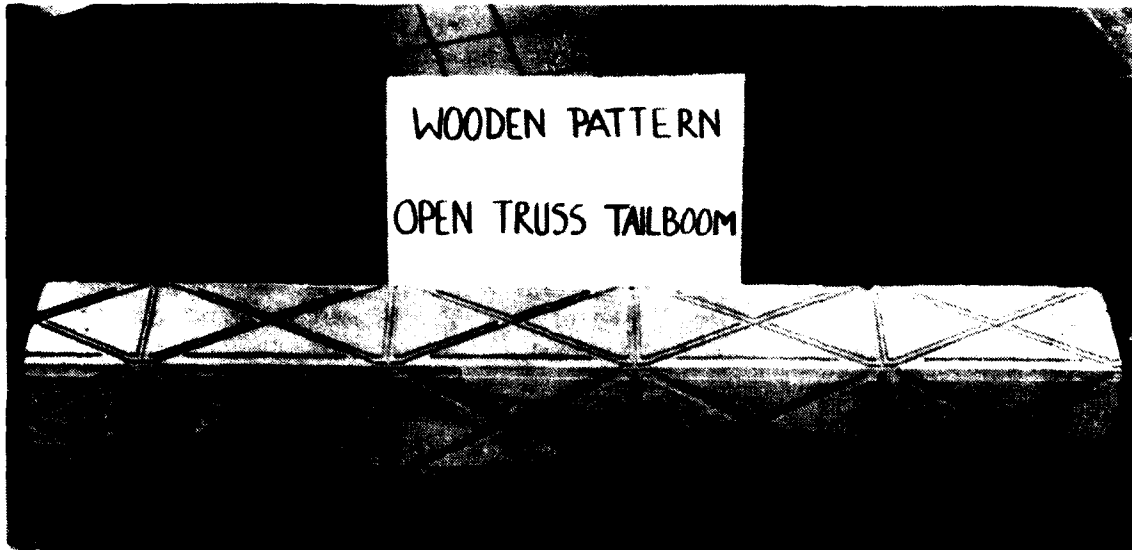


Figure 28. Wooden Tooling Pattern

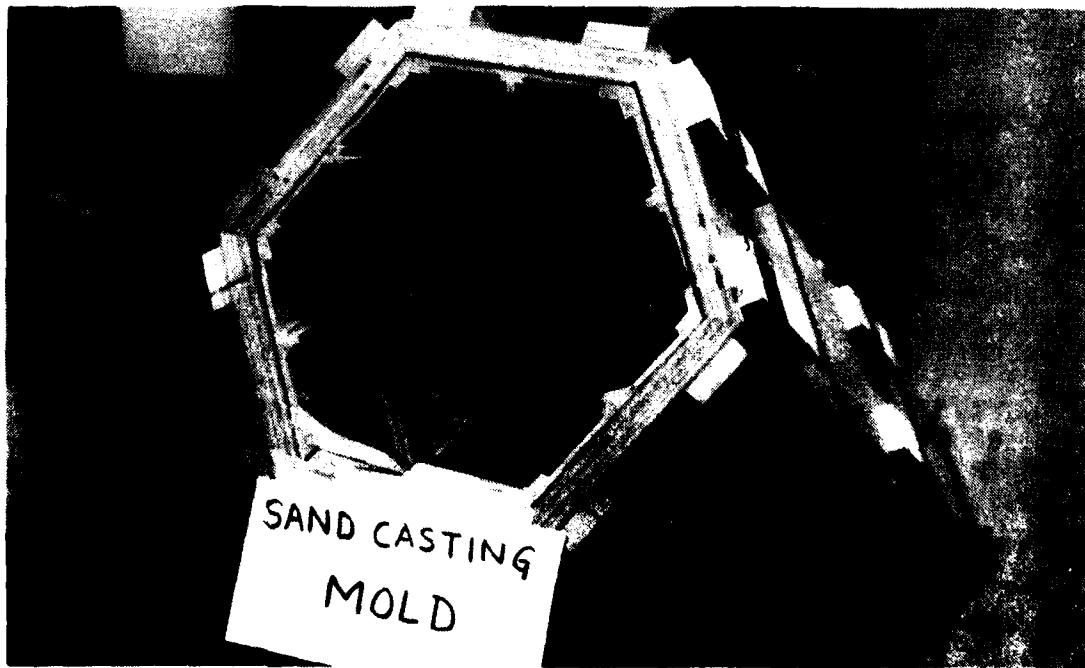


Figure 29. Sand Casting Mold



Figure 30. Sand Casting



Figure 31. Wet Lay-Up

BALLISTIC TESTING

Ballistic testing was conducted at Fort Eustis, Virginia, during the week of 19 November 1979. The ballistic testing phase consisted of single shots at three different truss specimens. All specimens were loaded prior to ballistic impact. Specimens one and two were loaded with high-speed level flight loads while specimen number three was loaded with 150 percent of high-speed level flight loads. Loads were applied to the truss specimens using lead weights and a welded steel load application frame. This loading arrangement is shown in Figures 32 and 33.

The loads listed in Table 10 were applied at the free end of the tail boom specimens.

TABLE 10. SPECIMEN APPLIED LOADS

Test Specimen 1

FX = 0	MX = 3497* in.-lb (clockwise looking fwd)
FY = 201 lb rt	MY = 3131 in.-lb (comp on lower surface)
FZ = 417.5 lb down	MZ = 14222 in.-lb (comp on RHS)

Test Specimen 2

FX = 0	MX = 2211 in.-lb (clockwise looking fwd)
FY = 201 lb rt	MY = 3131 in.-lb (comp on lower surface)
FZ = 449.5 lb down	MZ = 15312 in.-lb (comp on RHS)

Test Specimen 3

FX = 0	MX = 3300 in.-lb (clockwise looking fwd)
FY = 300 lb rt	MY = 5066 in.-lb (comp on lower surface)
FZ = 675.5 lb down	MZ = 28166 in.-lb (comp on RHS)

* Lateral load was input a wrong W.L. attachment. Correct MX loading is 2211 in.-lb.

All moments taken about the center of the aft (free) bulkhead.

LEVEL FLIGHT LOADS APPLIED AT THE CENTER OF REAR PLATE.

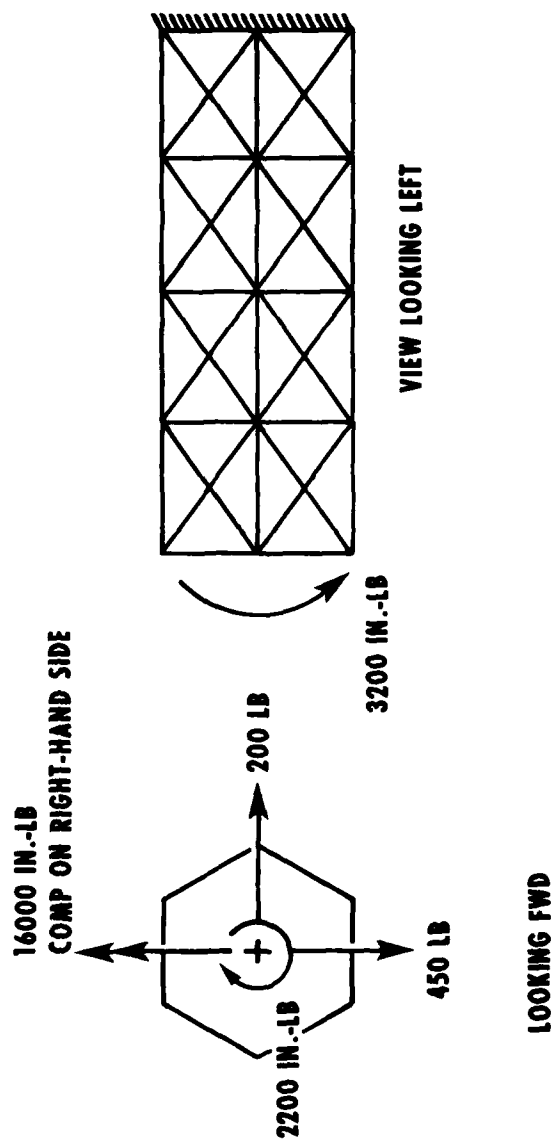


Figure 32. Truss Loading Diagram

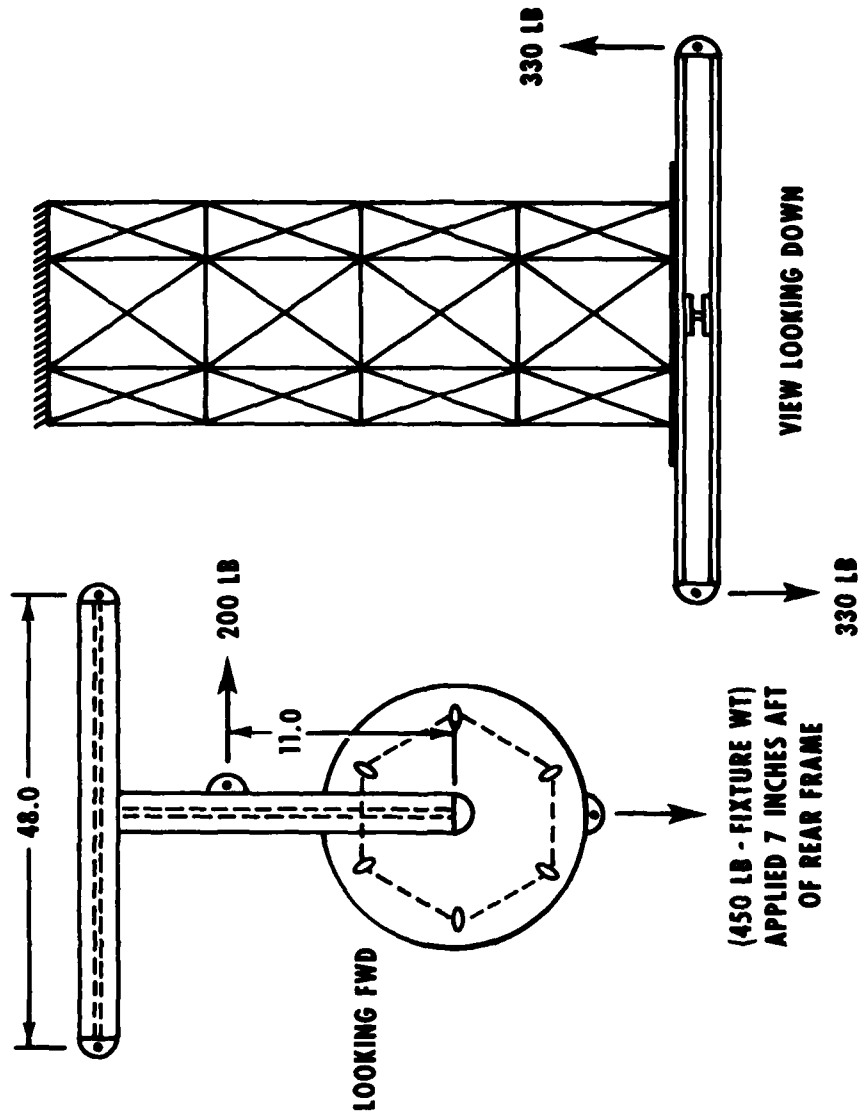


Figure 33. Load Application Frame

The test plan for specimen number 1 called for ballistic impact to be at the center of the most outboard compressive longeron in the center of the second bay, B.S. 25.00 (see Figure 34).

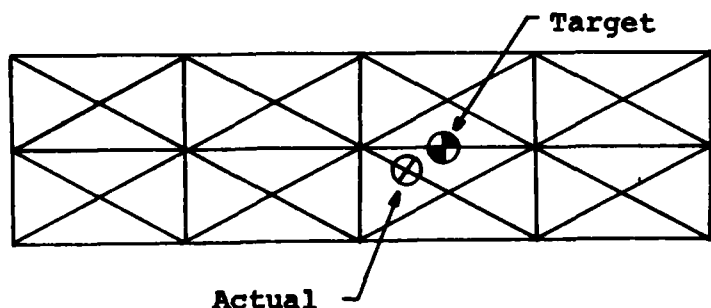


Figure 34. Targeted Impact Area, Specimen 1

The round impacted a point below and aft of the target point, with the fuse being initiated by contact with a diagonal member.

Fragments destroyed the three tension side longerons and numerous diagonal members on the upper, lower, and exit sides of the truss. Figure 35, view looking inboard at the exit side of the truss, shows the fragment damage. Figure 36 shows the approximate amount of damage done to each member. The fraction shown by each member is the percentage of area damaged by the shell fragments.

The specimen continued to hold level flight loads for 30 minutes after impact.

Vertical deflections were taken immediately before and after ballistic impact, and in three 10-minute intervals after impact. These deflection measurements are shown in Figure 37. All measurements were taken from a point on the bottom of the load application frame to a fixed point on the ground directly underneath the measurement point.

The change in angle before and after impact can be calculated as

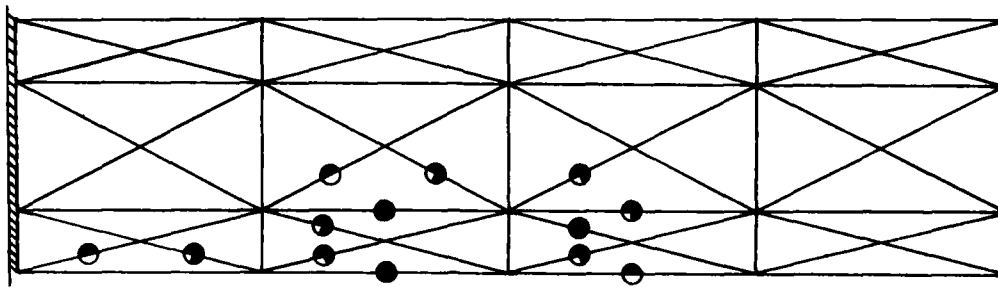
$$[\tan^{-1} (.375)/B.S. 60.00 - B.S. 25.00)] = .61 \text{ degree}$$

Even when the additional 1/8-inch creep deflection is included, the angle $[\tan^{-1} .5/35]$ of .82 degree is within the tail rotor driveshaft misalignment angle allowable of 1.5 degrees.

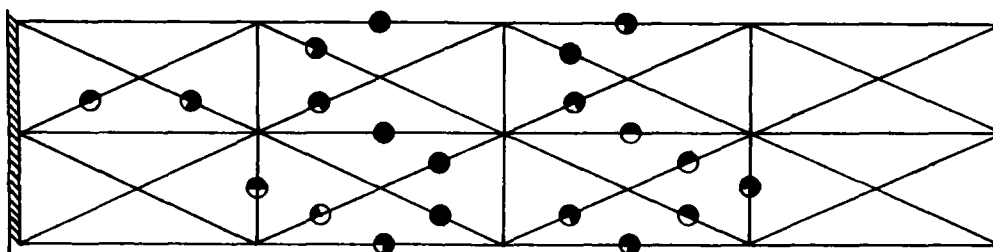


Figure 35. Exit Side Damage, Specimen 1

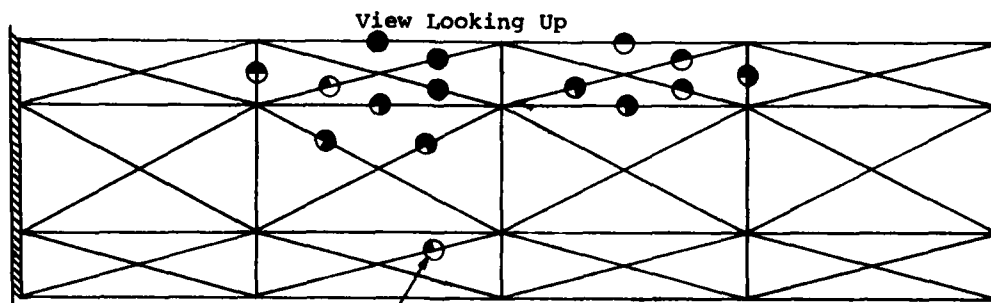
● Darkened area represents amount of damaged material



View Looking Down



View Looking Right



Impact Point

Figure 36. Individual Member Damage, Specimen

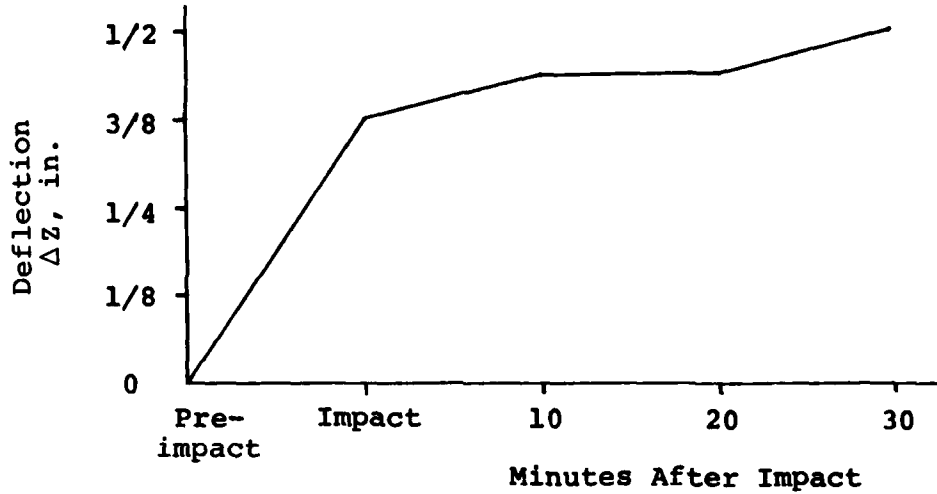


Figure 37. Boom Deflection After Impact

The test plan for specimen number 2 called for the ballistic impact to be at the most outboard compression longeron/frame joint at B.S. 30.00.

The round impacted a point on the outermost compression longeron slightly aft of the targeted joint (Figure 38).

Fragments did not completely sever any of the longeron members but did completely destroy several diagonal and frame members (Figures 39 and 40). The back (exit) side of Figure 39 is shown in Figure 41. Figure 42 shows the approximate amount of damage done to each member. The fraction shown for each damaged member is the percentage of area damaged by shell fragments.

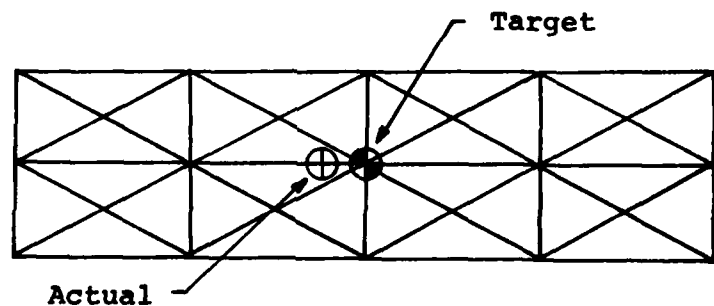


Figure 38. Targeted Impact Area, Specimen 2



Figure 39. Projectile Entry Hole, Specimen 2

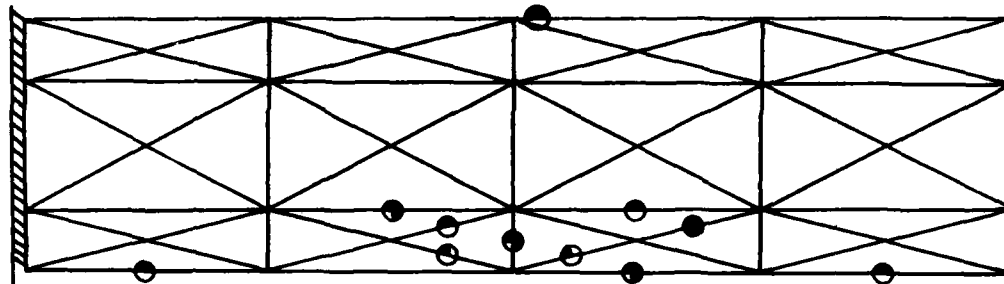


Figure 40. Exit Side Fragment Damage, Specimen 2

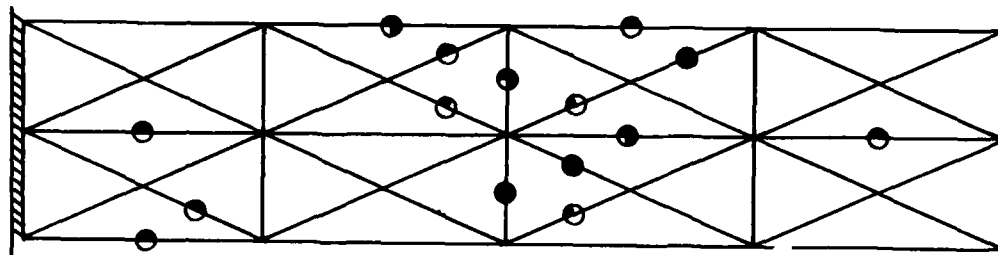


Figure 41. Exit Side of Entry Hole, Specimen 2

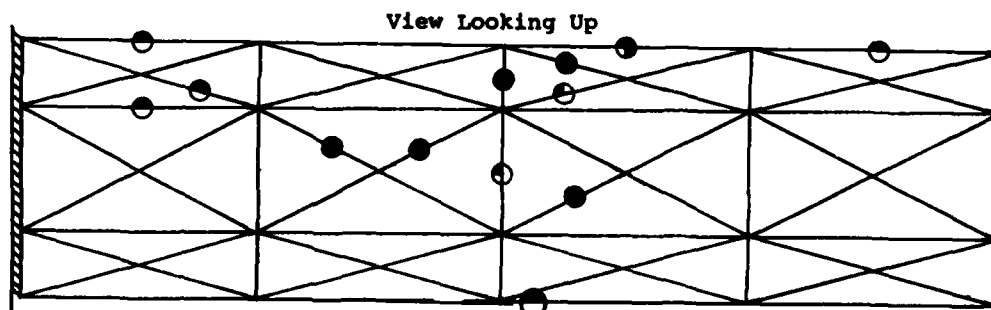
● Colored portion represents percent of damaged fibers



View Looking Down



View Looking Right



View Looking Up

Impact Point

Figure 42. Individual Member Damage, Specimen 2

The specimen continued to carry level flight loads for 30 minutes after impact.

Vertical and horizontal deflections were taken immediately before and after ballistic impact, and in three 10-minute intervals after impact. These deflection measurements are shown in Figure 43. Vertical deflection measurements were taken from a point on the bottom of the load application frame to a fixed point on the ground directly underneath the measurement point. Horizontal displacements were taken from the vertical movement of the horizontal load application tray.

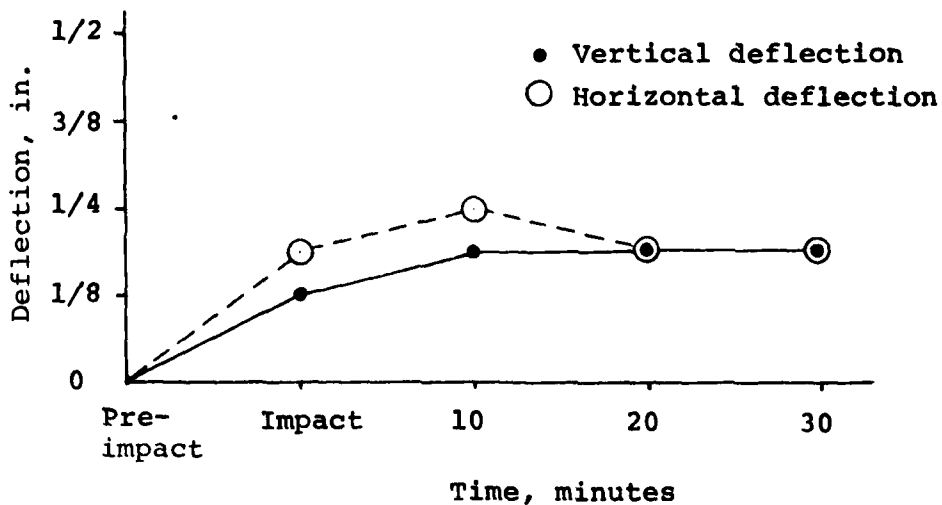
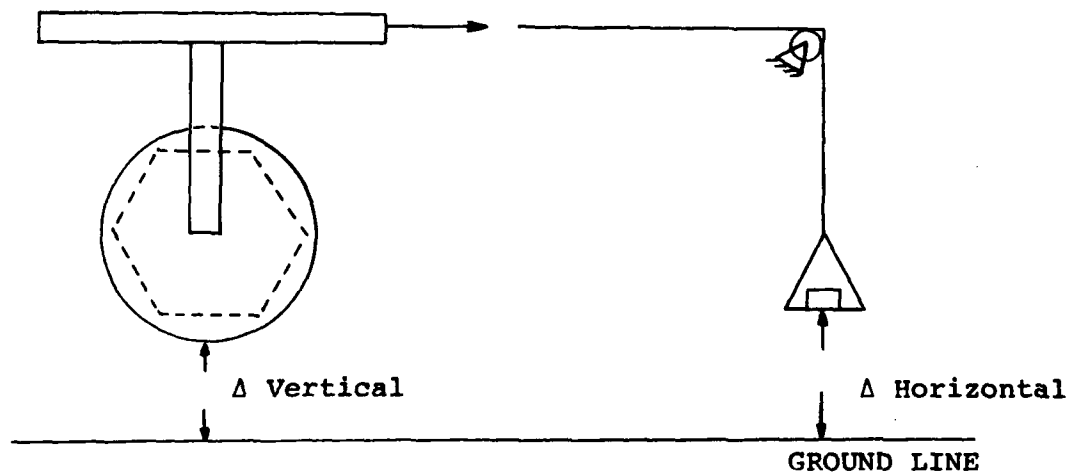


Figure 43. Boom Deflection After Impact, Specimen 2

Using a combination of vertical and horizontal deflections to calculate the change in angle after impact, the misalignment angle can be calculated as

$$[\tan^{-1} ((.125^2 + .1875^2)^{1/2}) / (B.S. 60.-0 - B.S. 30.00)]$$

$$= .43 \text{ degree}$$

This value is well within the allowable tail rotor driveshaft misalignment angle.

The test plan for specimen number 3 called for the ballistic impact to be at the most outboard compression longeron/ frame joint at B.S. 30.0 (Figure 44).

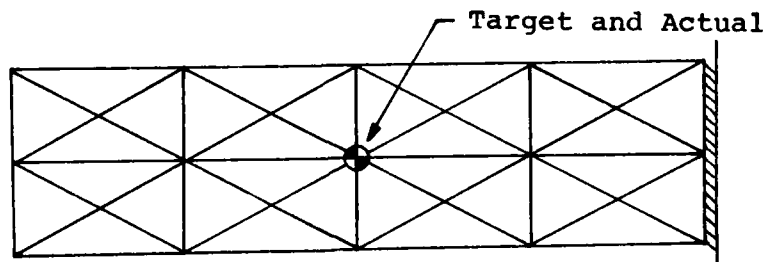


Figure 44. Targeted Impact Area, Specimen 3

The round impacted the target area, completely destroying continuity between the frame, diagonal, and longeron members. The base fragment destroyed the majority of the outboard tension longeron/frame joint (Figure 45). Other longeron and diagonal members were blown away, indicating that multiple fragment hits may have detached some members from the structure. The most outboard tension longeron between B.S. 30.0 and B.S. 45.0 and part of the exit side frame at B.S. 30.0 appears to have been severed at both ends. These members were among those found several feet away from the test specimen. Both the upper and lower tension longerons were subjected to fragment damage. Figure 46 shows the upper tension longeron. The upper half appears to have been cut with a fragment, leaving the lower leg to fail under a tensile load.

Only the upper and lower compression longerons survived and retained the majority of their structural integrity after impact. These members could not support the applied loads and the truss collapsed immediately after impact.

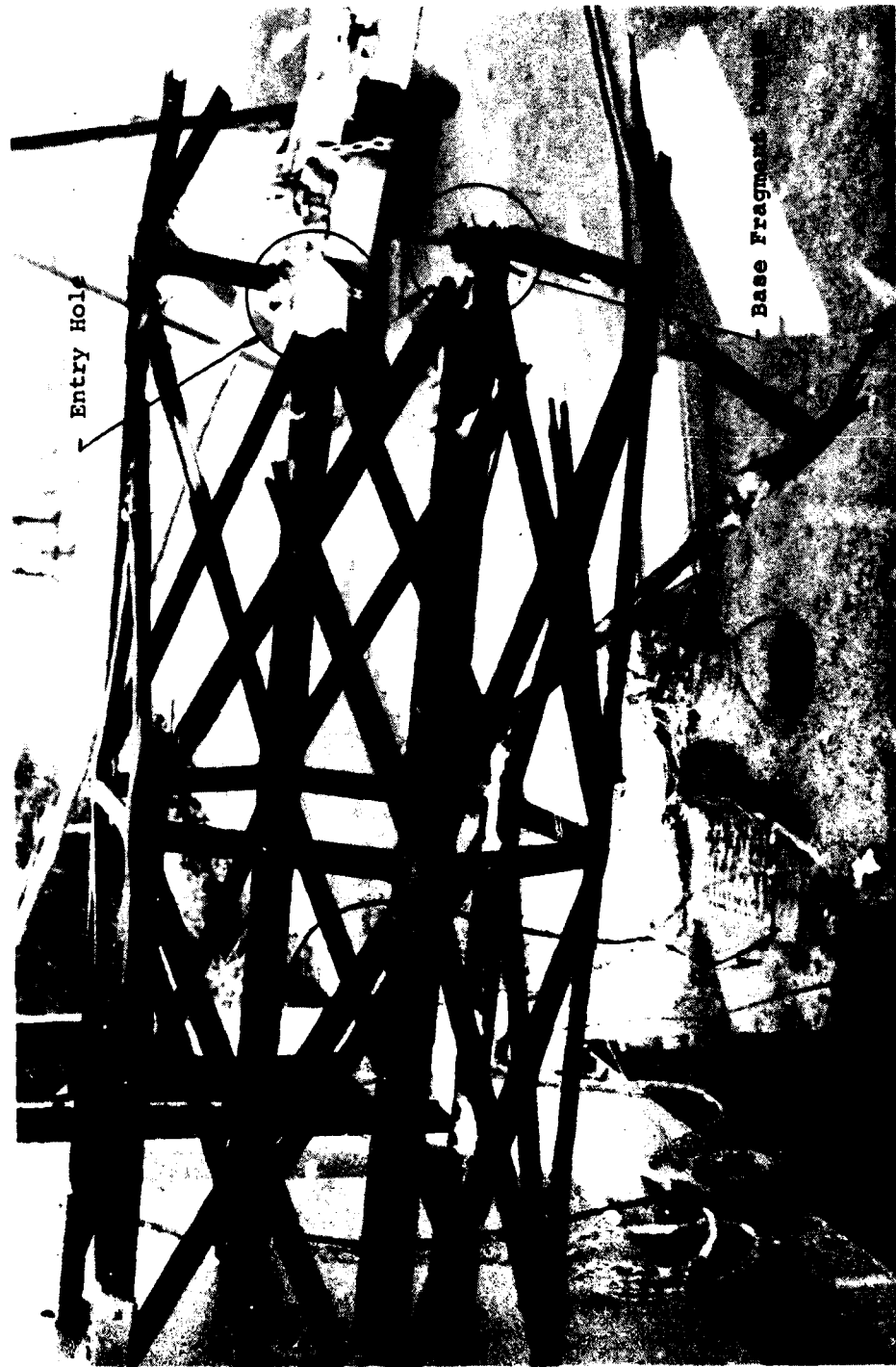


Figure 45. Fragment Damage, Specimen 3



Figure 46. Upper Tension Longeron, Specimen 3

In general, the fragments passed through the composite members cleanly. Very little delamination was seen in the area surrounding a fragment hit. When delamination did occur, only a few plies on the exit side of the hole were affected. Cracks did not develop in the areas around the fragment puncture holes. An example of fragment damage is shown in Figure 47.

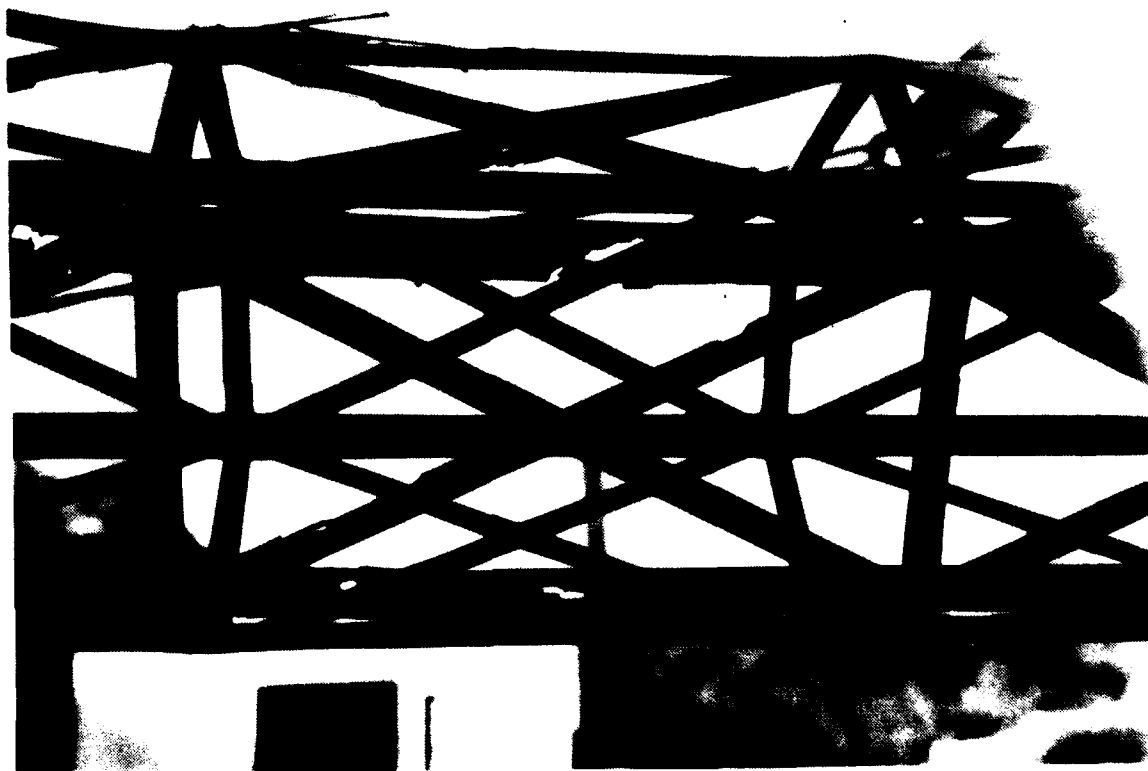


Figure 47. Typical Fragment Damage

STATIC LOAD CORRELATION

Each of the three specimens was instrumented with 12 strain gages. Readings were taken before and after ballistic impact. Tables 11, 13 and 14 show the correlation of NASTRAN-predicted strain with the measured values before impact.

TABLE 11. CORRELATION OF MEMBER LOADS
BEFORE BALLISTIC IMPACT
TEST 1

Gage No.	Member* ID	Measured** Strain ϵ in./in.	Predicted Strain ϵ in./in.	% Diff.
2	1	108	119	10
3	1	-167	-154	8
4	2	72	65	10
7	3	-196	-199	2
8	3	-409	-262	36
9	3	-132	-149	13
10	4	170	192	13
11	4	142	190	34
12	4	217	205	6

Note: Pre-impact data not available for gages 1, 5 and 6.

* Reference Figure 48

** Reference Appendix A, pages 86 through 95.

Predicted strains at the gage locations were obtained by reducing the NASTRAN force and moment output data for the members of interest.

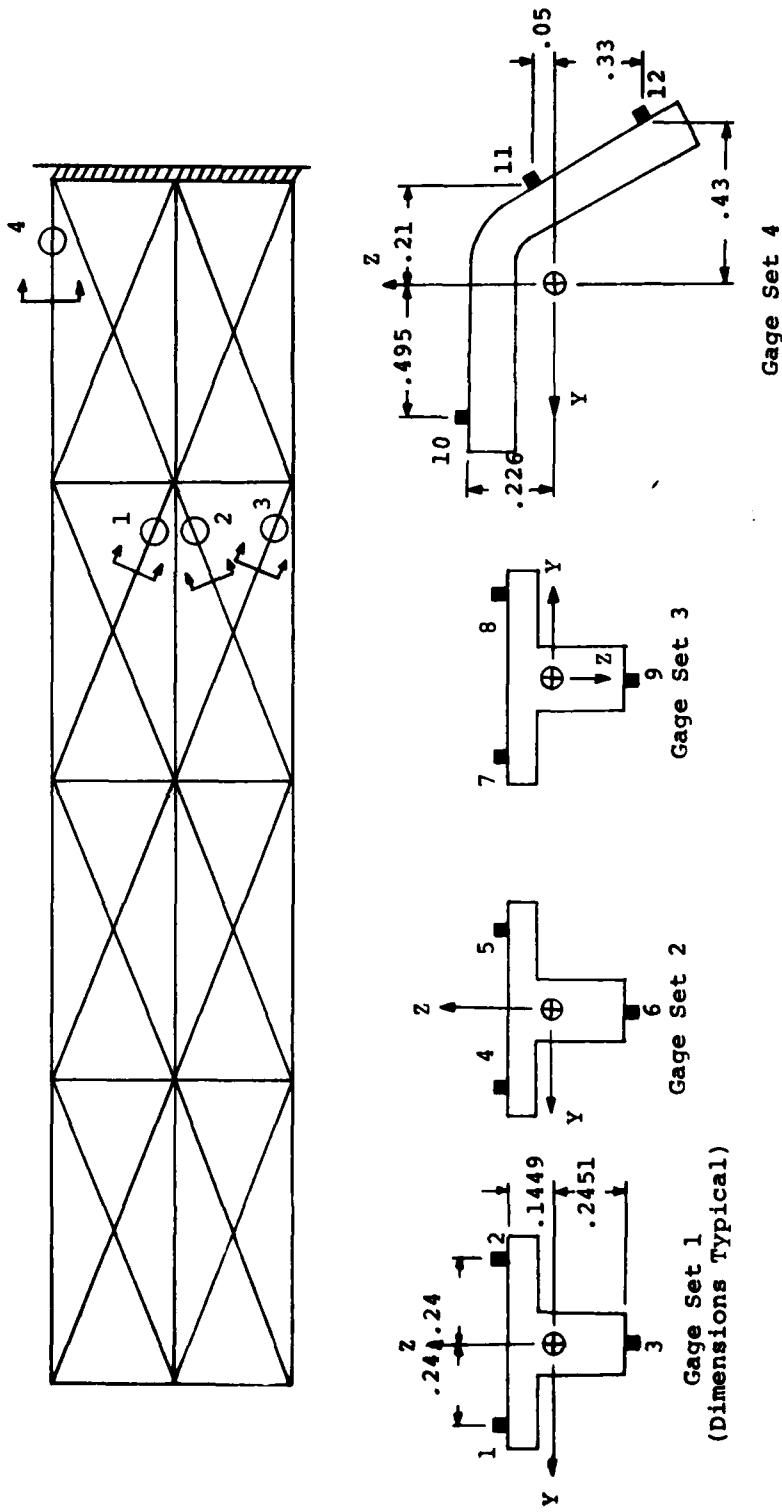


Figure 48. Strain Gage Locations, Specimen 1

TABLE 12. NASTRAN MEMBER FORCES AND MOMENTS

MEMBER	M_y (in.-lb)		M_z (in.-lb)		P_x (lb)
	END 'A'	END 'B'	END 'A'	END 'B'	
TEST 1					
1	-4.97	-.7	1.84	-5.23	-322
2	.38	-.2	2.73	-.21	183
3	-9.39	-4.31	6.25	8.24	-500
4	10.54	.95	-7.36	-1.88	723
TEST 2					
3	7.62	2.7	2.51	-8.22	-1140
4	-2.63	.58	17.04	8.54	957
TEST 3					
1	4.21	2.69	6.54	10.88	-549
2	-5.26	-1.43	-7.79	-9.72	-706
3	.4	.1	8.01	11.3	-254
4	6.68	4.83	13.68	7.98	664

Using the forces and moments from the NASTRAN run shown in Table 12, the strain at the gage locations were calculated as follows:

Forces and moments are output from NASTRAN at the member end points. The gages were located approximately three inches from the 'A' end of the NASTRAN element. A straight line moment distribution was used to calculate the stress at the gage location. Axial force is considered to be constant throughout the length of the member (Figure 49).

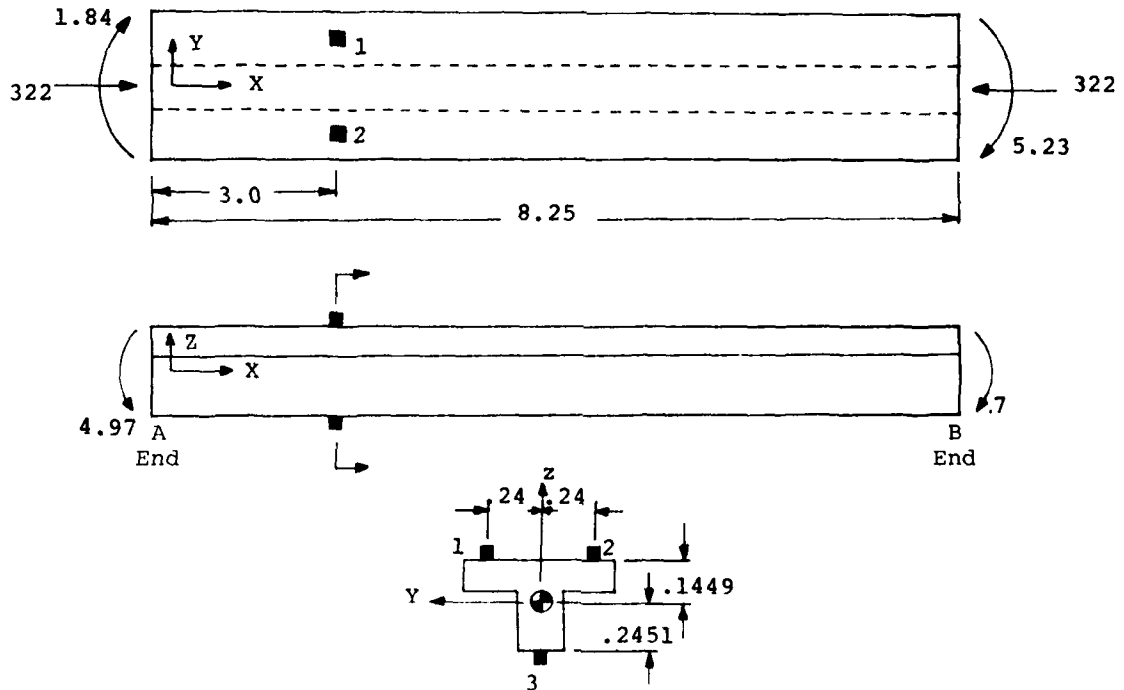


Figure 49. NASTRAN LOADS, Member 1, Specimen 1

Looking at gage 2 (located on the outboard flange) the stress due to bending at the 'A' end is $f_b = \frac{M_C}{I_2} + \frac{M_C}{I_1}$

$$f_b = \frac{1.84(.24)}{.00322} + \frac{4.97(.1449)}{.001896} = 516 \text{ psi}$$

At end 'B'

$$f_b = \frac{5.23(.24)}{.00322} + \frac{.7(.1449)}{.001896} = - 336 \text{ psi}$$

Using a straight line moment distribution between points 'A' and 'B', the bending stress at a point 3 inches from end 'A' is

$$516 - \frac{3}{8.25}(516 - (-336)) = 206 \text{ psi}$$

The stress at gage 2 is

$$\frac{P}{A} + f_b = \frac{322}{.1347} + 206 = -2184 \text{ psi}$$

Looking at gage 3 (located on the centerline of the lower web, the stress due to bending at the 'A' end is

$$f_b = \frac{-4.97(.2451)}{.001896} = -642 \text{ psi}$$

at end 'B'

$$f_b = \frac{-.7(.2451)}{.001896} = -90 \text{ psi}$$

The bending stress at gage 3 is

$$-642 + \frac{3}{8.25}(-642 - (-90)) = -441 \text{ psi}$$

The stress at gage 3 is

$$\frac{P}{A} + f_b = \frac{-322}{.1347} - 441 = -2831 \text{ psi}$$

Using a material E_c of 18.37 (Table 2), the NASTRAN predicted strain for gage number 2 is

$$-2184/18.37 = -119 \text{ } \mu\text{in./in.}$$

The predicted strain for gage number 3 is

$$-2831/18.37 = -154 \text{ } \mu\text{in./in.}$$

Strains for the remaining diagonal members were calculated in a similar manner.

Predicted strain values for the longeron members were obtained as follows (Figure 50):

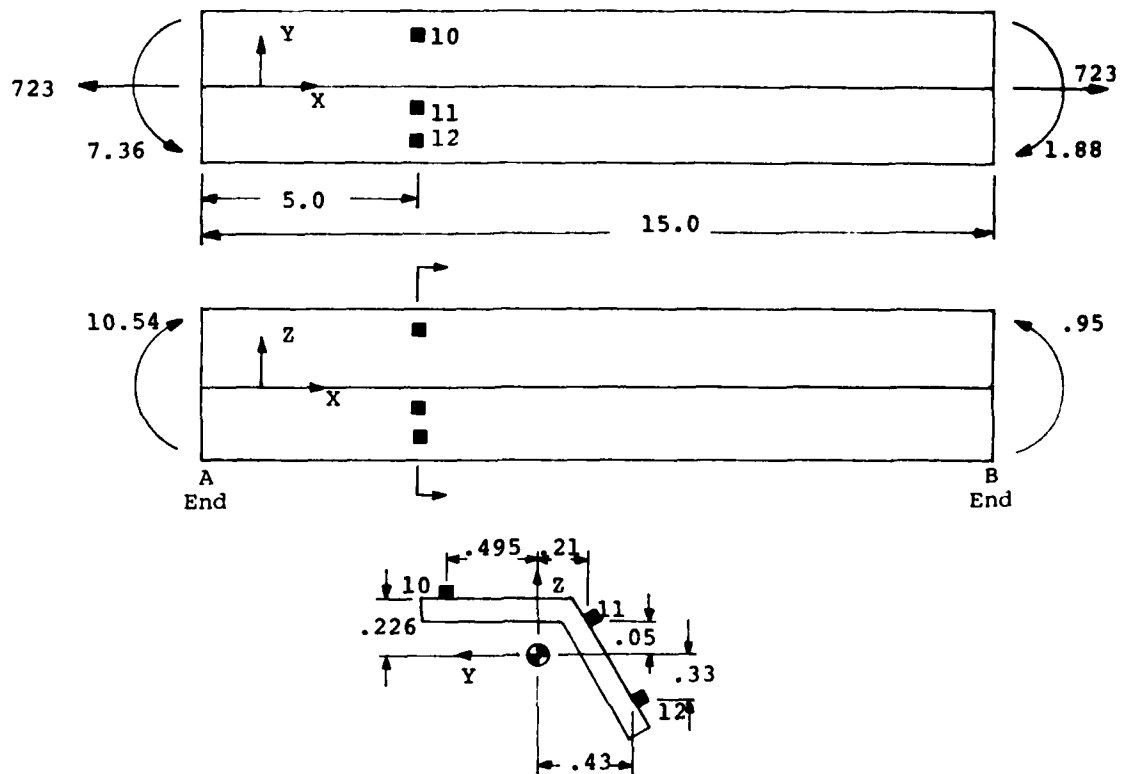


Figure 50. NASTRAN LOADS, Member 4, Specimen 1

At gage 10 (level leg, inboard), the bending stress at the 'A' end is

$$f_b = \frac{7.36(.495)}{.019372} - \frac{10.54(.226)}{.007946} = - 111 \text{ psi}$$

At end 'B'

$$f_b = \frac{1.88(.495)}{.019372} - \frac{.95(.226)}{.007946} = 21 \text{ psi}$$

Using a straight line moment distribution between points 'A' and 'B', the bending stress 5 inches away from point 'A' is

$$-111 + \frac{5}{15} (21 - (-111)) = -67 \text{ psi}$$

The stress at gage 10 is

$$\frac{P}{A} + f_b = \frac{723}{.1957} - 67 = 3627 \text{ psi}$$

At gage 11 (inboard gage on outboard leg), the bending stress at the 'A' end is

$$f_b = \frac{-7.36(.21)}{.019372} - \frac{10.54(.05)}{.007946} = -146 \text{ psi}$$

At end 'B'

$$f_b = \frac{-1.88(.21)}{.019372} - \frac{.95(.05)}{.007946} = -26 \text{ psi}$$

Using a straight line moment distribution between points 'A' and 'B', the bending stress 5 inches away from point 'A' is

$$-146 + \frac{5}{15} (-26 - (-146)) = -106 \text{ psi}$$

The stress at gage 11

$$\frac{P}{A} + f_b = \frac{723}{.1957} - 106 = 3588 \text{ psi}$$

At gage 12 (outboard gage on outboard leg), the bending stress at the 'A' end is

$$f_b = \frac{-7.36(.43)}{.019372} + \frac{10.54(.33)}{.007946} = 274 \text{ psi}$$

At end 'B'

$$f_b = \frac{-1.88(.43)}{.019372} + \frac{.95(.33)}{.007946} = -2 \text{ psi}$$

At a point 5 inches away from point 'A'

$$f_b = 274 - \frac{5}{15}(274 - (-2)) = 182 \text{ psi}$$

The stress at gage 12 is

$$\frac{P}{A} + f_b = \frac{723}{.1957} + 182 = 3876 \text{ psi}$$

Using a material E_t of 18.88 (Ref. Table 2) the NASTRAN-predicted strain for gage 10 is

$$3627/18.88 = 192 \text{ } \mu\text{in./in.}$$

For gage 11

$$3588/18.88 = 190 \text{ } \mu\text{in./in.}$$

For gage 12

$$3987/18.88 = 205 \text{ } \mu\text{in./in.}$$

Strains measured in various members during tests 2 and 3 are presented in Tables 13 and 14 respectively. The NASTRAN-predicted strains for these elements were calculated in the same manner as shown on the preceding pages.

TABLE 13. CORRELATION OF MEMBER LOADS BEFORE BALLISTIC IMPACT TEST 2

Gage No.	Member* ID	Measured** Strain ϵ in./in.	Predicted Strain ϵ in./in.	% Diff.
7	3	-519	-303	42
8	3	-316	-316	0
9	3	-449	-307	31
10	4	242	211	13
11	4	273	253	7
12	4	285	301	6

NOTE: Pre-impact data not available for gages 1-6.

* Reference Figure 51.

** Reference Appendix A, pages 96 through 105.

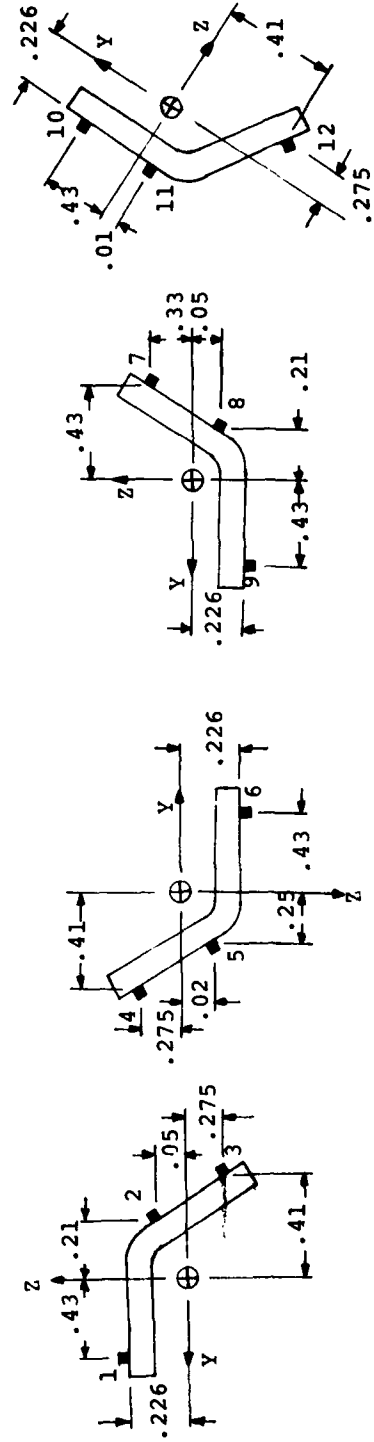
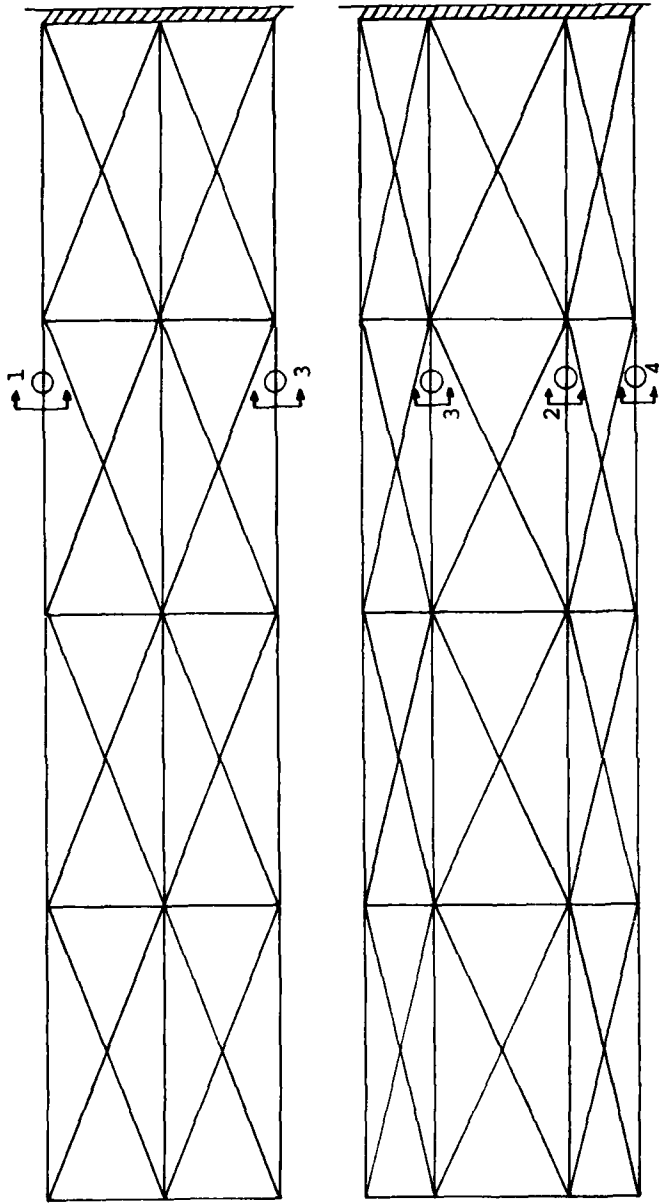
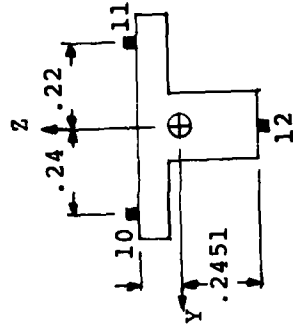
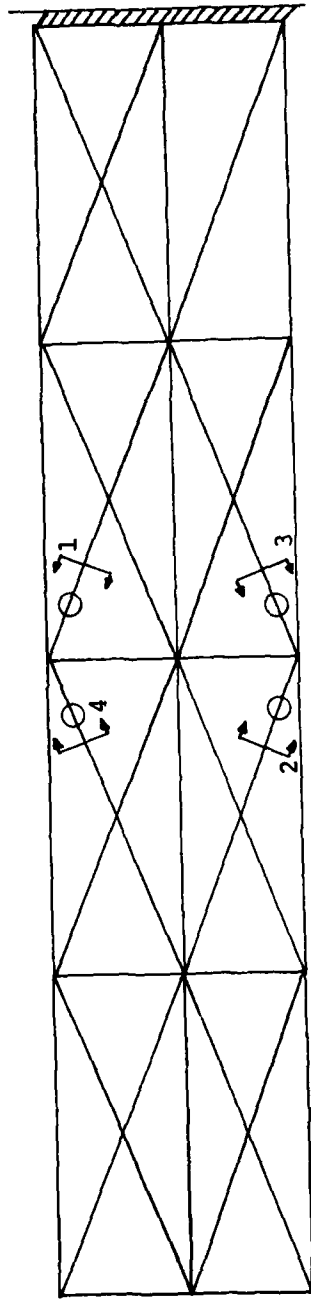
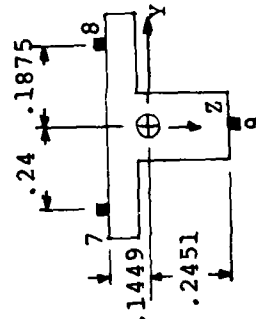


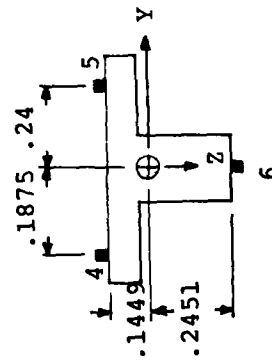
Figure 51. Strain Gage Locations, Specimen 2



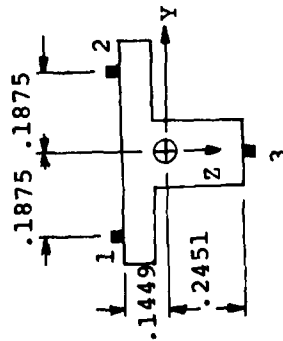
Gage Set 4



Gage Set 3



Gage Set 2



Gage Set 1

Figure 52. Strain Gage Locations, Specimen 3

TABLE 14. CORRELATION OF MEMBER LOADS BEFORE BALLISTIC IMPACT
TEST 3

Gage No.	Member* ID	Measured** Strain ϵ in./in.	Predicted Strain ϵ in./in.	% Diff.
1	1	-225	-174	23
2	1	-307	-240	21
3	1	-319	-248	22
4	2	-422	-337	20
5	2	-277	-267	4
6	2	-198	-259	31
7	3	-199	-141	29
8	3	-72	-67	7
10	4	138	191	38
11	4	242	282	16
12	4	380	302	20

NOTE: Pre-impact data not available for gage 9

* Reference Figure 52.

** Reference Appendix A, pages 106 through 115.

The reason for the lack of better correlation was the large tolerances allowed for manufacturing. Tolerances of .01 inch were allowed for thickness dimensions while a .03-inch window was allowed for all length dimensions. A 15-percent increase in area can be obtained using the maximum dimensions rather than the minimum dimensions for a diagonal member. Minimum section properties were used for all members in the NASTRAN loads. Large dimensional tolerances were provided in order to hold down tooling costs. It was felt that these tolerances would not affect the evaluation of the truss for ballistic purposes.

DYNAMIC LOAD IMPULSES

Strain gages were placed on members which exhibited the largest change in static load after elements were removed to simulate ballistic damage. It was felt that these members would also exhibit the largest dynamic impulse loads following ballistic impact. Continuous readings were taken starting approximately 4 msec before impact until the principal shock wave had passed the gage locations. Gage readouts are shown in Appendix A.

Analysis of the readout data revealed that the compression buckling allowable for both the diagonal and longeron members was exceeded by the dynamic impulse loads. Dynamic plus steady-state strain is presented in Tables 15 and 16.

No dynamic impulse information was available for test 3.

Investigation of the test specimens after ballistic impact did not reveal any damage that could be attributed to the impulse loads. The allowable tension strain (Ref. Table 2) was not exceeded. The compressive strain caused by the impulse wave traveled through the truss at a velocity that was faster than the reaction time of the structure. Thus, those elements subjected to a compressive impulse stress in excess of the design allowable did not buckle. It is felt that had a tension strain greater than the design allowable been experienced, failure would have occurred.

TABLE 15. DYNAMIC IMPULSE STRAIN
 (REF. APPENDIX A, PAGES 86 THROUGH 89)

Test 1

Gage Number	Member	Max Dynamic Strain μ in./in.	Steady State Strain μ in./in.	Combined Strain μ in./in.	Design Allowable μ in./in.
1	Diagonal	+ 640	N/A	640	9799
		- 569		- 569	-1341
2		+1850	-108	1742	9799
		-1317		-1425	-1341
3		+1424	-167	1257	9799
		-1349		-1516	-1341
4		+1475	72	5147	9799
		-1106		-1034	-1341
5		+ 925	N/A	925	9799
		-1174		-1174	-1341
6		+1104	N/A	1104	9799
		- 966		- 966	-1341
7		+1590	-196	1394	9799
		-1244		-1440	-1341
8		+ 394	-409	- 15	9799
		-1907		-2316	-1341
9		+1281	-132	1149	9799
		-1993		-2125	-1341
10	Longeron	+ 641	170	811	9799
					-1611
11		+ 712	142	854	9799
					-1611
12		+ 983	217	1200	9799
		- 605		- 388	-1611

TABLE 16. DYNAMIC IMPULSE STRAIN
 (REF. APPENDIX A, PAGES 96 THROUGH 99)

Test 2

Gage Number	Member	Max Dynamic Strain μ in./in.	Steady State Strain μ in./in.	Combined Strain μ in./in.	Design Allowable μ in./in.
1	Longeron	+ 890	N/A	+ 890	9799
		- 854		- 854	-1611
2		760	N/A	760	9799
		-1139		-1139	-1611
3		+ 880	N/A	+ 880	9799
		-1907		-1907	-1611
4		+1027	N/A	+1027	9799
		-1466		-1466	-1611
5		+ 733	N/A	+ 733	9799
		-1833		-1833	-1611
6		+1452	N/A	+1452	9799
		-1797		-1797	-1611
7		430	-519	- 89	9799
		-2135		-2654	-1611
8		0	-316	-2956	9799
		-2640			-1611
9		2053	-449	+1604	9799
		- 852		-1301	-1611

NOTE: Fragment cut sensor leads of gages 10-12.

CONCLUSIONS AND RECOMMENDATIONS

Analysis of the results of this study indicates that an open truss constructed of composite materials is a viable concept for a ballistically tolerant tail boom.

Use of filament winding techniques in the manufacturing phase demonstrated the manpower and time savings that could be achieved by using these techniques in a production environment. The use of a collapsible metal winding mandrel machined to close to tolerances would be needed to produce production quality parts of uniform weight and stiffness. Use of such tooling was not included in the scope of this program because of the extra cost involved.

Because of the openness of the truss, blast pressure did not play a part in boom damage after impact. A tearaway covering could be incorporated into future designs without reducing the ability of the truss to carry load after impact. The addition of such a covering would, however, eliminate the possibility of a round passing completely through the boom without detonating. The truss configuration tested had approximately 50 percent open area. Tail booms having a larger diameter could be designed with even more open area, thus increasing the chance for a complete miss.

Exit-side fragment damage was much more extensive than expected. Even though the truss design provided for approximately 50 percent open area, almost all members on the exit side suffered some fragment damage. A larger diameter truss would allow for more open area, thus reducing the chance that a fragment would strike a member. A larger boom diameter would also allow for the placement of more members outside of the fragment dispersion cone, thus reducing the chance for damage.

Fragment holes were clean cuts with only limited ply delamination on the exit side. No cracks were seen propagating from the holes. The unidirectional fiber orientation used in the fabrication of diagonal and frame members was satisfactory from a crack propagation standpoint. The brittle nature of graphite did not prove to be a cause of excessive member damage. It could not be determined from this program if cracks would develop in damaged members as a result of the continued application of level flight oscillatory loads. Fatigue testing of damaged specimens should be a part of any future program.

Dynamic impulse loads did not play a role in the truss design. Compressive strain caused by the impulse wave traveled through the truss at a velocity that was faster than the reaction time

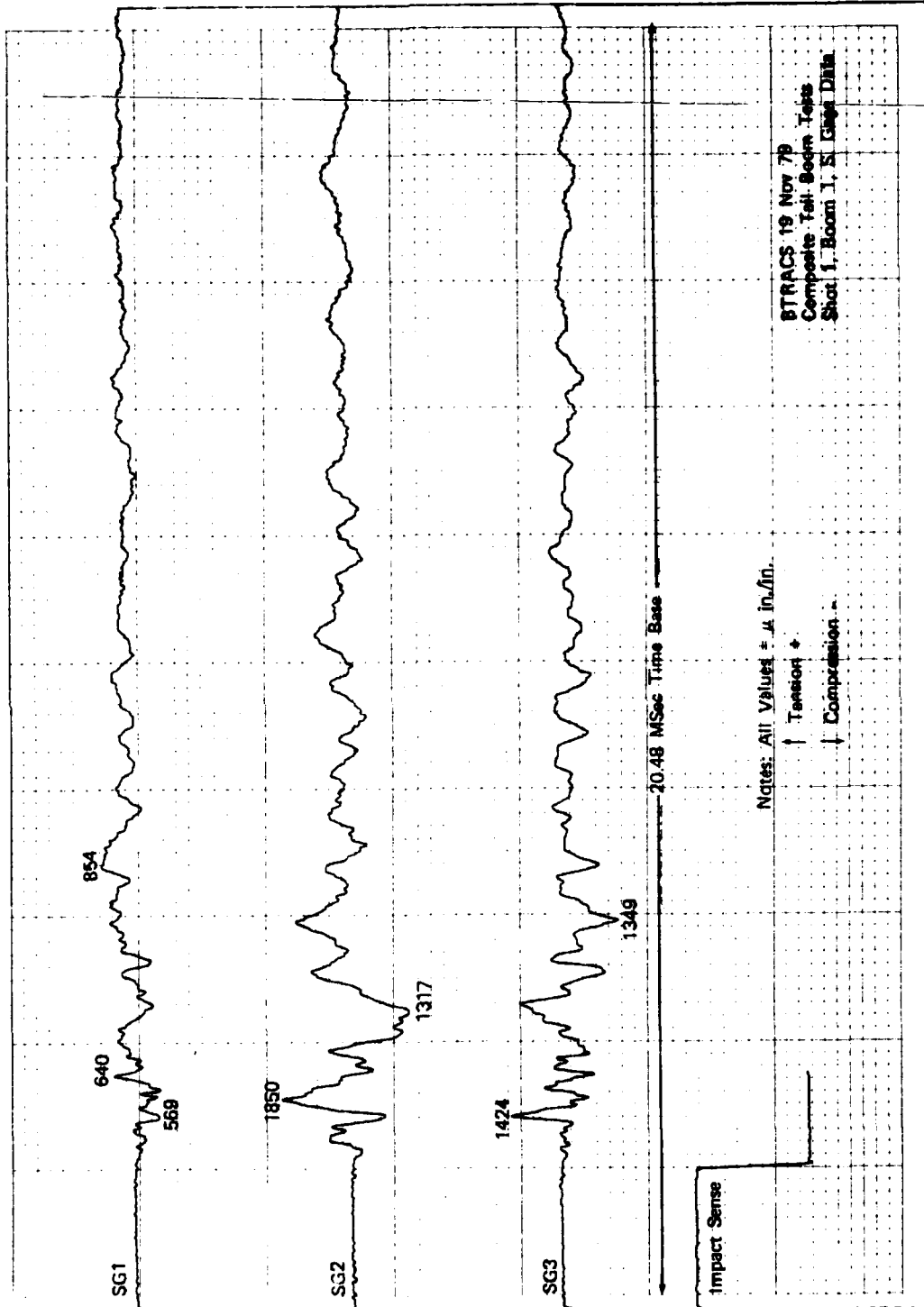
of the structure and thus did not cause members to buckle. The high strength of the graphite provided a large margin of safety for any tensile impulse strains. It is felt that the addition of material in anticipation of dynamic impulse loading requirements is not necessary in future designs.

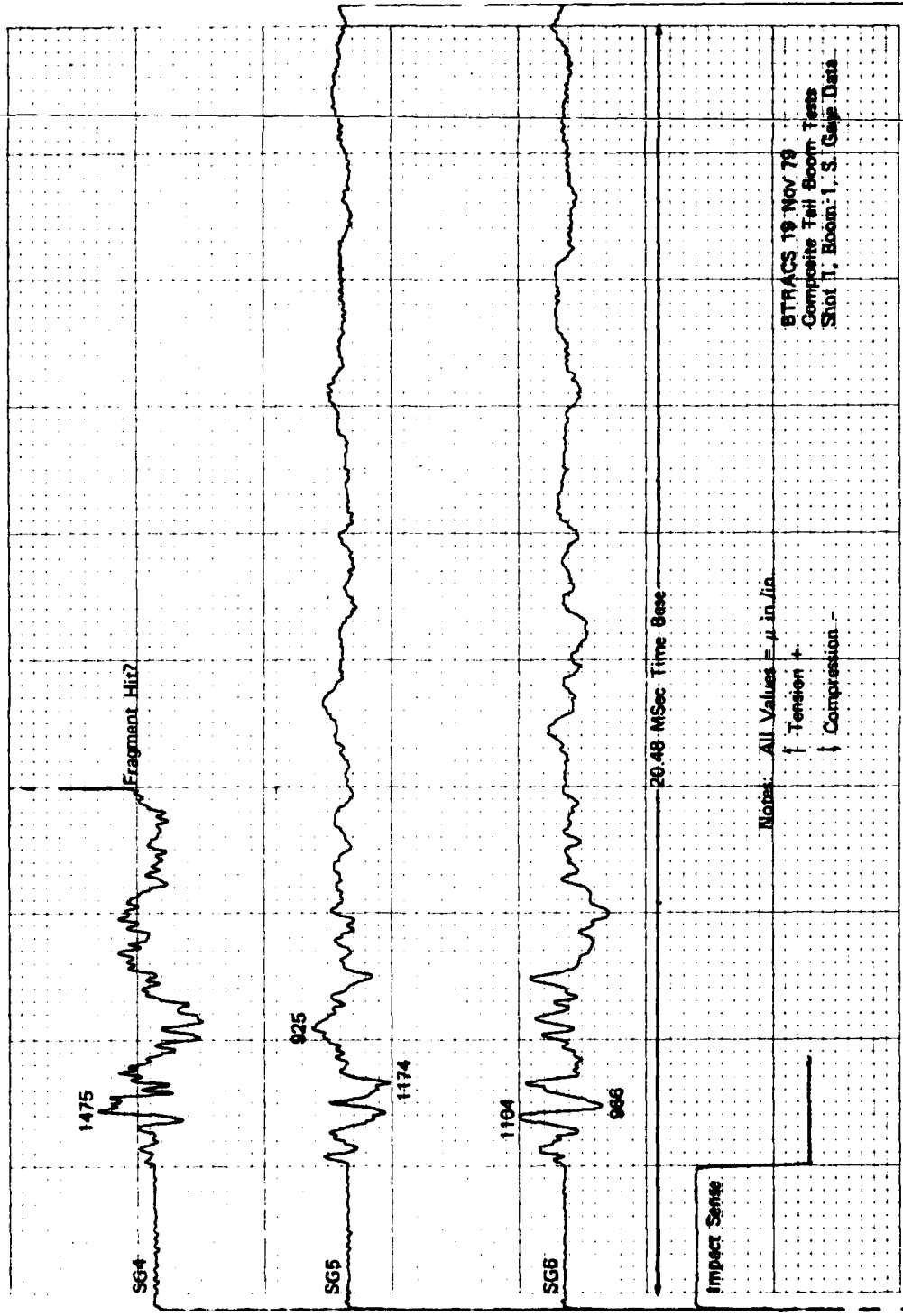
REFERENCES

1. ~~ADVANCED COMPOSITE DESIGN GUIDE~~, Rockwell International Corporation, Contract F33615-74-C-5075, Air Force Flight Dynamics Laboratory, Air Force Systems Command, Wright-Patterson Air Force Base, Ohio, April 1976.
2. McCormick, Caleb W., NASA SP222(03) NASTRAN USER'S MANUAL, National Aeronautics and Space Administration, Washington, D.C., July 1978.
3. Wilson, H. E., COMPOSITE ANALYSIS PROGRAM SC1701, Bell Helicopter Textron Report 599-162-927, April 6, 1977.

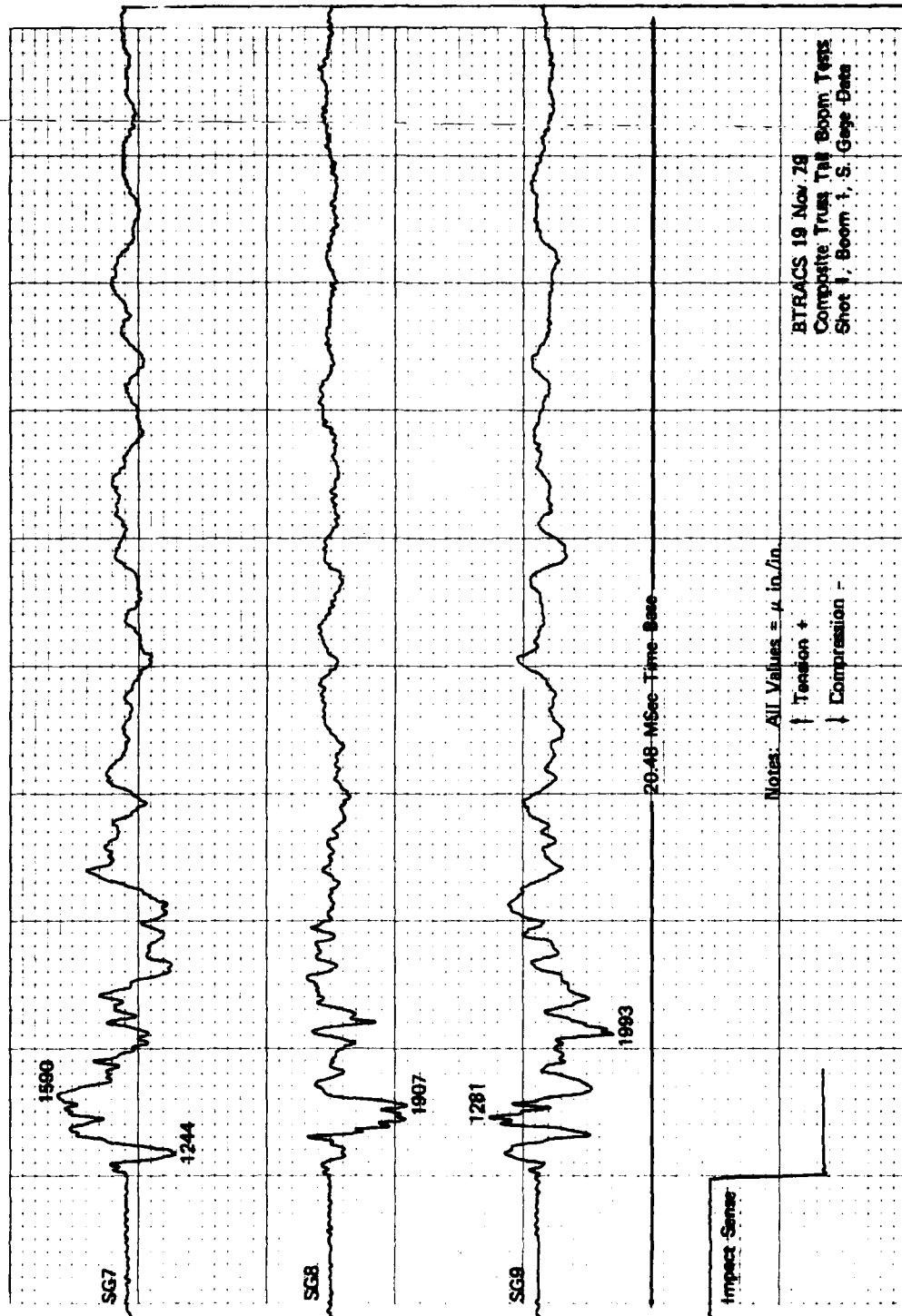
APPENDIX A
COMPOSITE TRUSS TAIL BOOM TESTS

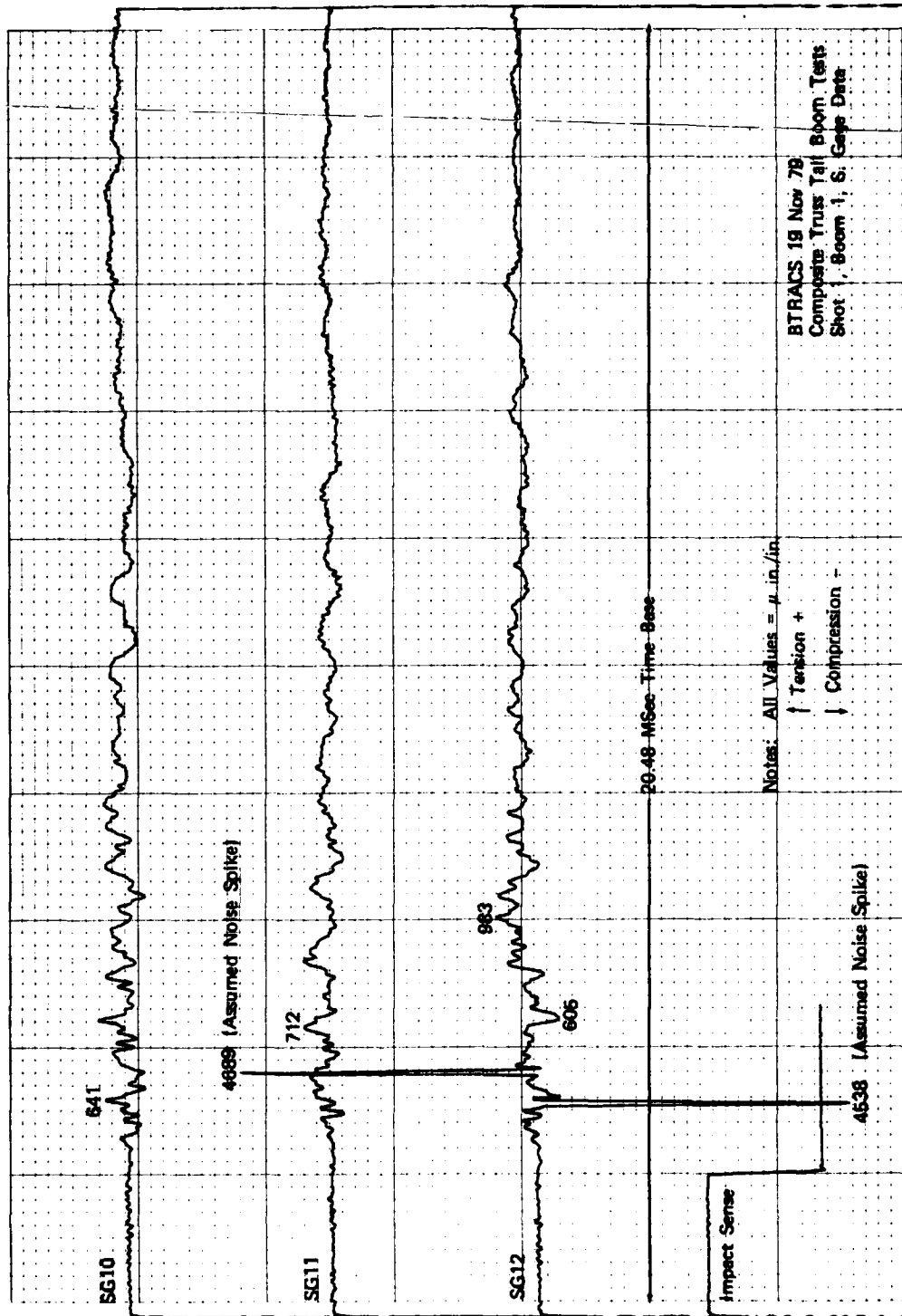
This appendix contains the measurements of the composite truss tailboom tests.

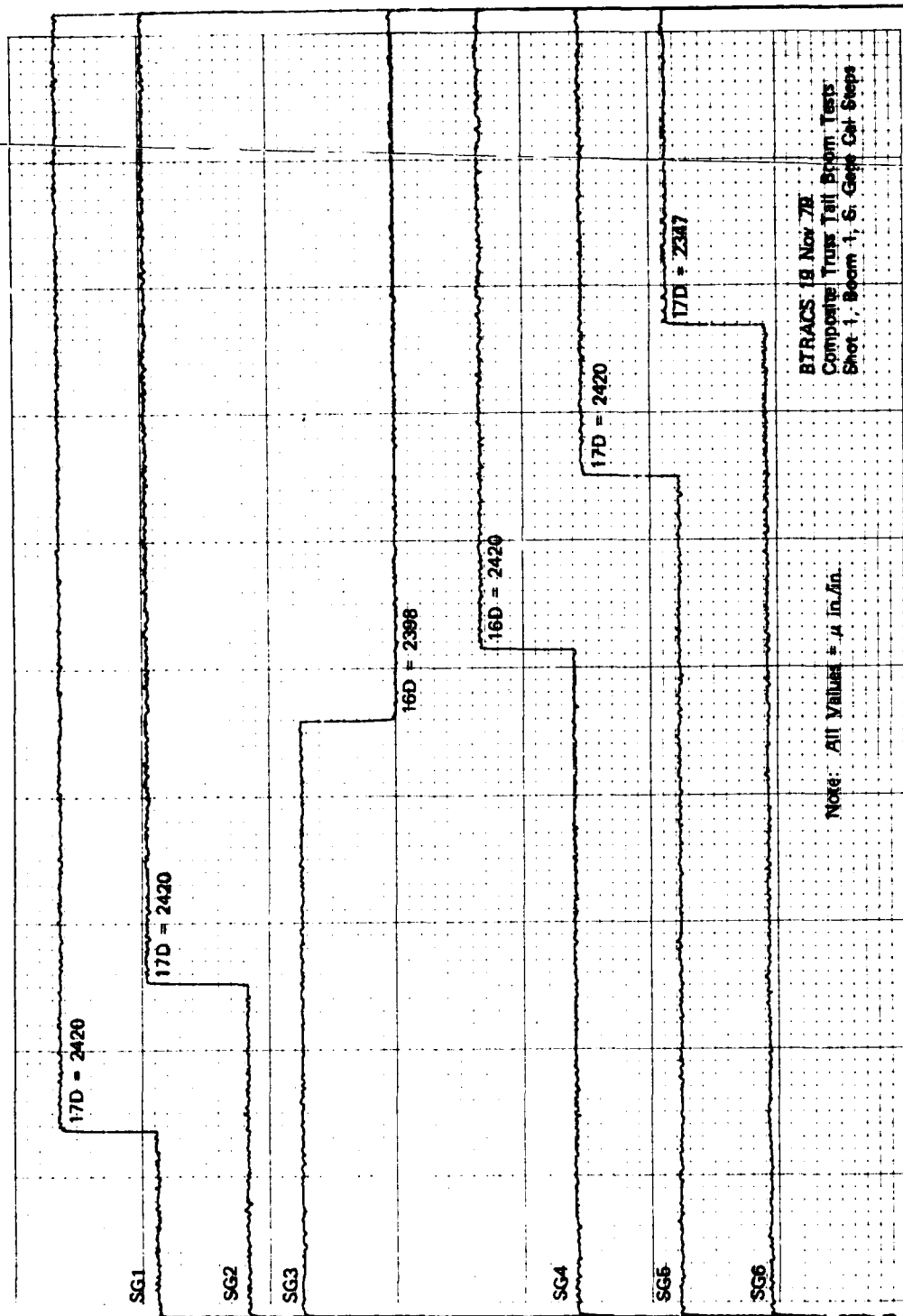




BTRACS 19 Nov 79
 Composite Tail Boom Tests
 Slot 1, Boom: 1, S, Gals Data

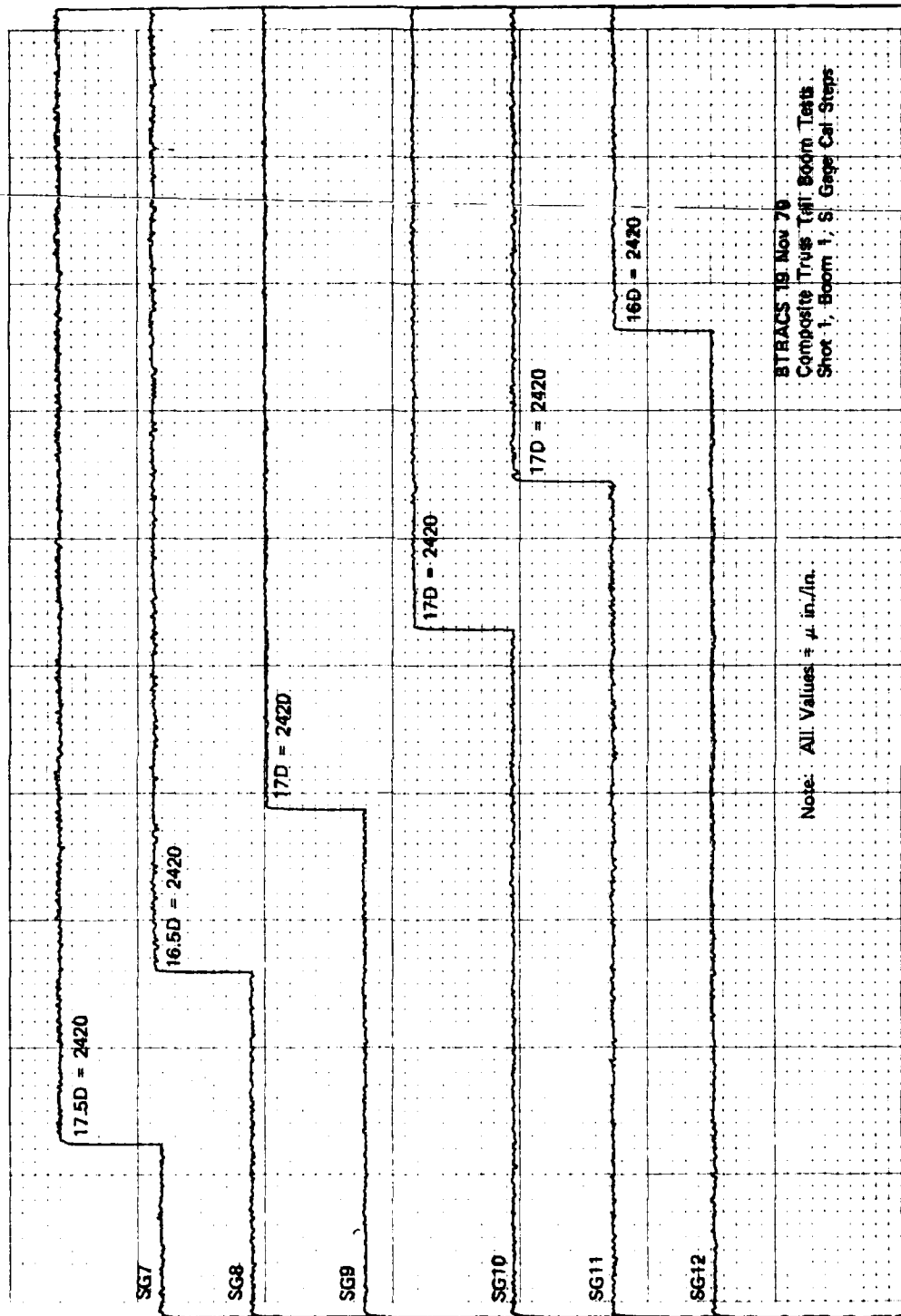


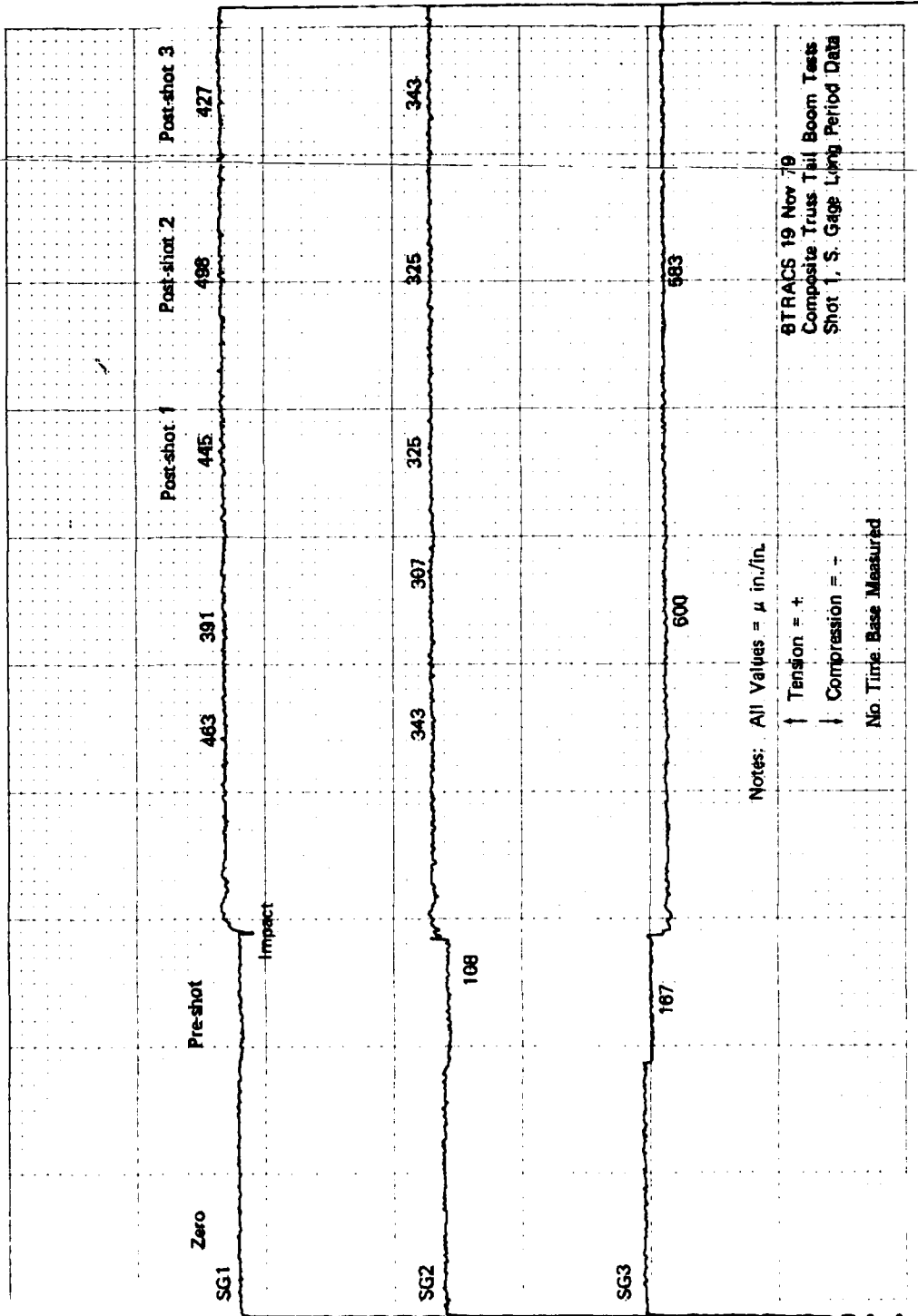


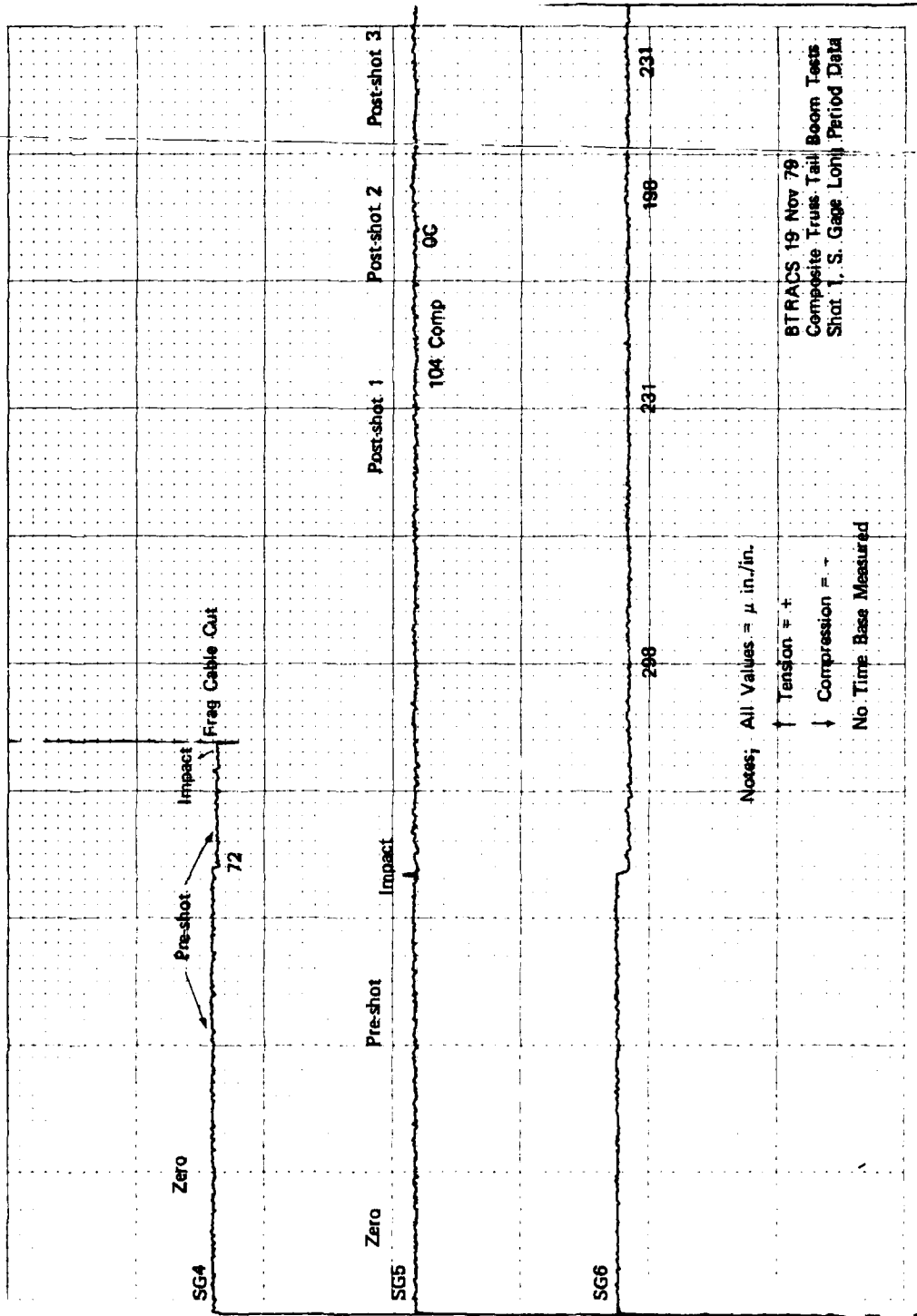


BTRACS 19 Nov 78
 Composite Truss Tail Boom Tests
 Shot 1, Boom 1, 5, Geop Cal Steps

Note: All Values ± .4 in./in.







BTRACS 19 Nov 79
 Composite Truss Tail Boom Tests
 Shot 1, S. Gage Lohij Period Data

AD-A085 132

BELL HELICOPTER TEXTRON FORT WORTH TX

F/G 1/3

CONCEPTUAL DESIGN OF A HELICOPTER COMPOSITE TRUSS TAIL ROOM.(U)

APR 80 D A GALLIAN

DAK51-78-C-0016

UNCLASSIFIED

USAAVRADCOM-TR-80-D-R

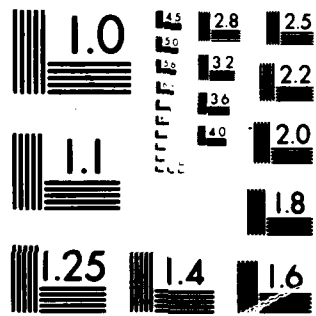
NL

2 2

28 APR 80



END
DATE
FILMED
7 80
DTIC



MICROCOPY RESOLUTION TEST CHART
NATIONAL BUREAU OF STANDARDS-1963-A

Zero	Pre-shot	Impact	Post-shot 1	Post-shot 2	Post-shot 3
SG10	170	477	511	511	511
SG11	142	267	289	285	285
SG12	217	885			

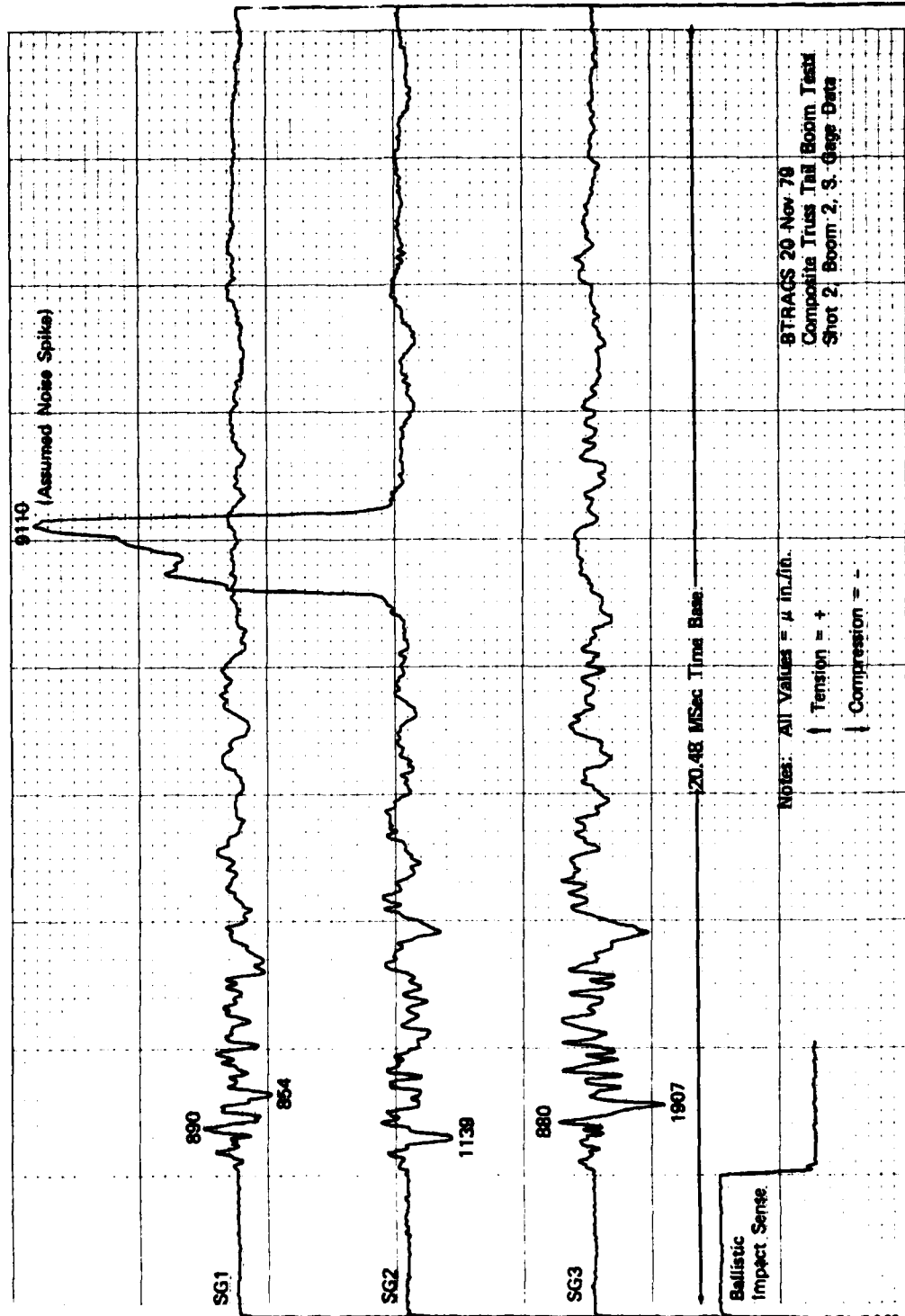
Notes: All Values = μ in./in.

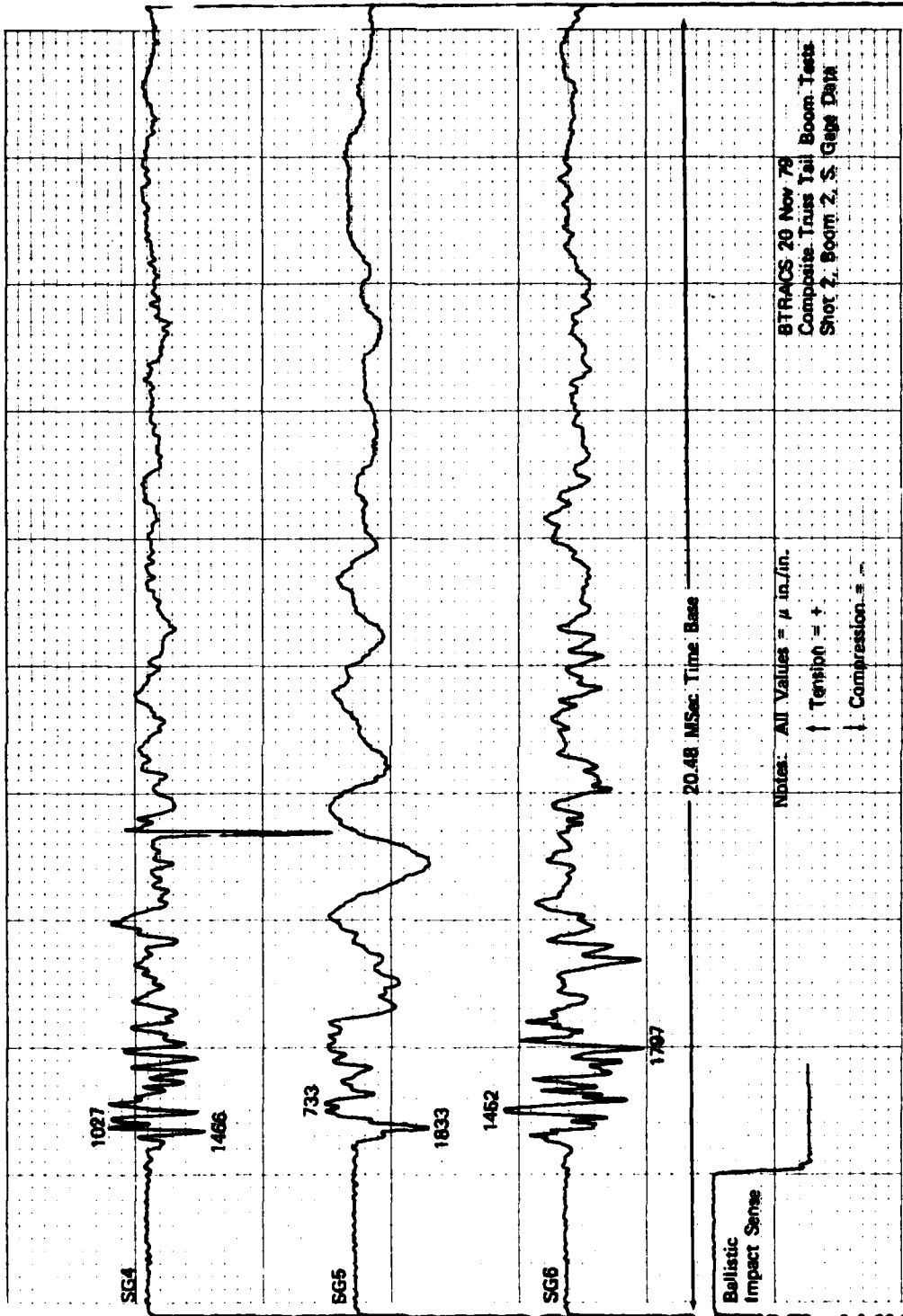
↑ Tension = +

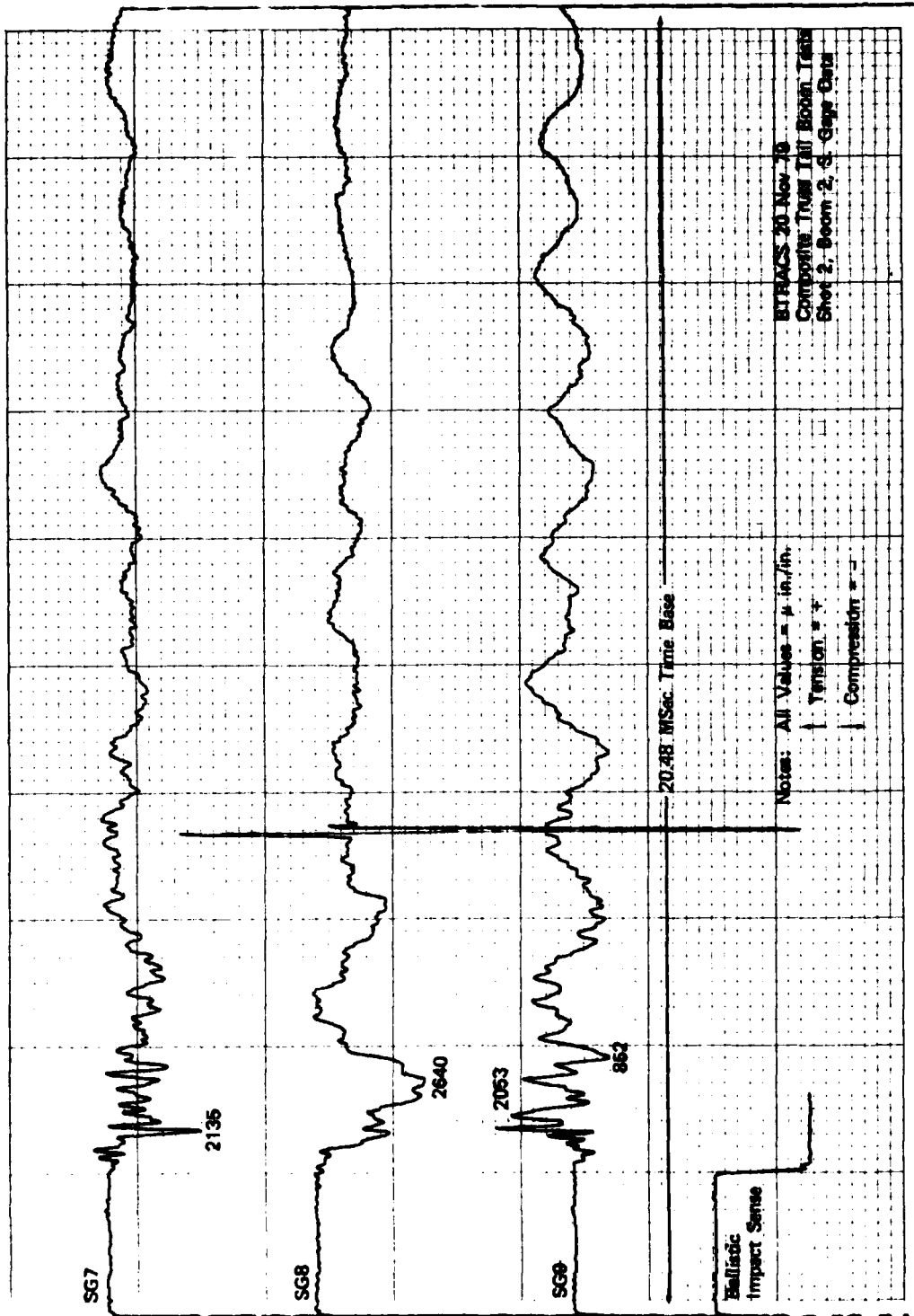
↓ Compression = -

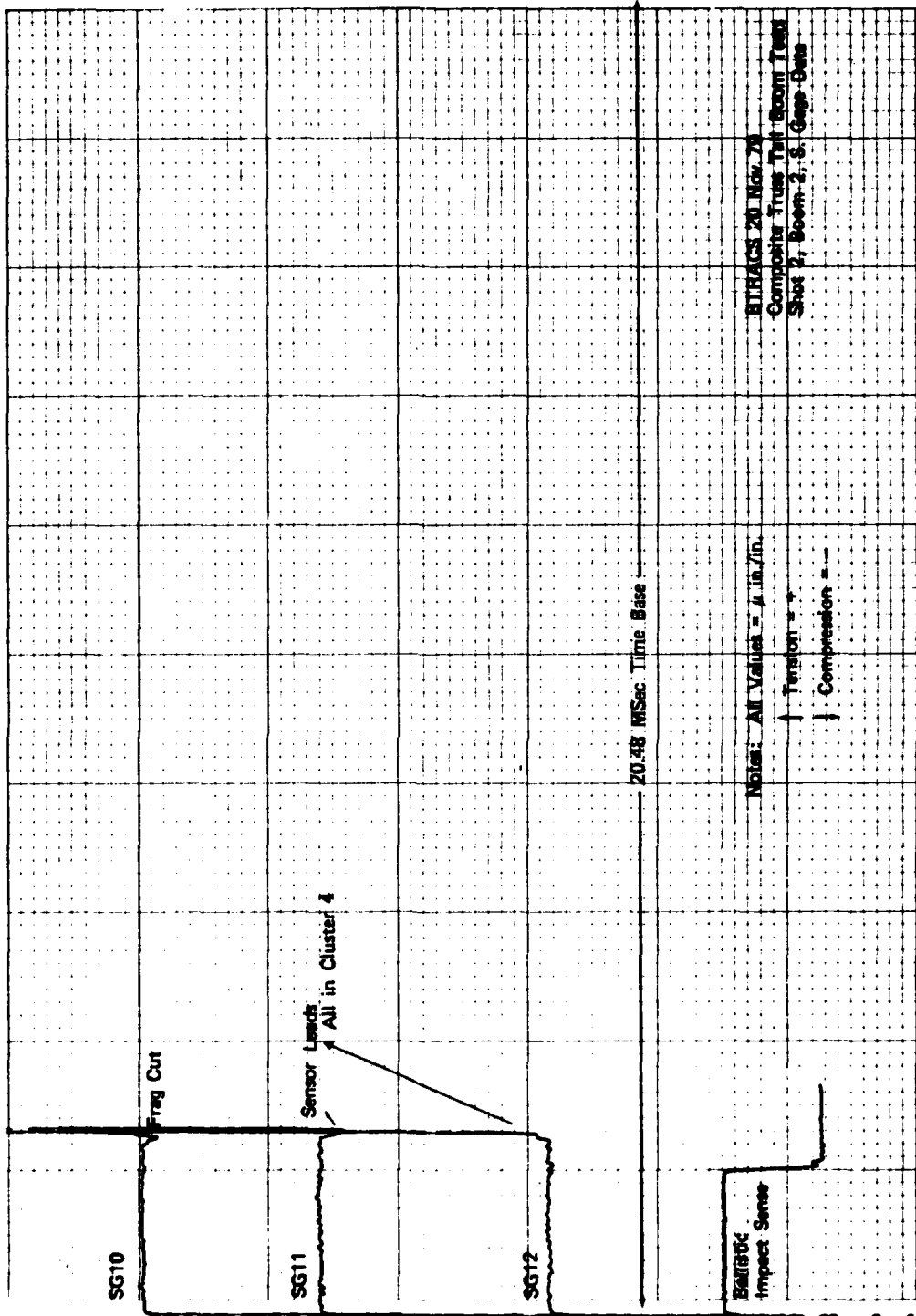
No Time Base Measured

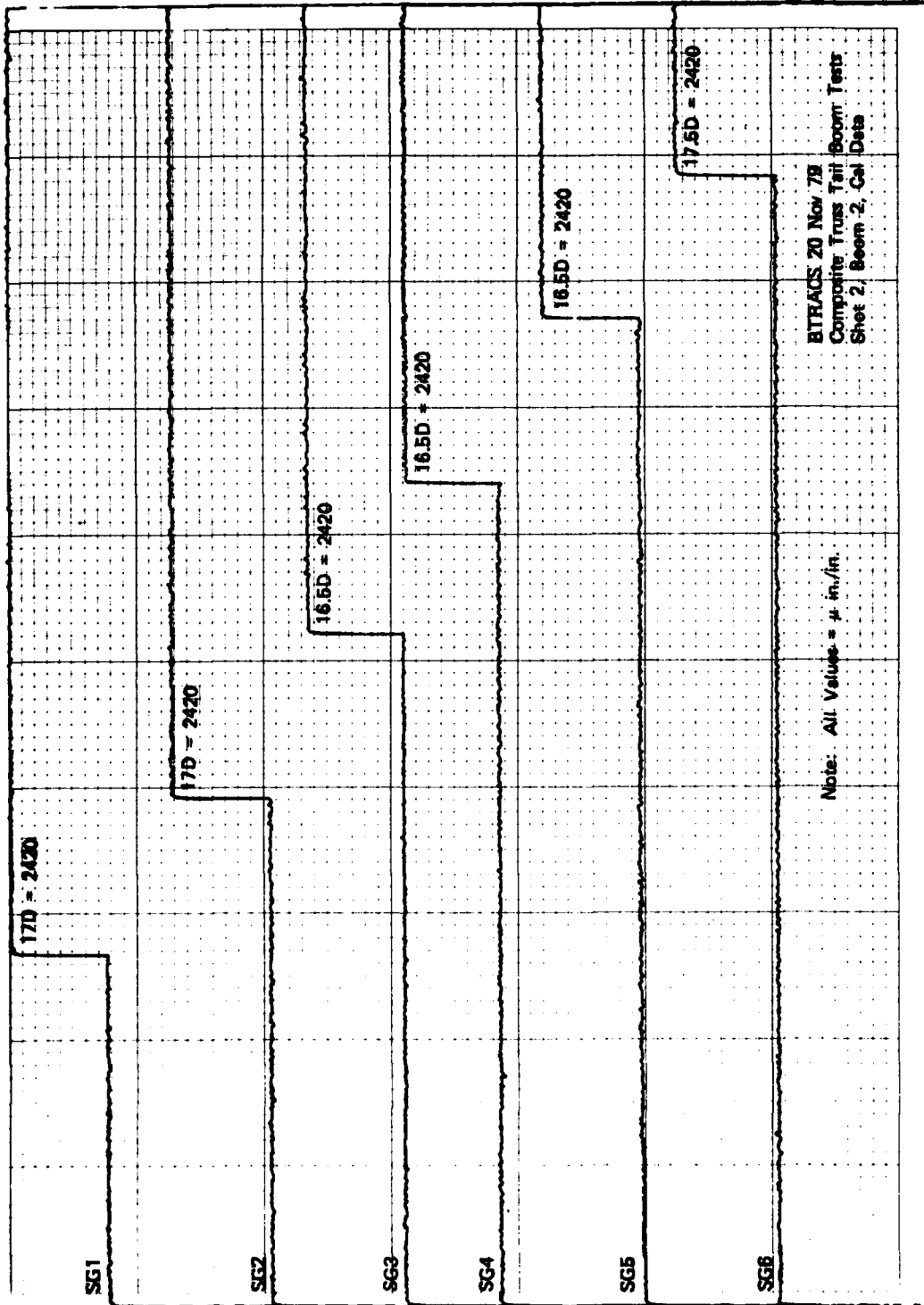
BTRACS 19 Nov 79
Competition Trans: Fall Beam Tests
Shot 1, 2, 3, 4, 5, 6, 7, 8, 9, 10, 11, 12, 13, 14, 15, 16, 17, 18, 19, 20, 21, 22, 23, 24, 25, 26, 27, 28, 29, 30, 31, 32, 33, 34, 35, 36, 37, 38, 39, 40, 41, 42, 43, 44, 45, 46, 47, 48, 49, 50, 51, 52, 53, 54, 55, 56, 57, 58, 59, 60, 61, 62, 63, 64, 65, 66, 67, 68, 69, 70, 71, 72, 73, 74, 75, 76, 77, 78, 79, 80, 81, 82, 83, 84, 85, 86, 87, 88, 89, 90, 91, 92, 93, 94, 95, 96, 97, 98, 99, 100

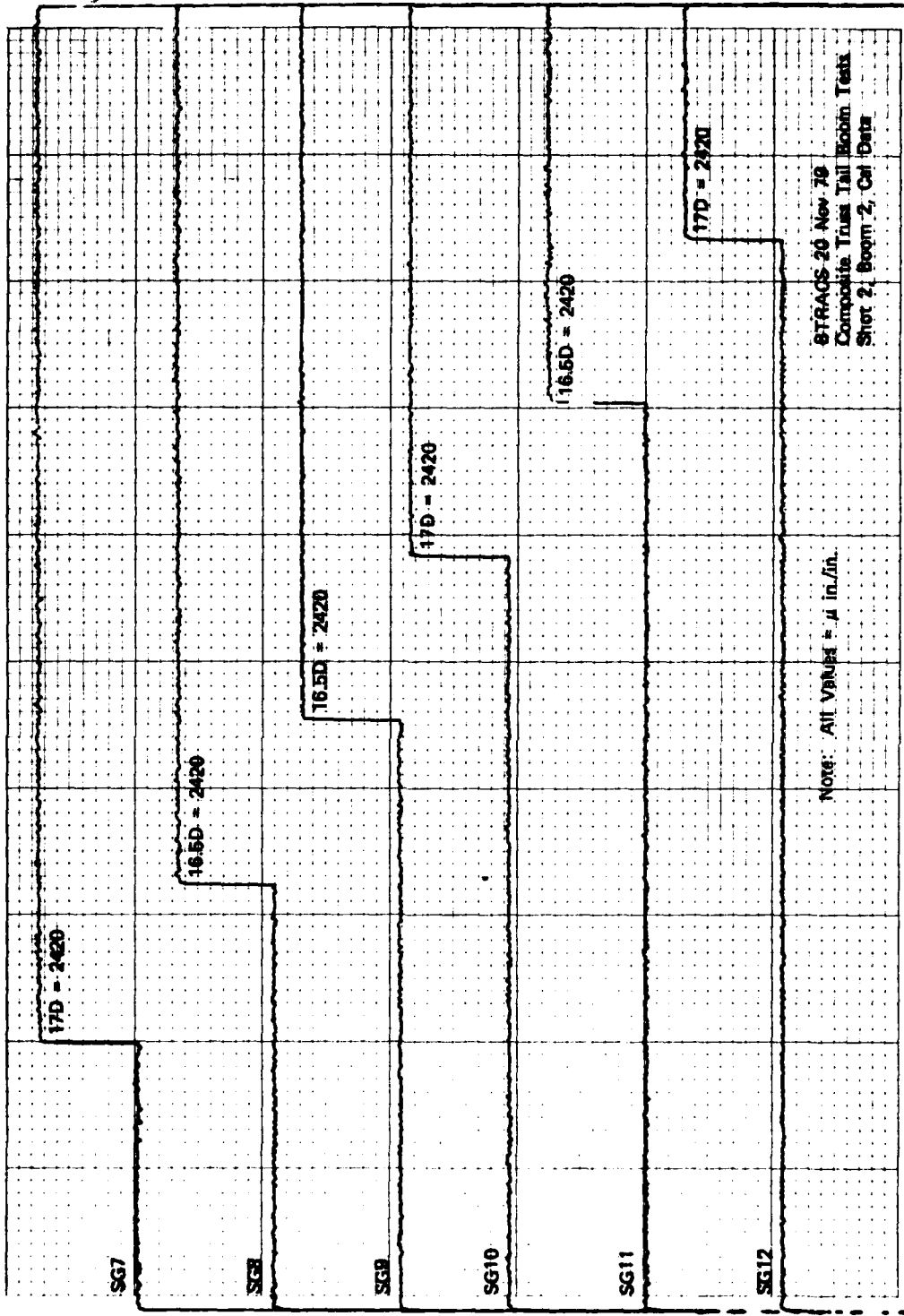












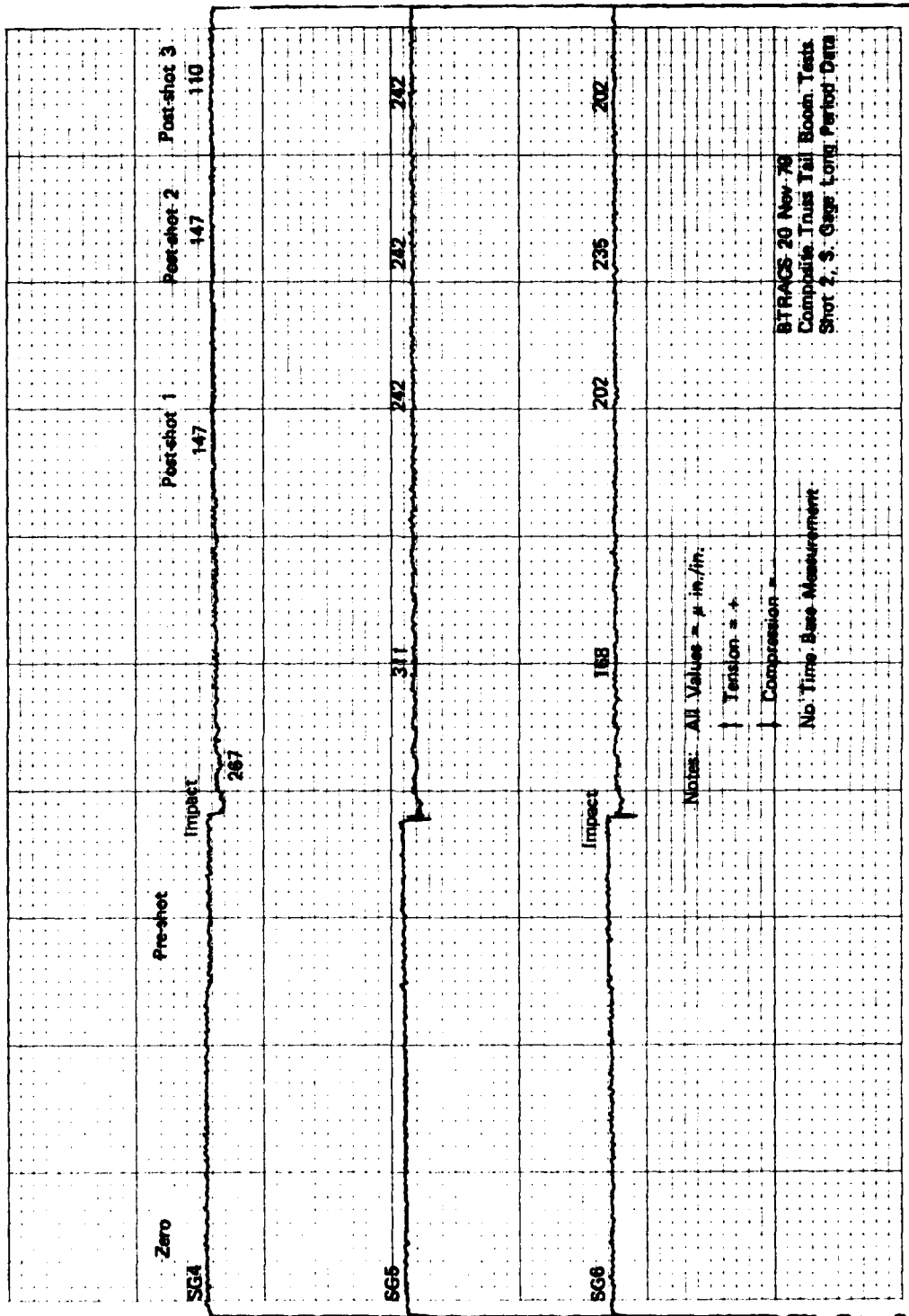
8TRACS-20 Nov 78
Composite Truss Tail Bobbin Test
Shot 2, Boom 2, Cal Data

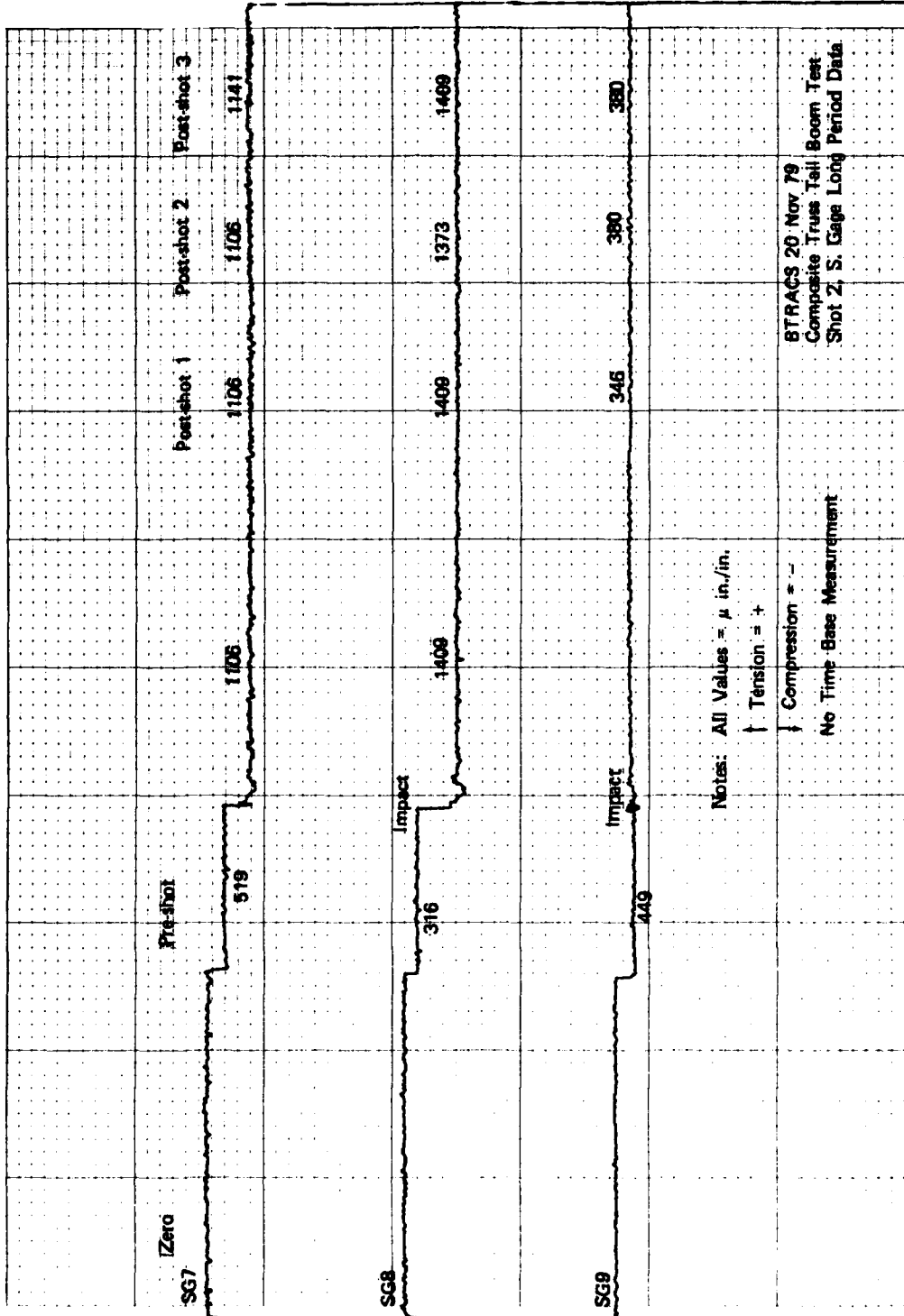
Note: All Values = μ in./in.

	Pre-shot	Impact	Post-shot 1	Post-shot 2	Post-shot 3
SG1	Zero	Impact 106	140	140	123
SG2		Impact 136	136	136	123
SG3		Impact			

Notes: All Values μ in./in.
 ↑ Tension = +
 ↓ Compression = -
 No Time Base Measurement

ETRACS 20 Nov 79
 Composite Train Tail Boom Tests
 Shot 2 - S. Gege Long Period Data





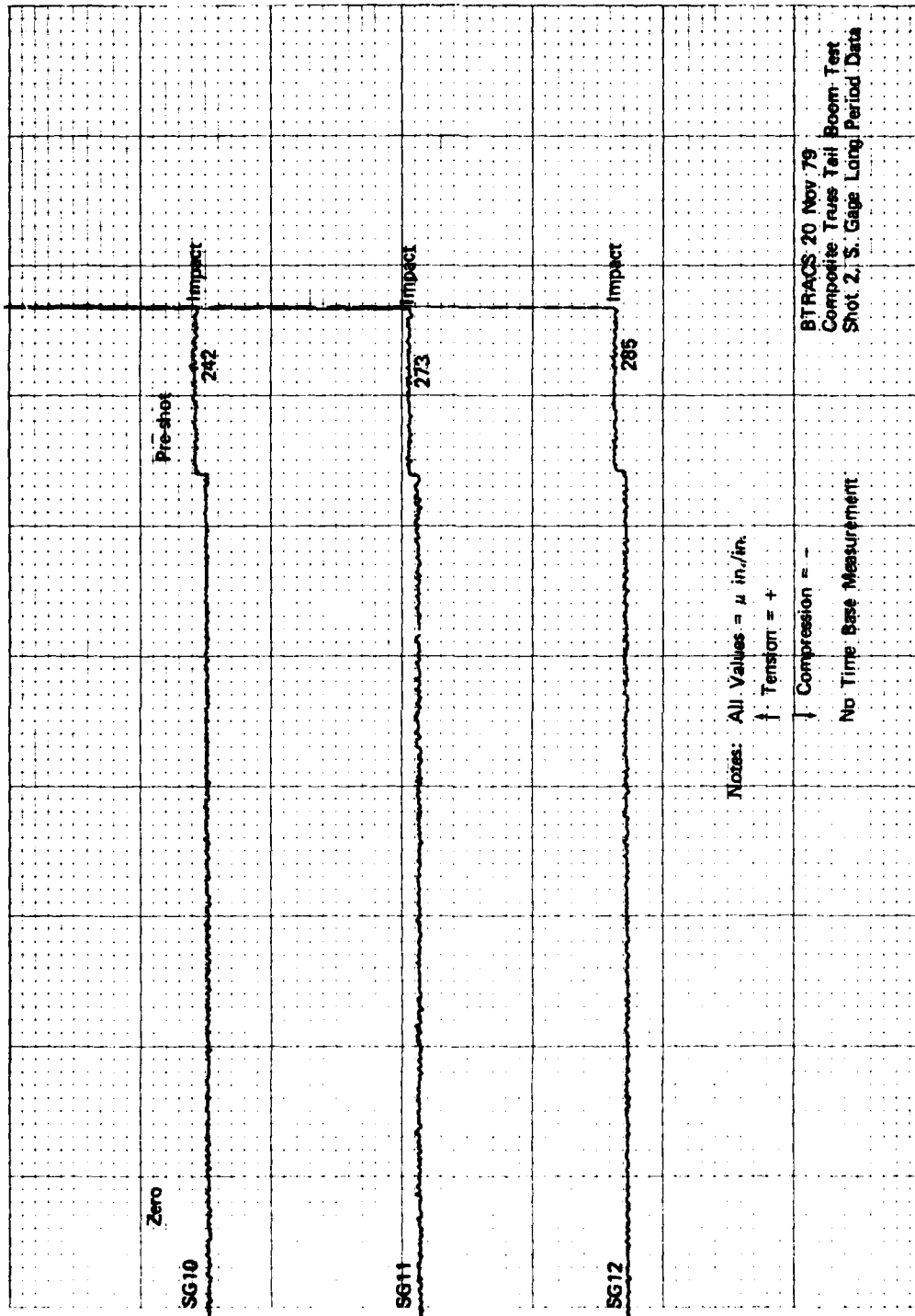
Notes: All Values = μ in./in.

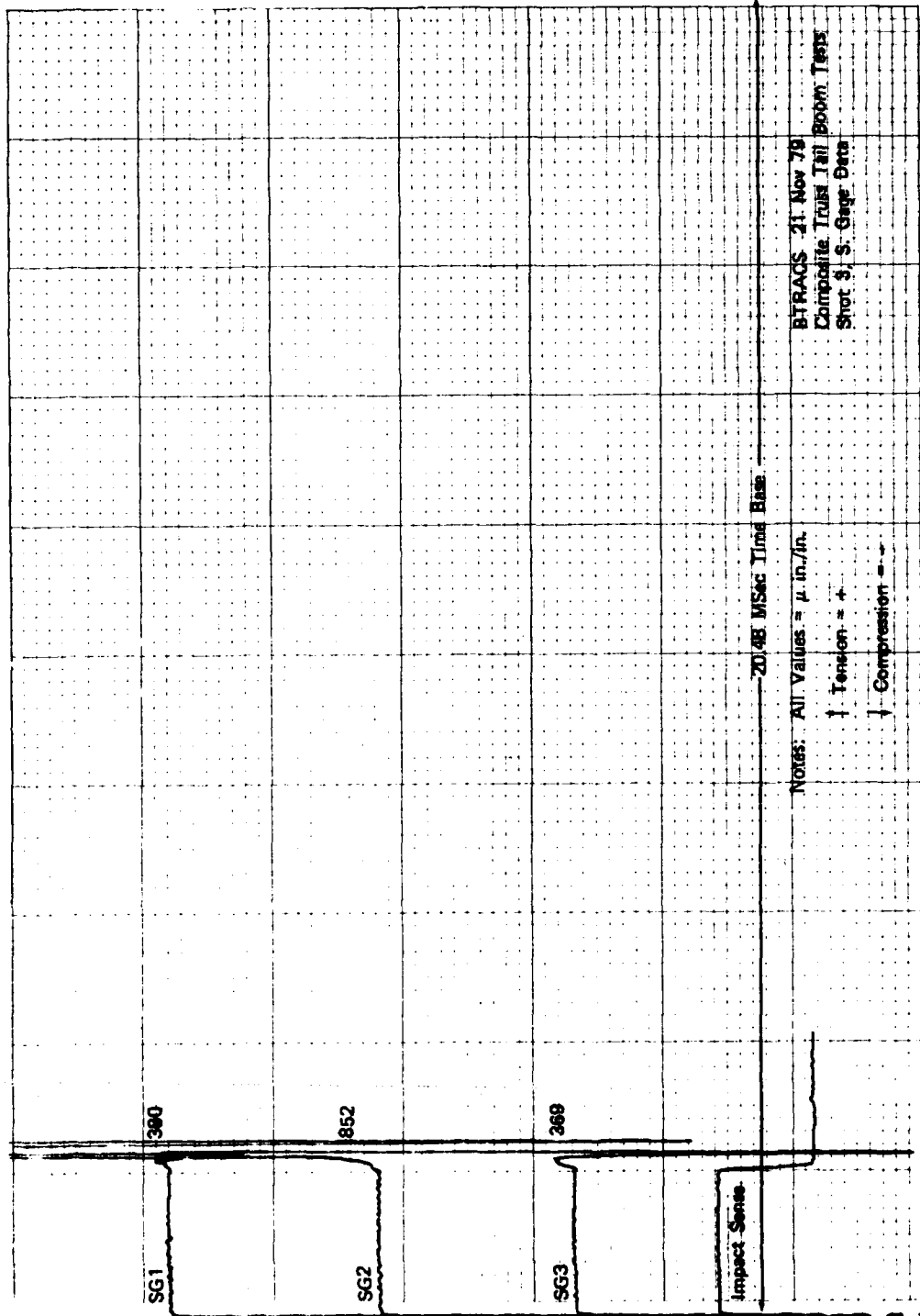
↑ Tension = +

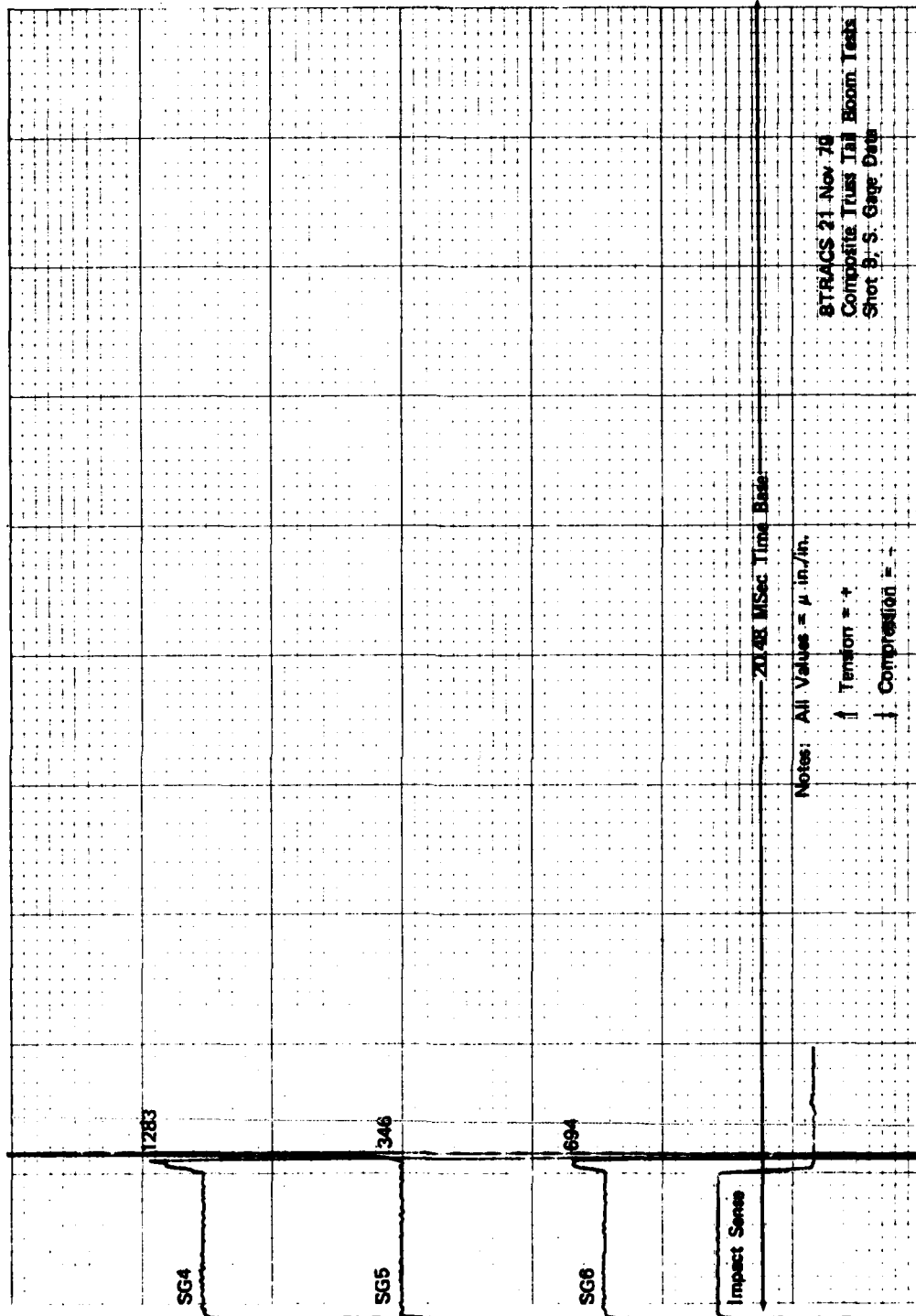
↓ Compression = -

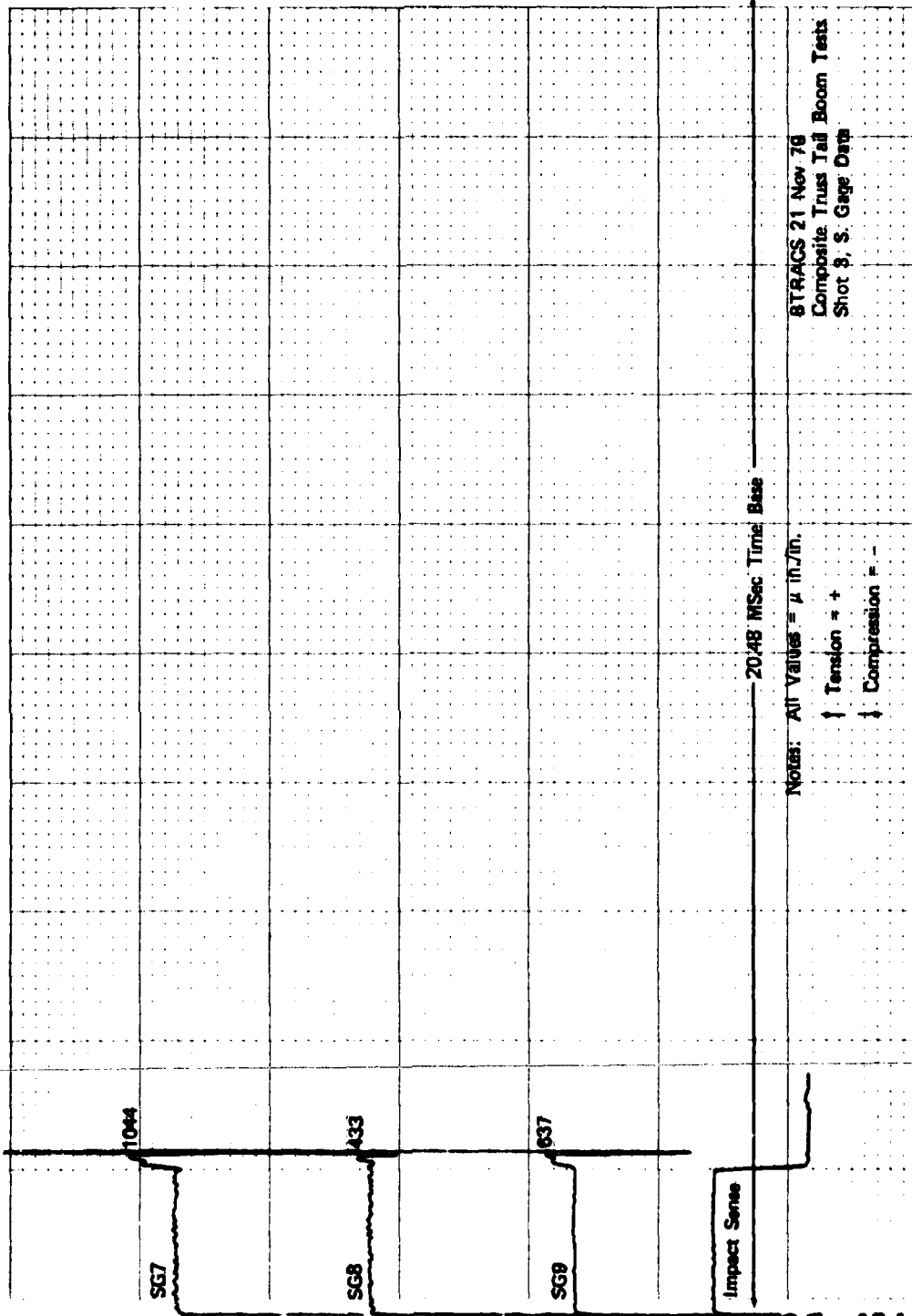
No Time Base Measurement

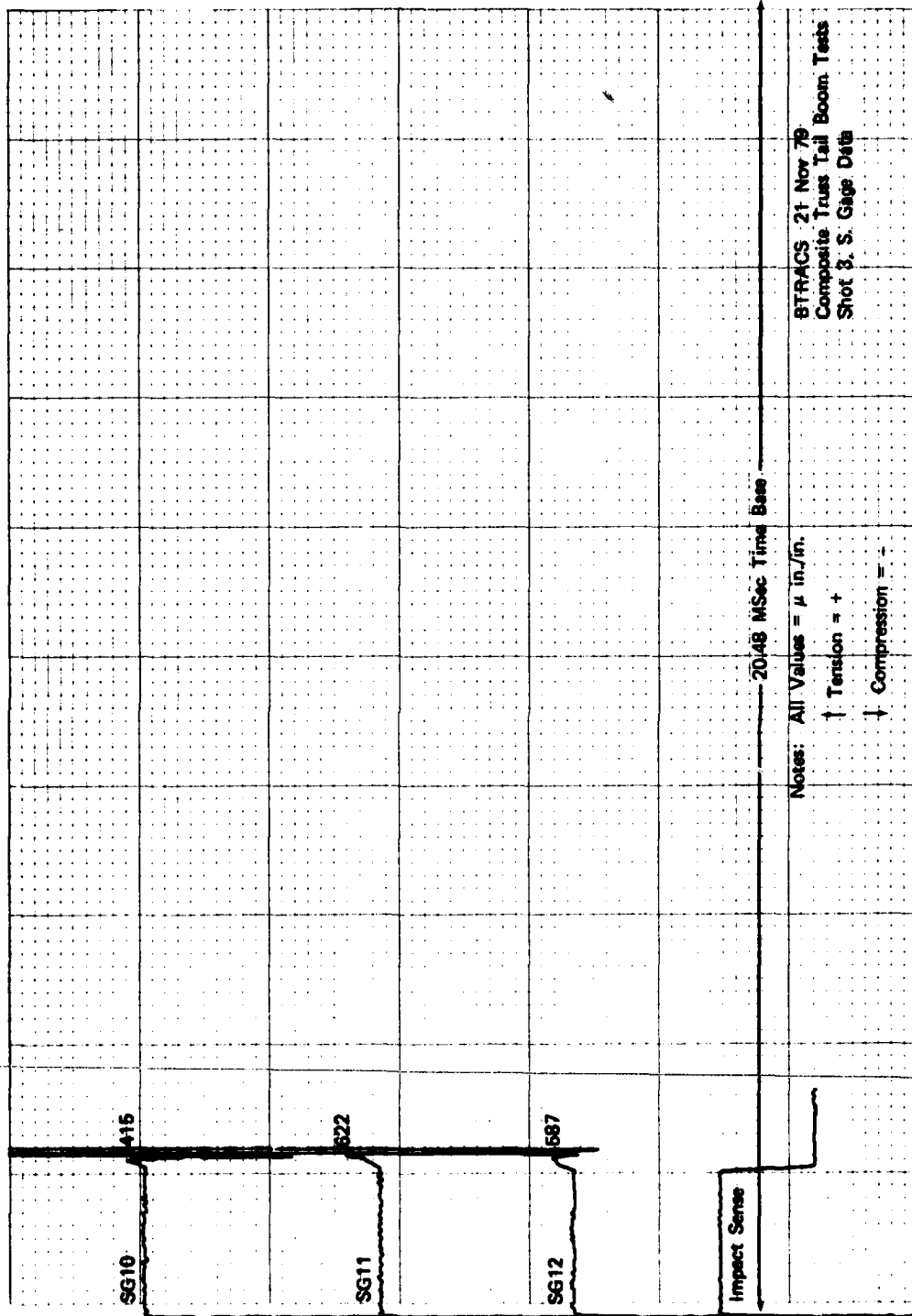
BTRACS 20 Nov 79
Composite Truss Tail Boom Test
Shot 2, S. Gage Long Period Data

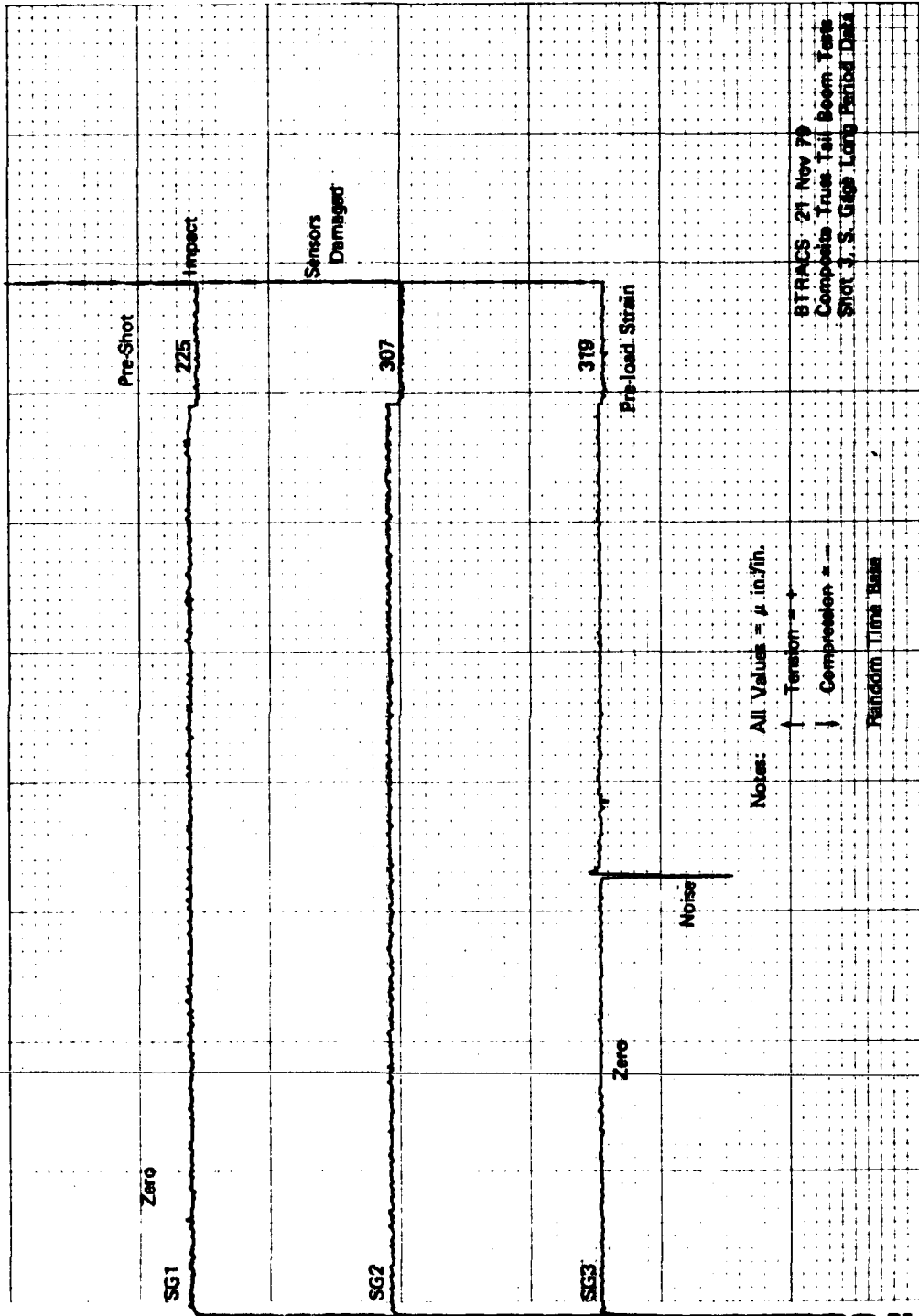


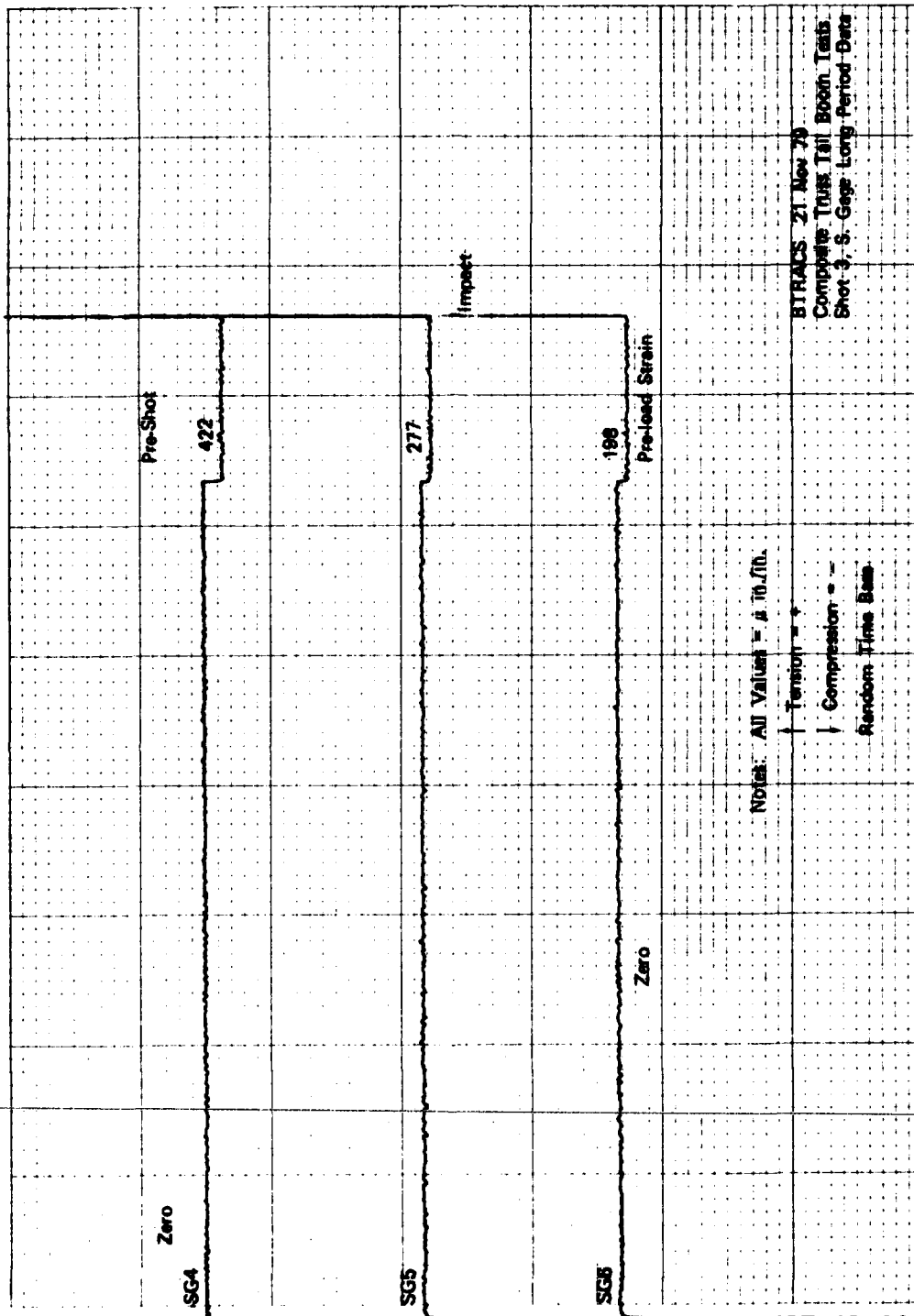












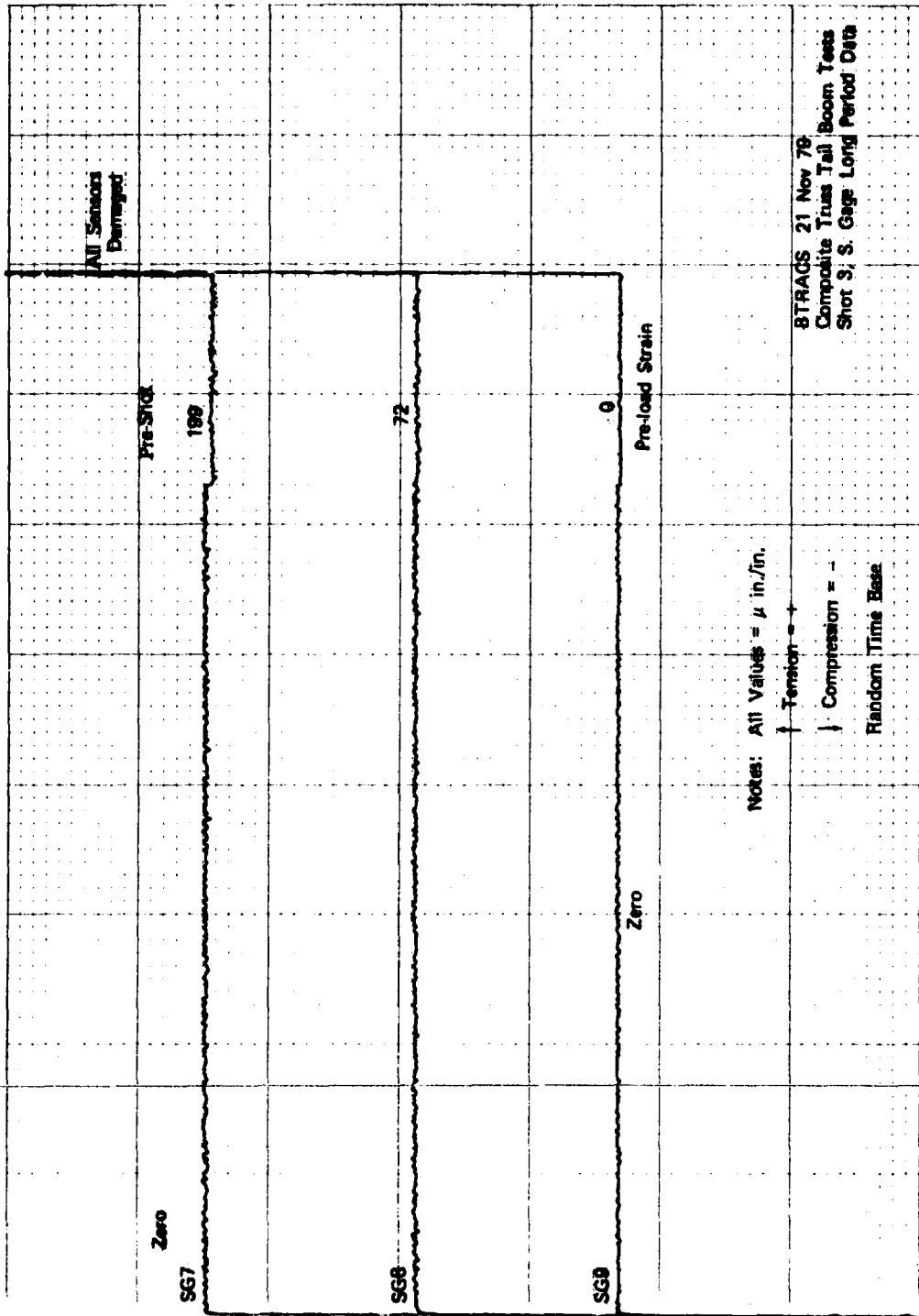
Note: All Values = μ in./in.

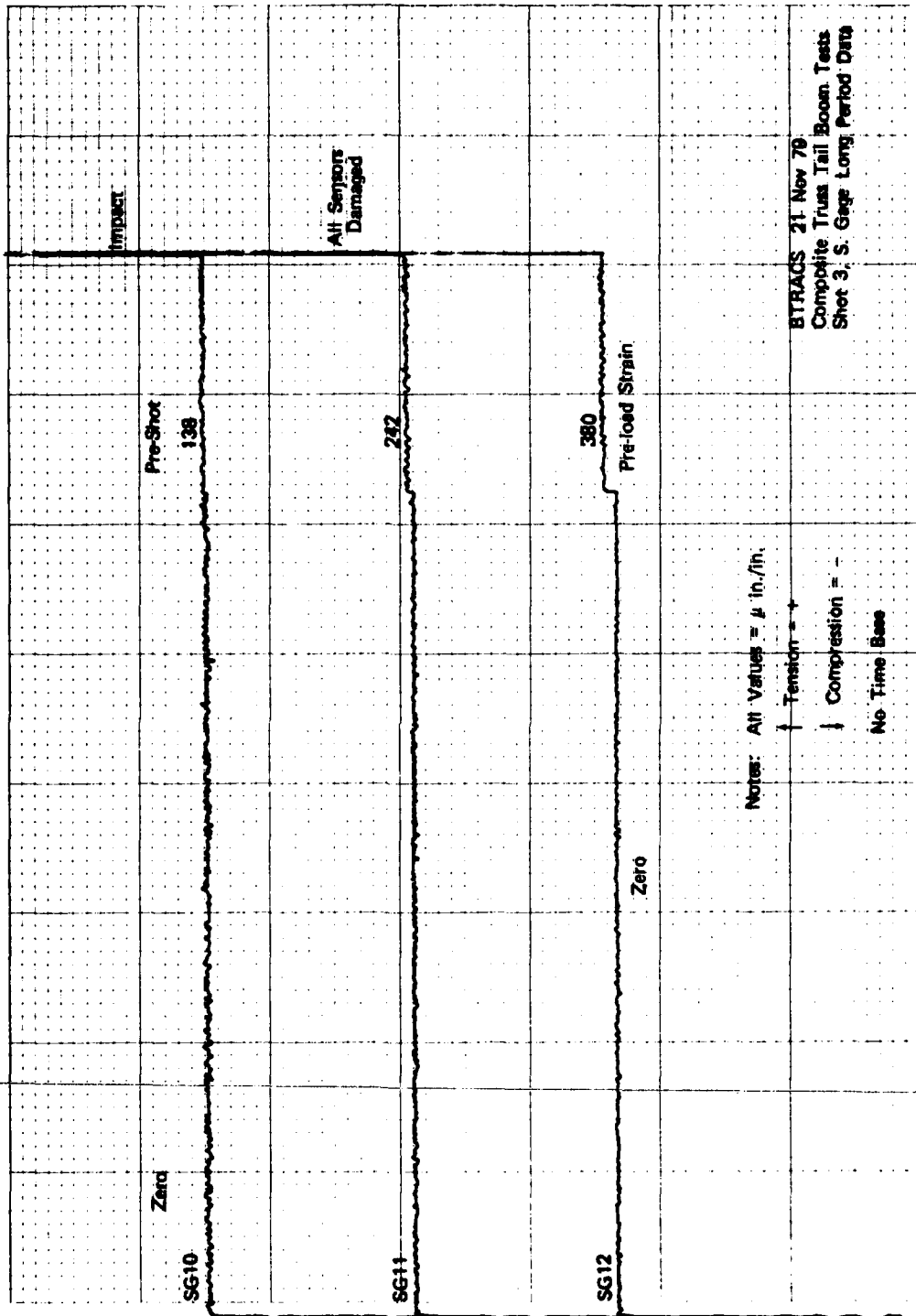
Tension = +

Compression = -

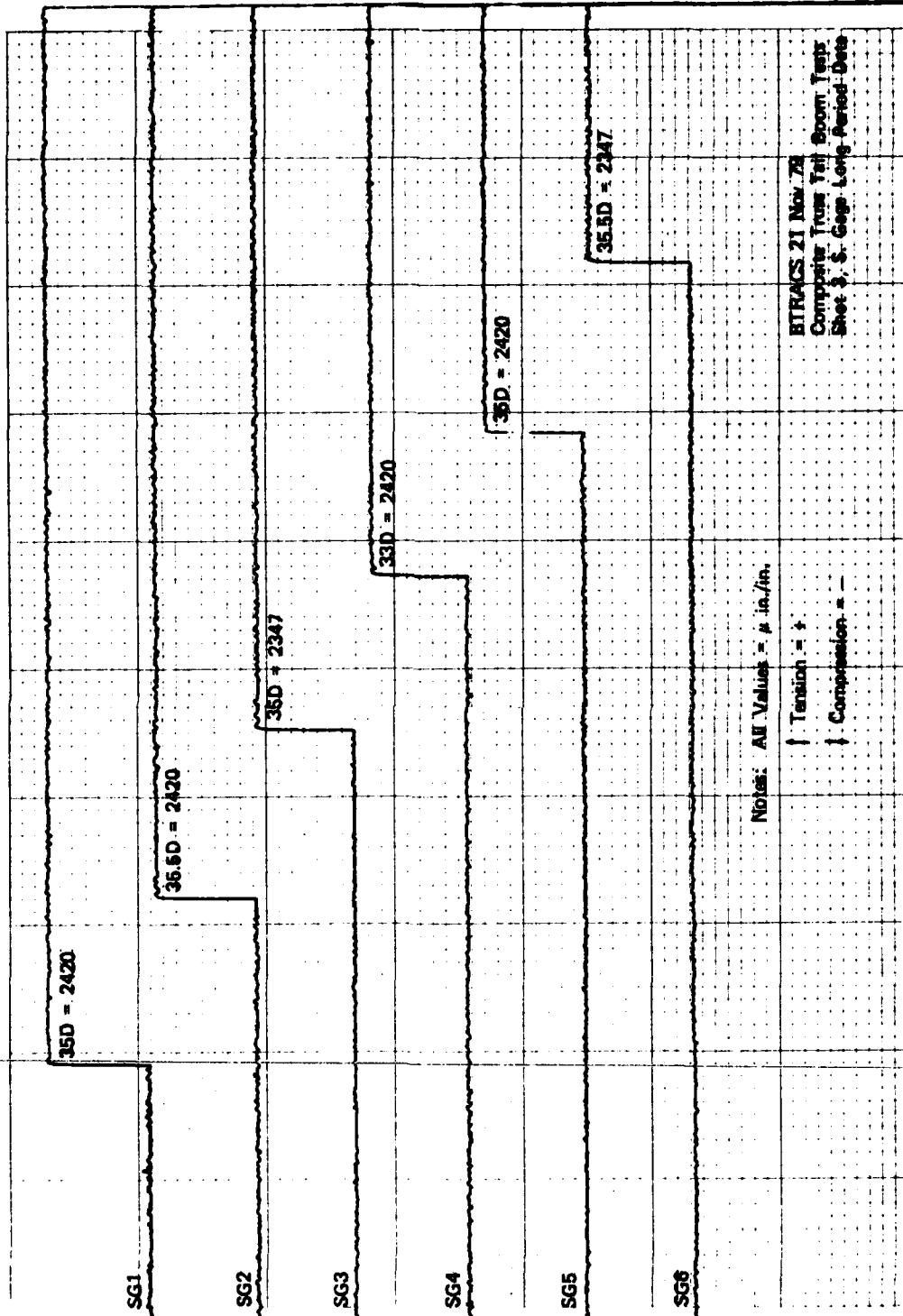
Random Time Base

BTRACS 21 Nov 79
Complete Truss Tail Boom Tests
Shot 3, 5. Gage Long Period Data





BTRACS 21 New 79
 Composite Truss Tail Boom Tests
 Shot 3, S. Gage Long Period Data



ETRACS 21 Nov 78
 Computer Trans Tail Boom Tests
 Sheet 3 of 6. Geop. Long. Period. Data

